FAULT DIAGNOSIS METHODOLOGIES FOR AUTOMOTIVE ENGINE AIR INTAKE PATH

by

Qadeer Ahmed
PE093006

A thesis submitted to the
Electronic Engineering Department
in partial fulfillment of the requirements for the degree of
DOCTOR OF PHILOSOPHY IN ELECTRONIC ENGINEERING

Faculty of Engineering and Applied Sciences
Mohammad Ali Jinnah University
Islamabad

October 2011

Dedicated to Ammi, Abbu, Hira, Hamnah & Abdul Ahad

ACKNOWLEDGMENT

First and foremost I would like to thank Allah Subhana Wataallahu, who gave me the strength, guidance and opportunity to carry on my postgraduate studies in Pakistan. The perseverance granted by Almighty Allah helped me to bear the hard times in writing this thesis.

I acknowledge intimate support of my parents who kept me motivated and assured every kind of moral and financial support throughout my doctoral studies. I also appreciate my spouse for her cooperation, support and providing stress free atmosphere during my doctorate's tenure.

I am very much grateful to my supervisor Dr. Aamer Iqbal Bhatti, who's keen observance & directives helped me to develop and enhance my skills & research work well in time. His exceptional guidance has always enabled me to get out of difficulties of research work.

I extend my special thanks to team members; Mr. Mudassar Abbas Rizvi, Mr. Umer Arfi, Mr. Ghulam Yaseen, Mr. Amin Akram, Mr. Mohsin Raza, Mr. Sohaib Qamar and Mr. Waqas Khawaja, of ICT R & D funded project, "Information System for Early Fault Warning in Automotives". Working with these nobles was a unique experience.

I also recognize the constructive comments and suggestions of Control and Signal Processing Research Group members: Mr. Muhammad Iqbal, Dr. Sohail Iqbal, Mr. Qareb Raza, Mr. Khubaib Ahmed, Mr. Armaghan Mohsin, Mr. Syed Ijaz Kazmi, Mr. Qudrat Khan, Mr. Ussama Ali and many others, who contributed a lot in improving this research work.

In the last, I acknowledge financial concessions granted by the Muhammad Ali Jinnah University, Islamabad and ICT Research & Development Funds, for fiscal help in setting up lab facilities for this research work.

ABSTRACT

On-board model based condition monitoring of an automotive spark ignition engine is still a challenging task for automotive industry. The diagnostic system aims to enhance fuel efficiency and to reduce harmful exhaust emissions. Among various subsystems of gasoline engine, air intake system holds prime importance as it is responsible to ensure proper air and fuel proportions in combustion mixture. This subsystem exhibits highly nonlinear behavior due to its components like throttle body, intake manifold etc. Health monitoring of such nonlinear system cannot be performed by conventional diagnosis methods. That is why On-Board Diagnostic (OBD-II) standard kits do not have the provision to diagnose various air intake system faults. These faults include air leakages in intake manifold, clogged air filter, reduced throttle body efficiency and certain sensor faults. This manuscript presents a novel nonlinear health monitoring scheme based on sliding mode theory for on-board diagnostics of air intake system. Sliding mode theory is extensively used in fault diagnosis methodologies. Sliding mode observers based on nonlinear dynamics deliver robust platform for the estimation of un-measurable system variables. The estimation of such parameters can be exploited for fault diagnosis of dynamical systems. In this dissertation, second order sliding mode observers are designed for air intake system. The designed observers are used to estimate un-measurable and critical parameters/states. Five of the estimated critical parameters are: frictional torque, combustion efficiency, volumetric efficiency, air filter discharge coefficient and throttle discharge coefficient. These parameters are estimated from a two state nonlinear model of gasoline engine based on inlet manifold pressure and rotational speed dynamics. These parameters are extremely helpful in engine modeling, controller design and fault diagnosis/prognosis. Another contribution of this thesis is the development of virtual sensors for air intake system. Pressure dynamics are estimated from crankshaft sensor measurements and vice-versa. The outlined parameters and virtual sensors are used to monitor various functions of air intake system. These functions cannot be routinely sensed/monitored by any sensor. The estimation of afore-mentioned parameters has been conducted under healthy and faulty operating conditions to generate residuals. These residuals are evaluated to identify/classify any malfunction in air intake system. A detailed procedure for three fault diagnostic schemes have been discussed. These scheme require no extra sensor/hardware for their evaluation, only conventional on-board diagnostics (OBD) equipments are mandatory. The validation of novel estimation and diagnostic scheme is performed on production vehicle engine equipped with engine control unit compliant to OBD-II standards. It has been shown experimentally that the above discussed faults have been timely identified. The proposed fault diagnosis scheme has the potential for online implementation as it operates sample-by-sample on OBD-II measurements.

LIST OF PUBLICATIONS

Journal Publications

1. **Q. Ahmed**, A.I. Bhatti, Q. Khan and M. Raza. Condition Monitoring of Gasoline Engine Air Intake system using Second Order Sliding Modes. *Special Issue: Variable Structure Systems in Automotive Applications, International Journal of Vehicle Design. 2011.* [**Impact Factor: 0.55**]

2. **Q. Ahmed** and A.I. Bhatti. Estimating SI engine efficiencies and parameters in second order sliding modes. *IEEE Transactions on Industrial Electronics*, vol.58, no.10, pp.4837-4846, Oct. 2011. [**Impact Factor: 4.678**]

3. **Q. Ahmed**, A.I. Bhatti and M. Iqbal. Virtual sensors for automotive engine sensors fault diagnosis in second order sliding modes. *IEEE Sensors Journal*, vol.11, no.9, pp.1832-1840, Sept. 2011. [**Impact Factor: 1.61**]

Conference Publications

1. Ahmed, Q.; Bhatti, A.I.; , "Second order sliding mode observer for estimation of SI engine Volumetric Efficiency & Throttle Discharge Coefficient," Variable Structure Systems (VSS), 2010 11th International Workshop on , vol., no., pp.307-312, 26-28 June 2010.

TABLE OF CONTENTS

LIST OF FIGURES

LIST OF TABLES

LIST OF ACRONYMS

AFR	Air to Fuel Ratio
AIS	Air Intake System
CBM	Condition Based Monitoring
DEM	Discrete Event Models
ECU	Electronic Control Unit
EGR	Exhaust Gas Recirculation
EKF	Extended Kalman Filter
EPA	Environmental Protection Agencies
FD	Fault Diagnosis
HMM	Hidden Markov Model
KF	Kalman Filter
MAP	Manifold Air Pressure
MAF	Manifold Air Flow
MIL	Malfunction Indication Light
MVEM	Mean Value Engine Model
OBD-II	On-Board Diagnostic Version II
RBF	Radial Basis Function
RLS	Recursive Least Squares
SI	Spark Ignition
SOSM	Second Order Sliding Mode
UKF	Unscented Kalman Filter
WOT	Wide Open Throttle

LIST OF SYMBOLS

Symbol	Description	Units
P_a	Pressure available after air filter	Pa
$\bar{P}_a$	Ambient pressure	Pa
P_{ini}	Maximum pressure drop by air filter	Pa
ϵ_{por}	Air filter porosity	%
ϵ_{dia}	Air filter pores diameter	mm
ϵ_{th}	Air filter pores thickness	mm
C_{af}	Air filter discharge coefficient	
A_E	Throttle effective area	m^2
D	Inlet diameter	m
α_{cl}	Throttle angle at closed position	$^\circ$
α	Throttle angle	$^\circ$
$\dot{m}_{in}$	Air flow entering the manifold	kg/sec
$\dot{m}_{out}$	Air flow entering the cylinder	kg/sec
P_m	Manifold pressure	Pa
V_m	Manifold volume	m^3
m	Mass of air	kg
T_m	Manifold temperature	K
R	Specific gas Constant	J/kg.K
T_a	Ambient temperature	K
ρ_a	Air density	kg/m^3
γ	Ratio of heat capacities	
P_{cr}	Critical pressure	Pa
C_D	Throttle discharge coefficient	
V_d	Displaced volume	$0.001294m^3$
η_{vol}	Volumetric efficiency	
ω_e	Engine speed	rad/sec
N_e	Engine speed	RPM
ρ_m	Air density in manifold	kg/m^3
T_b	Brake torque	N.m
J_e	Engine inertia	$0.25kg.m^2$
T_i	Indicated torque	N.m
T_l	Load torque	N.m
T_f	Frictional torque	N.m
T_p	Pumping torque	N.m
η_{th}	Thermal efficiency	
η_c	Combustion efficiency	
H_{net}	Net heat produced in combustion	J
H_{fuel}	Heat produced in combustion	J
c_v	Heat capacity at specific volume	$J/(m^3K)$
AFR	Air to fuel ratio	

Chapter 1

INTRODUCTION

Automobiles are one of the major means of transportation since last century. Due to constantly increasing demand of automobiles, the automotive technology has continuously evolved to meet the requirements of environment protection agencies and end-users. Automotive industry is among the fastest growing industries in the last few decades. A rough estimate shows that around 6920 1300cc and above vehicles were sold in June 2010 only in Pakistan [3].

Modern vehicles are heavily equipped with sensors, actuators, controllers and computer modules embedded inside the vehicle body. These electronics aim to provide comfort in driving, increase fuel economy and reduce harmful exhaust gases produced during combustion process. Among various electronic systems involved in any modern vehicle like anti-lock braking, electronic fuel injection etc, on-board diagnostics is an essential component.

1.1 Background

On-board fault diagnostics of an automotive engine is its integral part as it needs to be strictly monitored in uncertain operating conditions. The main aim of engine on board monitoring is to ensure proper portions of air and fuel in combustion mixture. Any deviation from desired proportions will lead to degraded engine performance and result in harmful pollutants in exhaust gases.

The incorporation of on board diagnostics (OBD) in any vehicle is also due to legislation requirements emerged in 1993 at California [4]. These legislation requirements aim to reduce hazardous pollutants produced by the automobile engines. The same legislations are imposed in every country like in Pakistan, Environment Protection Agency (EPA) ensures vehicle health under its rules defined in [5]. The main focus of the legislation rules is to regulate *Smoke* and *Noise* produced by any vehicle. In case of smoke, the carbon content should be minimized along with other hazardous chemical components like nitrogen oxides, lead etc. According to

[5], noise level should remain under 85 dB. These legislative requirements can only be ensured if the vehicle is equipped with on-board diagnostics systems.

OBD-II is a standard issued by Society of Automotive Engineers (SAE) and International Standard Organization (ISO). This standard describes the interchange of digital information between on-board emission-related Electronic Control Units (ECUs) of road vehicles and an OBD-II scan tool. OBD-II also commonly refers to the physical on-board diagnostic system of a vehicle, which consists of an ECU, Malfunction Indicator Light (MIL), Diagnostic Link Connector, and the wiring that connect the different elements.

On-board diagnostics have various advantages besides fulfilling the legal requirements. One of the main advantages is: the maintenance schedule is adaptively updated according to engine health indicated by Malfunction Indication Light. Similarly, the mechanics can access the stored fault code and replace the respective component without any hesitation instead of diagnosing by hit and trial methodology. To ensure engine optimal performance, the announced faulty component is excluded from engine control loop and suboptimal control strategy is employed until the vehicle gets repaired. Above all, the emissions are under check and balance.

1.2 Motivation

Automotive engine is a system with highly nonlinear dynamics. These nonlinear dynamics are induced due to its components like throttle/butterfly valve, intake pressure manifold etc. It has been elaborated in [6], [7] that for the health monitoring of a nonlinear system like engine, methodologies from linear systems theory do not possess the desired capability. Thus for an automotive gasoline engine a nonlinear fault diagnosis scheme is mandatory.

This task can be achieved if one can develop a nonlinear model of engine subsystems dynamics and later on these dynamics can be used for the formulation of diagnosis scheme. The nonlinear model based fault diagnosis scheme will inherit the engine behavior that will result in efficient health monitoring. This practice

can benefit us with the monitoring of such malfunctions that cannot be routinely detected and isolated.

It has been often claimed that certain gasoline engine malfunctions are still not monitored in available on-board diagnostics. It was reported by the owners of electronically controlled engine vehicles that faults like throttle body blockade and manifold leakages effect engine performance but these faults are not reported by the on-board diagnostic systems. Like, in case of manifold leakages the engine stumbled during start-up and halted later on. The on-board diagnostic system failed to report the air leakage problem. In second case, due to throttle area blockade the engine used to start but was unable to continue its operation during idling conditions. Once again the on-board diagnostic system did not announce any fault in engine.

The current on-board diagnostic system monitors numerous engine faults with the help of sensor measurements thresholding, look-up table and experience based techniques. But some of the faults of nonlinear engine, including above mentioned malfunctions, still remain undiagnosed. Although, one can find many solutions to the above mentioned problems but the available techniques lack the ability to get incorporated in on-board diagnostic system. All of the available methodologies either require extra sensors or hardware for their applicability.

The above discussion motivates the development of a diagnostic algorithm based on a nonlinear engine model. This algorithm should be able to diagnose such fault which effect the engine dynamics negatively and yet these fault are not routinely monitored.

1.3 Objectives

In order to meet the requirements of OBD-II bylaws for gasoline engine, the following subsystems must be strictly monitored.

- Air Intake System
- Fuel and Combustion System

- Exhaust After-treatment System

If any of these subsystem starts to malfunction, engine performance will deteriorate and it will result in poor fuel efficiency.

Air intake subsystem holds prime importance in maintaining engine performance. This subsystem is responsible to deliver clean air to avoid wear and tear in engine due to abrasive pollutants. At the same time it is also liable for desired amount of air for combustion process. If air intake subsystem is properly functioning the engine can deliver desired power and torque performance. These tasks are achieved by retaining proper proportions of air and fuel in combustion chamber.

Keeping in view the importance of air intake system, the main objective of this thesis is to monitor its operations rigourously. This task can be achieved by employing nonlinear engine model for the estimation of critical parameters. These critical parameters are un-measurable in nature and carry useful information of system health. These parameters can be identified using sliding mode based estimation techniques. The nominal and faulty values of the parameters can be used to generate residuals to identify any fault in air intake system, thus ensuring strict health monitoring.

1.4 Contributions

The major contribution of the research work is the development of model based fault diagnosis scheme for air intake system. The proposed scheme delivers higher fault detection performance i.e. smaller faults can be detected in shorter time. The developed scheme will work on nonlinear model thus there is no limit on its operating range. Another benefit of model based fault diagnosis is the possibility of isolating various faults. The proposed model based fault diagnosis scheme evaluates the residuals being generated from the parameters estimated from sliding mode techniques. The input to this technique is the measurements that are readily available from OBD-II scanner, thus declaring the scheme readily online implementable.

Following are main contributions of the presented research work.

- Estimation of five critical & un-measurable engine parameters
- Development of virtual sensors for air intake system
- Air filter health monitoring
- Manifold leakages diagnosis
- Throttle body efficiency monitoring
- Supervision of air intake system sensors functions

The above mentioned tasks are conducted on OBD-II measurements with no extra hardware requirement.

1.5 Overview

Rest of the thesis is organized as discussed below;

Chapter 2 will introduce the reader to basic terminologies used with in fault diagnosis community. It will also include numerous fault diagnosis schemes used by the researchers around the world. The discussion will brief the advantages of second order sliding mode observer based parameter estimation and fault diagnosis over other schemes. It also covers an introduction about the faults that can occur in air intake system of gasoline engine and their effects on engine performance. Later on these effects will be exploited for fault identification and classification.

Chapter 3 contains automotive engine modeling based on its pressure and angular speed dynamics. These nonlinear dynamics provide solid ground for health monitoring of air intake system. The pressure dynamics are modeled based on air flow across the intake manifold. The angular speed dynamics are described by the torques produced by combustion process, frictional and pumping actions. These engine dynamics will be used to develop model based fault diagnosis scheme for engine health monitoring.

Chapter 4 contains the main contribution of this dissertation. It will discuss about the estimation of gasoline engine parameters. Several engine parameters that cannot be routinely measured can reveal information about engine health. In this chapter a second order sliding mode observer based estimation scheme will be formulated. It also contains a discussion about the verification of the presented scheme for identification of production vehicle engine parameters.

Chapter 5 contains some novel fault diagnosis methodologies proposed in this manuscript. This chapter encompasses three fault detection schemes for monitoring air intake system functions. The proposed schemes will help in monitoring clogged air filter, manifold leakages, throttle body efficiency and certain sensor faults. The proposed methodologies will be verified by implementing it for the health monitoring of production vehicle gasoline engine. In addition this chapter will give a detailed overview of the experimental setup used for validation of the proposed model based fault diagnosis scheme.

Chapter 6 will conclude the thesis by outlining its major contributions alongwith a list of tasks that can be performed in future.

Chapter 2

INTRODUCTION TO FAULT DIAGNOSIS AND GASOLINE ENGINE FAULTS

An introduction to basic terminologies used in fault diagnosis literature is discussed in this chapter. The definition of the terminologies are adopted as outlined in *IFAC* workshop on *SAFEPROCESS* in 1996. These terminologies will be used throughout the thesis. This chapter also elaborates upon the fault diagnosis techniques being exercised by researchers around the world. An overview of model and model free fault diagnosis techniques is provided along with their applications. The possible faults that can occur in air intake path of automotive engine are also explored in detail. The overview explains the past efforts of the researchers to diagnose these faults using various diagnosis techniques. Moreover, it has been argued that on-board model based engine fault diagnosis, to ensure fuel efficiency and reduced emissions, is still a challenging task for automotive industry. It is still an open research task as the current diagnosis techniques lack the ability to be employed for on-board engine diagnostics.

2.1 Fault Diagnosis Terminology

The terminologies and their definitions used in the field of fault diagnosis was standardized at IFAC workshop on SAFEPROCESS in 1996 [8]. This effort was aimed at synchronizing the terminologies used by researchers in fault diagnosis field.

These terminologies are categorized as follows;

1. States and Signals.
2. Functions.
3. Models.
4. Fault Types.

2.1.1 States and Signals

States and signals in fault diagnosis comprise of Fault, Residual, Malfunction, Error, Disturbance and Perturbation. *Fault* is unacceptable deviation of at least one property or parameter of the system from its usual behavior. *Residual* is defined as fault indicator. It is measure of the deviation between measurements and model-equation-based computations. The definition of other terminologies can be seen in [8].

2.1.2 Functions

The tasks involved in fault diagnosis are termed as Functions. These tasks include Fault Detection, Fault Isolation, Fault Identification, Fault Diagnosis, Monitoring, Supervision and Protection. *Fault detection* is defined as determination of faults present in a system and time of detection. Similarly, *Fault isolation* is determination of kind, location and the time of detection of a fault. *Fault Identification* is determination of the size and time-variant behavior of a fault and *Fault diagnosis* is determination of kind, size, location and time of a fault. *Monitoring* is a continuous real time task of determining the conditions of a physical system, by recording information recognizing and indicating anomalies of the behavior. Other functions can be seen in [8].

2.1.3 Models

Models are mathematical equations that are used to reconstruct and to diagnose faults in a particular engineering system. The models used to diagnose faults in engineering system can be *Quantitative model*, *Qualitative model* and *Diagnostic model*. These models are based on static and dynamic relations among system variables and parameters in order to describe systems behavior [8]. Another terminology in this context is *Analytical redundancy*, which is the concept of utilizing two or more methods to determine a variable that is prone to fault. This approach is also practiced for fault diagnosis.

2.1.4 Fault Classification

Faults can be classified according to time dependency, their nature and component type. These classifications are explained below;

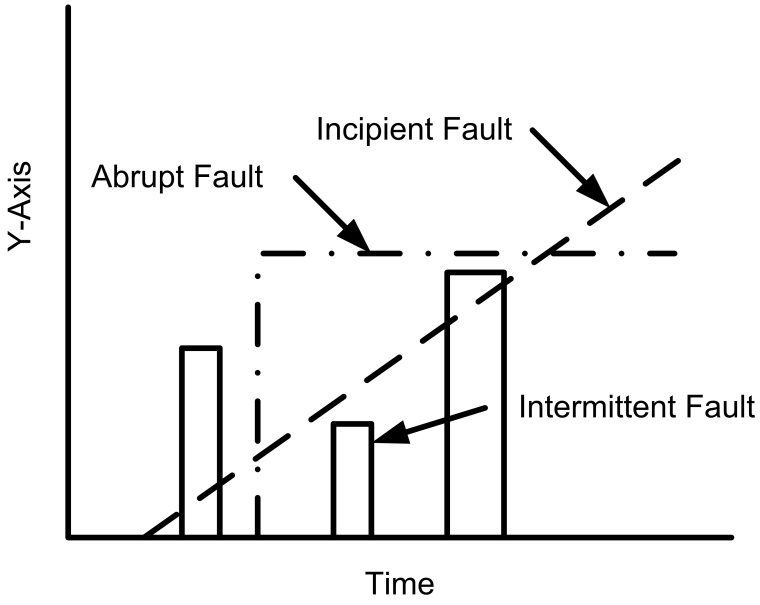

FIGURE 2.1: Fault types with respect to time

2.1.4.1 Time Dependency Based Fault Classification

The occurrence and growth of faults with the time in system are covered under this category. The faults in the system may occur suddenly due to any accident. It may grow with time due to aging of the components or it may occur randomly due to make-break of electrical connections. The time based fault categorization is shown in Figure 2.1 and can be done as;

- *Abrupt Fault* is sudden and permanent occurrence of fault in the system or its components. It is modeled as a step function. Abrupt fault sometimes exhibits itself as bias in the monitored signal.
- *Incipient fault* represents slow growth of the fault in the system or its components. It can be modeled as ramp function. Incipient fault may show itself as time dependant deviation of the monitored signal from real measurement.
- *Intermittent faults* are the faults that occur randomly in the system. It may be a combination of impulses with different amplitudes.

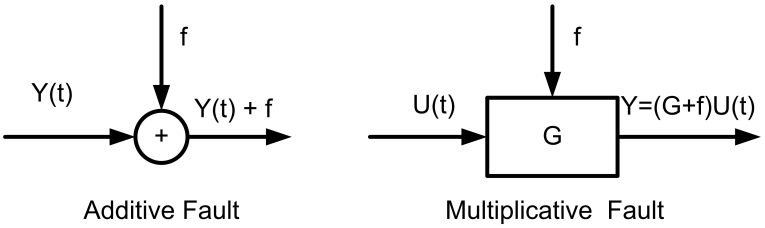

FIGURE 2.2: Additive and Multiplicative Faults

2.1.4.2 Fault Nature based Classification

How the faults interact with the system itself or its output is explained by fault nature. Figure 2.2 explains the fault nature symbolically, where $Y(t)$ is system output, $U(t)$ is system input, f represents fault and G represents system. Depending on fault nature, the faults can either be additive or multiplicative;

- *Additive faults* influence the system output/variable by an offset. This offset can be expressed by addition. Additive faults can be due to noise or disturbance in the system. A common additive fault is offsets in sensor measurements.
- *Multiplicative faults* appear as a result of parametric changes in the system. These parametric changes appear in multiplication with the system states or inputs.

2.1.4.3 Components Based Faults

The faults can occur in each component of the system. The broad classification of the components include sensors, process/system and actuator. Based on these components the faults can be classified as;

- System Faults
- Actuator Faults
- Sensor Faults

These faults can be comprehensively explained by representing a system mathematically as

$$\dot{x}(t) = Ax(t) + Bu(t)$$
$$y(t) = Cx(t) \qquad \textit{Eq (2.1)}$$

where,

x $\in \Re^n$ is the system state vector.
u $\in \Re^l$ is the control input vector.
y $\in \Re^p$ is the output vector.
A $\in \Re^{(n\times n)}$ is the system matrix.
B $\in \Re^{(n\times l)}$ is the input distribution matrix.
C $\in \Re^{(p\times n)}$ is the output distribution matrix.
The above mentioned faults can be explained as.

2.1.4.3.1 System Faults: System/process faults occur by change in system itself. Any change in system reflects itself in its parameters. So the system faults will reflect themselves in system matrix A. Hence, the faults in dynamical systems can be expressed as:

$$\dot{x}(t) = (A + \Delta A)x(t) + Bu(t)$$
$$y(t) = Cx(t) \qquad \textit{Eq (2.2)}$$

where, ΔA is change in system matrix A and represents system fault.
System faults can be due to damaging and aging of its components. Like in engine, manifold leakages and clogged air filter in gasoline engine can be termed as system fault.

2.1.4.3.2 Actuator Faults: Actuator faults correspond to the variation of the control input *u(t)* applied to the system. The faults reflect themselves in input

matrix. Mathematically, the actuator faults can be represented as,

$$\dot{x}(t) = Ax(t) + B^f x(t) \qquad \textit{Eq (2.3)}$$

where,

$$B^f = B(1 - \Gamma)$$
$$B^f = B - \Gamma B$$

ΓB is change in B caused by the fault. Where, $0 < \Gamma < 1$. 1 means component total failure and $\Gamma = 0$ represents healthy system actuators. Another mathematical representation of actuator faults representation as [9]:

$$u_a(t) = L_a(t)u(t) + (1 - L_a(t))f_a(t) \qquad \textit{Eq (2.4)}$$

where,

$L_a \leq 1$ is the efficiency gain.
$f_a \in \Re$ contains the values at which the actuators are stuck.

Actuator faults can be stuck-up of floating control valves in process industry. Similarly degraded motors for actuation purpose are also classified in this category.

2.1.4.3.3 Sensor Faults For each state to be measured a sensor is installed at a particular location. Faults that appear in the installed sensors are termed as Sensor Faults. Mathematically, $y = Cx$ represents measured outputs of the system. The sensor faults can be of the following types,

- *Degraded Efficiency:* In this case sensor will be showing false values but the changing trends will be same as the system behavior. Mathematically, loss in accuracy/degraded efficiency of sensor can be explained as $y = C(1 - s_{loss})x$, where s_{loss} represents the degraded efficiency.
- *Freeze:* In this case, the measurements taken from installed sensors will contain either '0' in case of fully damaged or any other value which will

remain constant through the system process. Freezing nature of sensor can be modeled as $y = s_{freeze}$, where s_{freeze} is constant value that sensor is sharing with the processor.

- *Drift:* If the sensor is showing increasing values of the measured state with time, this behavior is termed as *drift* and it can be modeled as $y = s_{drift}(t)Cx$, where $s_{drift}(t)$ is time dependant factor by which the value is drifting from its original value.

- *Bias:* The sensor measurements sometimes show biased value from true value, this can be modeled as $y = s_{bias} + Cx$, where s_{bias} is the bias added in the sensor readings.

2.2 Fault Diagnosis Methodologies

Optimum performance of engineering systems heavily rely on the proper functionality of sub-systems. Each sub-system should be precisely monitored for smooth operation of any engineering system. This motivation lead to the development of various fault diagnosis methodologies as shown in Figure 2.3. Fault diagnosis schemes are mainly classified into two main streams,

- Model based fault diagnosis techniques.

- Model free fault diagnosis techniques.

However in reality, none of the approach is completely either model-based or model-free in nature. Each of the model-free fault diagnosis schemes uses data that has some kind of an underlying model. Similarly, every model-based approach requires a certain amount of calibration based on available data. In truth, every approach is a combination of data-based (model-free) and physics-model-based (model-based) techniques [10].

2.2.1 Model-Free Fault Diagnosis Techniques

Model-free approaches typically do not rely on any physics based model for diagnosis of faults. These techniques utilize system characteristics and heuristics to

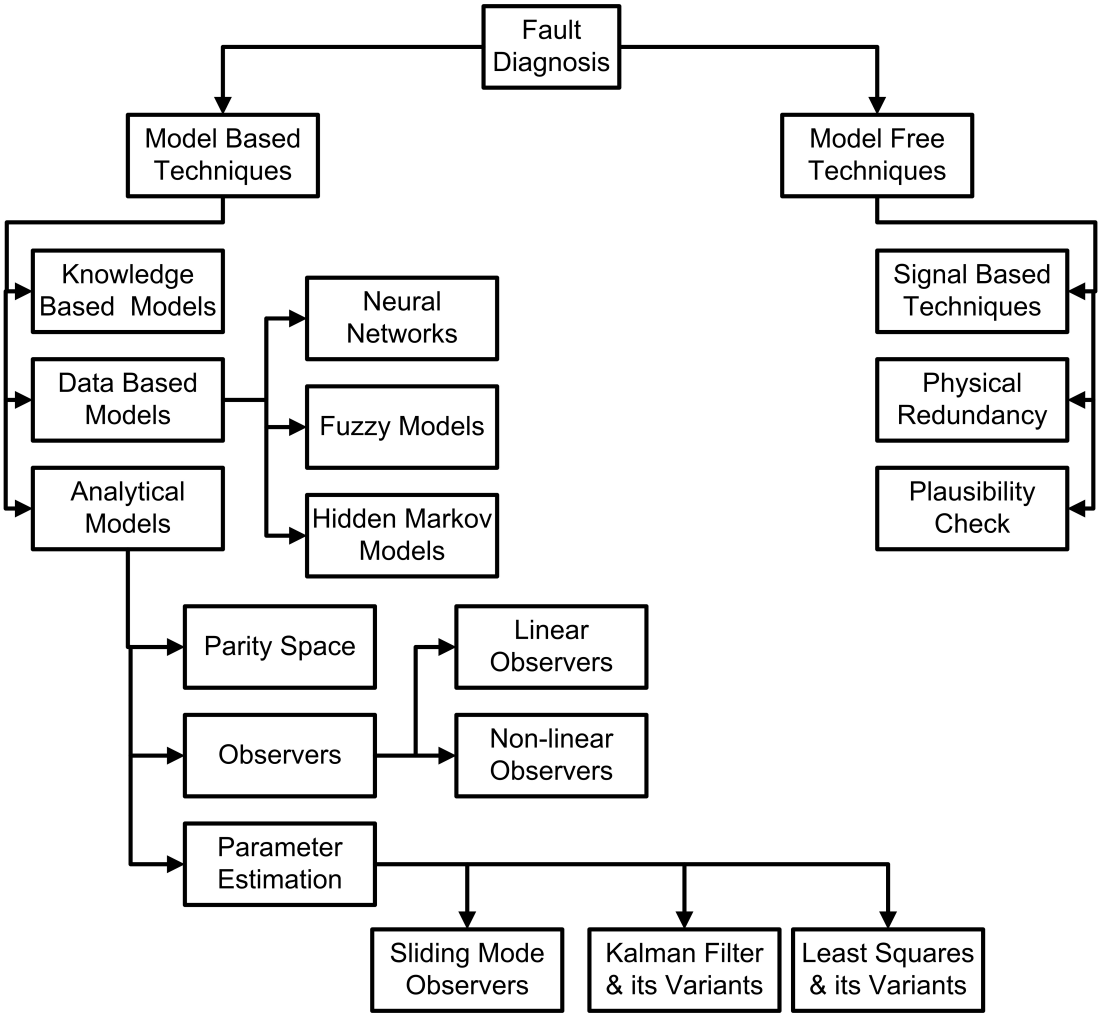

FIGURE 2.3: Classification of fault diagnosis methodologies

classify healthy and faulty system. A broad classification of model-free approaches is

- Signal Based Approach
- Physical Redundancy
- Plausibility Check

2.2.1.1 Signal Based Fault Diagnosis

Signal-based fault diagnosis approaches exploit system *features* for identifying healthy and faulty status of the system [11]. Figure 2.4 gives a brief idea about the methodology. Any fault in sensor, actuator or system will vary the features of the whole system. The features can be analyzed using signal processing techniques

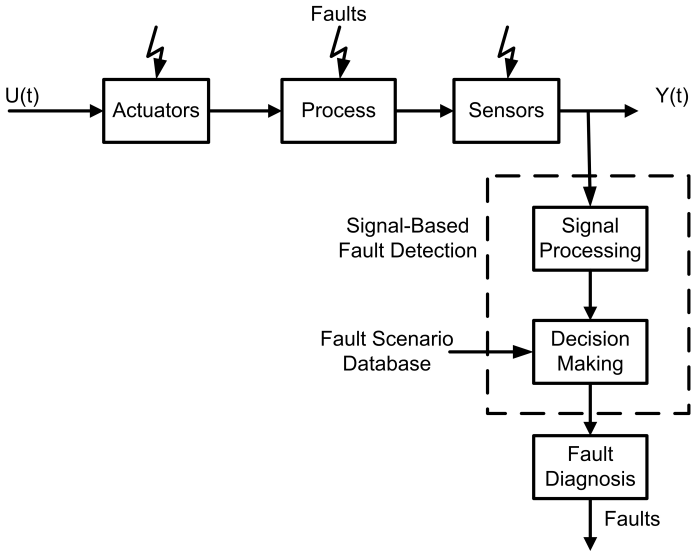

FIGURE 2.4: Signal based fault diagnosis methodology

like Periodogram, Welch periodogram, Scalogram, Spectrogram [12]. Based on archived fault scenarios, the respective system behavior is analyzed and classified accordingly. The authors in [13] proposed signal based fault diagnosis techniques for engine fault diagnosis. However, signal based fault diagnosis methodology ignores internal system dynamics to make its decision and fault scenarios database is not readily available.

2.2.1.2 Physical Redundancy

Physical redundancy is an expensive and naive way of monitoring system health. This approach requires installing of atleast three sensors to measure a single physical phenomena. The decision is made upon majority vote logic. Generally, *two out of three* logic is used to ascertain system health. If two sensors are declaring system faulty and the third one is declaring it normal, the decision will be faulty system. The authors in [14] employed physical redundancy with plausibility check approach to monitor sensor signals for vehicle health monitoring.

2.2.1.3 Plausibility Check

Plausibility check or signal analysis is performed on the sensor measurements installed in the system. The analysis involves the validation of system behavior against the physical laws. This is a preliminary phase of model-based fault diagnosis as it does not involve dynamic relation between system variables, thus

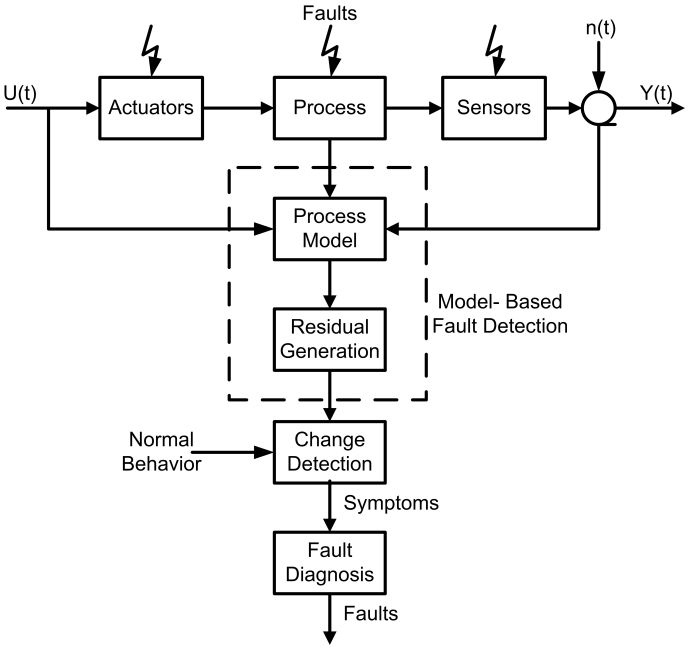

FIGURE 2.5: Model based fault diagnosis methodology

it lacks system insights. Versmold and Saeger [14] performed plausibility check based fault diagnosis from sensor signals for vehicle dynamics control systems.

2.2.2 Model Based Fault Diagnosis Techniques

A model based fault diagnosis scheme utilizes an underlying mathematical model that operates in parallel to monitor system health. The inputs and outputs of the actual system are provided to the developed model. The comparison of the actual system outputs and model outputs helps in generating residuals. These residuals are further explored to analyze and reconstruct faults. Figure 2.5 gives a brief idea about the model-based fault diagnosis schemes. Following are the popular model based fault diagnosis techniques.

2.2.2.1 Knowledge Based Models

Knowledge based models are the qualitative models that are developed on fuzzy-logic based techniques. The symptoms database and knowledge based models are combinely used to generate and evaluate residuals. Generally, knowledge models are used where the user is facing imprecise measurements and uncertain environment. This scheme increases the degree of abstraction, which plays a fundamental

role in reaching correct diagnosis in uncertain environment with imprecise measurement. Perschl and Schmidt [15] used knowledge based models to diagnose various fault in gas transmission networks. However, the major hurdle in developing this technique is the requirement of prior knowledge acquired through experience and symptoms database.

2.2.2.2 Data Based Models For Fault Diagnosis

Among model based fault diagnosis, the data based models are extensively used for condition monitoring of engineering systems. These models are developed by the data sets collected from the system to be monitored. The data set contains those features that can help in classification of all the possible system conditions/states. The conditions/states can either be healthy or faulty. This phase is termed as *training phase*. Once the algorithm is developed upon the training data sets, the data based diagnosis models are ready to classify system health status.

Following are some of the data based models fault diagnosis techniques:

Neural Networks: Neural network based models are composed of neurons, input and output layers. The coefficient of these neurons are trained in order to classify the system health status. The input features vectors are utilized to differentiate between normal behavior and faults. The neural network based model is first trained on the data of each class. The training data involves such features sets that can help in precise classification. Once the whole network in trained, the model can be used to diagnose the faults. Several authors have proposed fault diagnosis using neural network based models like in [16]. Similarly, the authors in [17] used auto-associative neural networks for fault diagnosis for automotive diesel engine. The major inconvenience in formulating neural network based diagnosis scheme is the requirement of large number of training samples to deliver efficient diagnosis results.

Fuzzy Models: These models are made up from fuzzy rules which describe the symptoms of faulty and fault-free operation in terms of predefined fuzzy reference sets. The models are based on expert knowledge or learned offline from the training data produced by computer simulation of typical plant,

with and without the faults. A particular model is defined by specifying the values of the elements of its associated fuzzy relational array. Each element of the array is a measure of the credibility or confidence that the associated rule correctly describes the behavior of the system around a particular operating point. The diagnosis of the fault is determined by comparing the rules of the reference models with the rules of a partial fuzzy model identified using normal operating data collected on-line from the real plant [18]. Lu et al. [19] proposed a fuzzy system for Automotive Fault Diagnosis. The fuzzy model comprised of the algorithms for automatically generating fuzzy rules and optimizing fuzzy membership functions. The diagnosis scheme was used for the detection of vacuum leaks in the automotive engine. Although fuzzy models are widely used for fault diagnosis, but detection results can be imprecise if system dynamics are ignored.

Hidden Markov Models (HMM): HMM is an statistical tool for modeling a wide range of time series data. This powerful statistical tool is used for modeling generative sequences that can be characterized by an underlying process producing an observable sequence. The observable sequence is used to train single HMM for each healthy and faulty status. After training process, each HMM corresponds to unique fault and it helps to diagnose that particular fault. The classified HMM is further explored to evaluate fault severity. Besides its extensive application in signal processing [20], HMM is widely used for estimation, Condition Based Monitoring (CBM), fault diagnosis and prognosis of engineering systems [21], [22], [23], [24], [25]. Although, HMM based fault diagnosis is widely practicely, but it requires extensive training from the data sets of various health status of the system, thus the devised methodology has its scope limited to particular system.

2.2.2.3 Analytical Models

The analytical models are popular tool for fault diagnosis in control systems community. This model based fault diagnosis scheme relies on a dynamical model of the system developed on the basis of physical laws. Each component i.e. actuators, sensors, process of the system is dynamically modeled. The dynamical

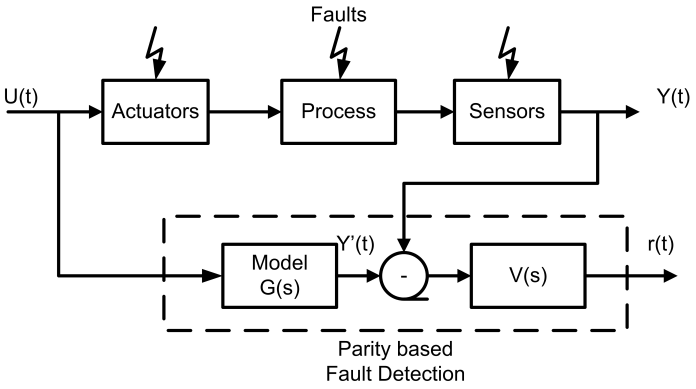

FIGURE 2.6: Parity space based fault diagnosis

model is then utilized to generate residuals based on the same inputs and outputs of the actual system to be diagnosed. The last stage involves the evaluation of the generated residuals to detect, quantify and isolate faults.

Some of the popular analytical model based fault diagnosis techniques are

- Parity Space
- Diagnostic Observers
- Parameter Estimation

2.2.2.3.1 Parity Space Parity space approach is based on consistency check (parity check) of parity equations. The parity equations are supplied by the same inputs as given the actual system. The deviation in the model and actual system output results in the generation of residuals. The parity equation can be developed using transfer functions or state space equations of the system. Figure 2.6 gives an outline of the parity space based residual generation for fault diagnosis. The same input (U(t)) is supplied to the parity space equation (G) and actual system. The output of the parity space (Y'(t)) and system (Y(t)) is then compared to generate residuals. The matrix (V(s)) is used to separate/isolate multiple faults in the system. Mostofi et al. in [26] used parity space relation to diagnose the faults of crankshaft sensor in gasoline engine. Karsihnaswami et al. [7] used nonlinear parity equations for the fault diagnosis of internal combustion engines. It can be

noticed that the parity based fault diagnosis does not consider noise effects and heavily relies on precise system model and precise models are rarely available.

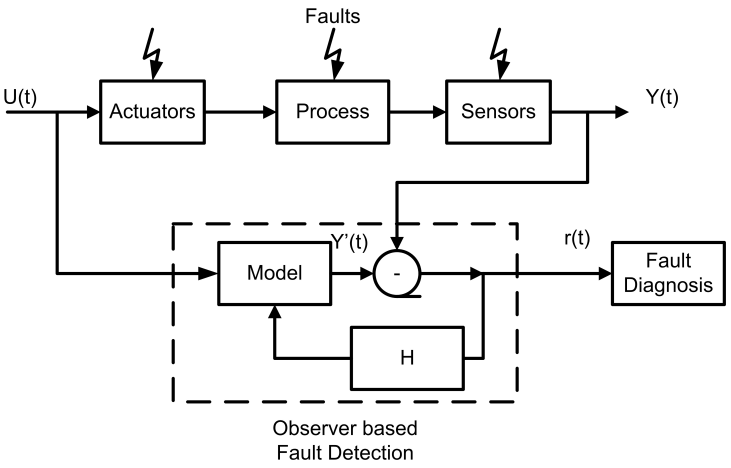

FIGURE 2.7: Observer based fault diagnosis

2.2.2.3.2 Diagnostic Observers Diagnostic observers are employed to reconstruct all of the system states from the available output measurements as shown in Figure 2.7. Linear diagnostics observers are extensively used to reconstruct the faults and diagnose the system health [27], [28]. Proportional observer, also known as *Luenberger Observer*, is a full state observer and provide solid ground to rebuild faults [29]. Similarly, proportional integral observers incorporate output error integral dynamics with conventional proportional error dynamics for convergence. This provides asymptotic and robust course of reconstruction of the states and residuals. Figure 2.8 explains the proportional-integral observer functioning. The dash-line box in Figure 2.8 represents the proportional observers functionality.

In Figure 2.8, A,B,C are system matrices. $\hat{x}$ and $\hat{y}$ are observed state and output vectors respectively. $\hat{v}(t)$ is the vector of the observed state variables of the effect system. $\hat{y}(t)$ is the vector of the observed output variables of the control system. $\hat{y}_v(t)$ is the vector of the reconstructed output variables of the effect system, interpreted as the vector of the reconstructed effect variables (fault variables, ...). L_E is the input matrix of the control system with respect to the type of influencing its behavior. L_C is the output matrix of the effect system. L_P is the matrix of the

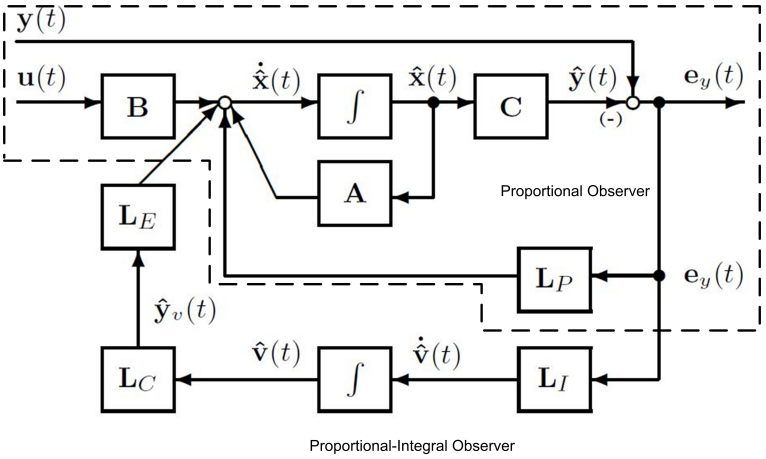

FIGURE 2.8: Proportional integral Observer Structure

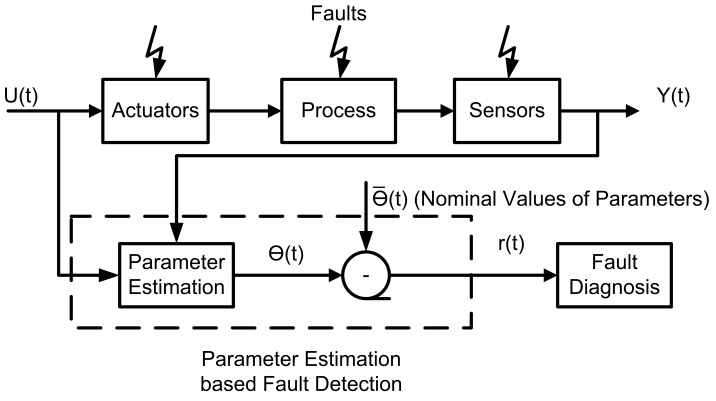

FIGURE 2.9: Parameter estimation based fault diagnosis

proportional gains. L_I is the matrix of the integral gains (both to be calculated). $e_y(t) = y(t)$ - $\hat{y}(t)$ is the vector of the reconstruction error of the output variables of the control system [30].

Proportional integral observers have been used for fault diagnosis also [31], [32], [33]. Z. Li and Jaimoukha [34] proposed observer-based fault detection and isolation filter design for linear time-invariant systems. The fault diagnosis can be done using a single observer excited by single/all output or bank of observers excited by single/all outputs [35].

2.2.2.3.3 Parameter Estimation Estimation of critical system parameters can be very useful for the diagnosis of engineering systems [36], [37]. A gray

system whose dynamics are known and time varying parameter need to be estimated/identified can be diagnosed by estimating its health indicating parameters. Figure 2.9 gives a brief idea about the parameter estimation methodology. The input (U(t)) and output (Y(t)) are supplied to parameter estimation technique. The estimated parameters are compared to their nominal operating values for the diagnosis of various faults. Some popular parameter estimation techniques are:

- Least Squares & its variants
- Kalman Filter & its variants
- Sliding mode techniques

Least Squares & its variants: The method of least squares is used to estimate the approximate solution of over-determined systems. By over-determined system it is meant that number of unknowns is more than number of available equations. The optimality criterion of standard least squares minimizes the squared sum of residuals between actual measured outputs and output values of the gray model being predicted from input observations. Once the residuals are minimized the respective parameters can be evaluated for condition monitoring. Figure 2.10 explains least square parameter estimation based fault diagnosis. This approach along-with its variants has been widely used for fault diagnosis [38], [39]. The least squares delivers an offline estimation solution for linear systems only. For a nonlinear dynamical system the estimation results are inaccurate and computational expensive [40].

Kalman Filter & its variants: Kalman filter is extensively used for state and parameter estimation of engineering systems [41], [42]. Standard Kalman filter requires linear model of the underlying system, initial measurement and process noise distribution and parameter/state estimates. Based on this information, the algorithm first predicts the estimates and rectifies the estimates using the measurements and Kalman filter gain. As standard Kalman filter is limited to linear system, a number of Kalman filter variants have been proposed to broaden its horizon. Among number of variants, few are:

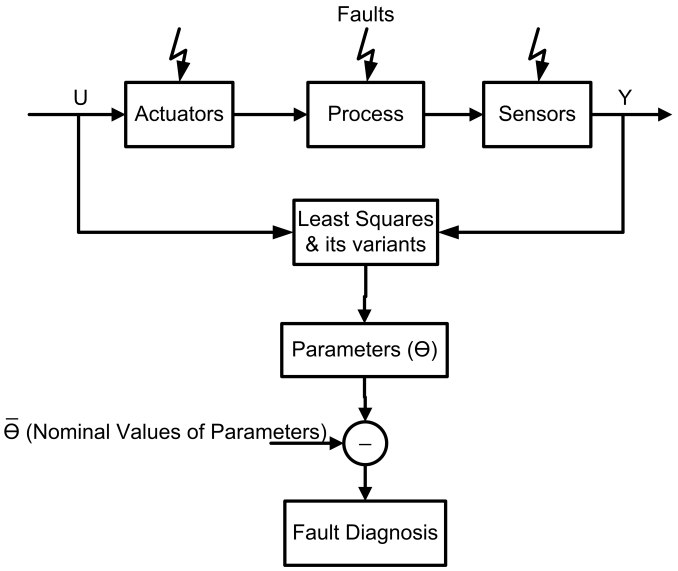

FIGURE 2.10: Least square parameter estimation based fault diagnosis

Extended Kalman Filter (EKF), being used for estimation of nonlinear system by linearizing it around a single operating point. Similarly, Unscented Kalman Filter (UKF) and its variants like Square-root UKF, performs standard unscented transform prior to recursive estimation [42]. Figure 2.11 gives a brief idea about the working of Unscented Kalman Filter. The unscented transformation is applied on initialized states. These transformed states are then utilized for estimation. If the parameters to be estimated are declared as states then the same procedure can be adopted for their estimation. Both tasks of state and parameter estimation can be performed in parallel using Joint Extended Kalman Filter or Dual Extended Kalman Filter. Wenael in [43] utilized dual extended Kalman filter for the estimation of vehicle states and parameters.

Sliding mode techniques: Sliding mode techniques are very powerful tool to estimate the parameters of uncertain systems. Figure 2.12 explains the sliding mode observer being used for parameter estimation. The actual system measurements are tracked using sliding mode observer. The uncertainty is modeled under the sliding mode injectors. These robust injectors eliminate the difference with actual and observed output. The detailed error analysis helps in estimating critical parameters being used to diagnose the faults of the system. Sliding mode techniques have been extensively used

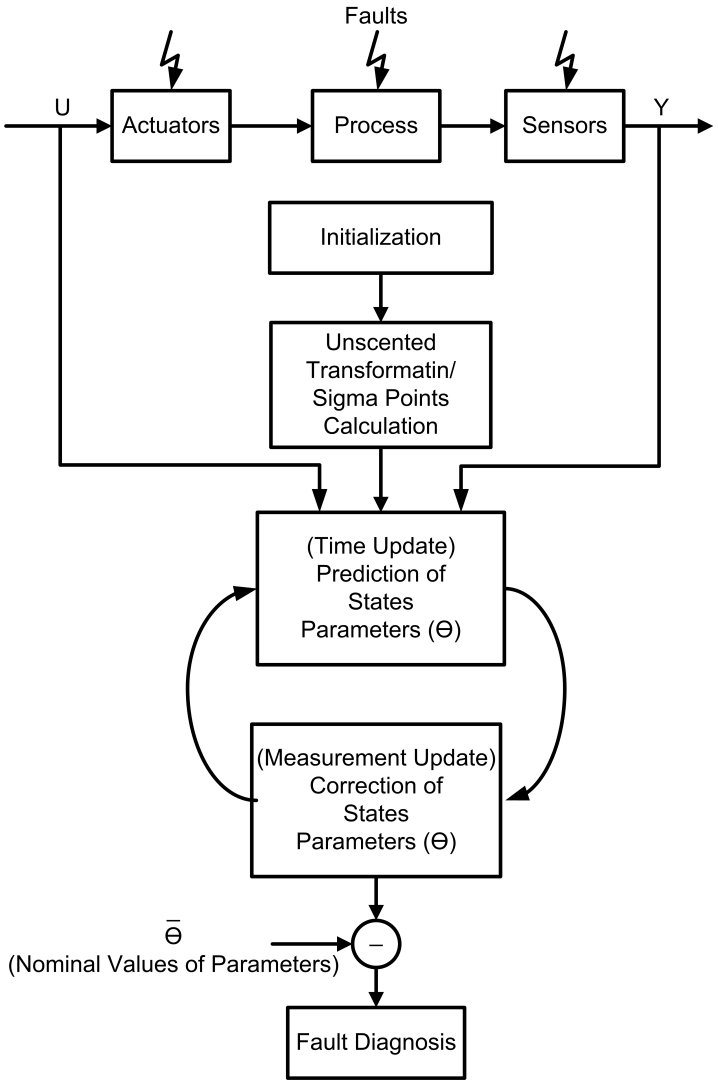

FIGURE 2.11: Unscented Kalman Filter state and parameter estimation based fault diagnosis

for estimation and control [44], [45], [46]. Currently, for the estimation of un-measurable and inaccessible system states, second order sliding mode techniques have been used by many researchers [47], [48], [49] [50], [51], [52].

2.2.2.4 Advantages of Second Order Sliding Mode Technique

After going through numerous fault diagnosis methodologies, it can be observed that each diagnosis scheme faces certain limitations. Like, physical redundancy needs extra sensors installation, which is expensive and obsolete approach. Other model free diagnosis techniques only work on sensor measurements without considering underlying working model and actual inputs to the systems. Knowledge based models require experience to develop model rules. Similarly, data based

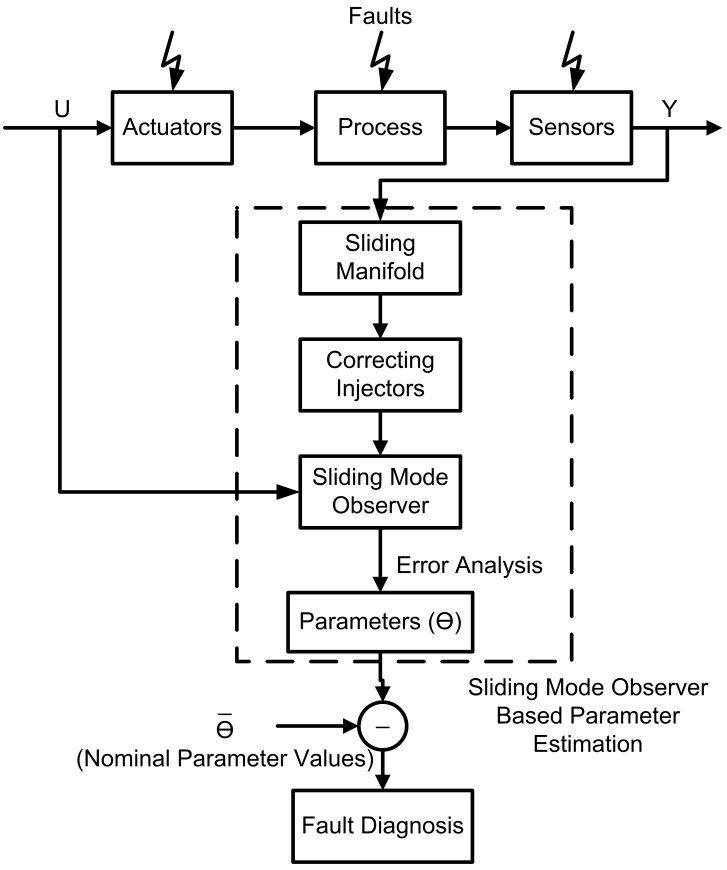

FIGURE 2.12: Sliding mode observer parameter estimation based fault diagnosis.

models require extensive training data sets. Insufficient training sets may lead to imprecise health monitoring. Another problem with data based schemes is their off-line execution for fault diagnosis.

Among analytical models, Proportional (Luenberger Observer) and proportional integral observers only work with linear models which makes fault diagnosis of highly nonlinear systems very difficult. The parity space approach often shows very good results in simulations, but it can be highly sensitive to measurement noise and process noise, since these are not taken into consideration in the design of the parity space. In the parameter estimation techniques, least squares and its variants work efficiently for linear systems only. First order sliding mode approach provides estimation of parameters with noise that needs to be filtered. This introduces a phase shift and bias. The need for filtering effects the finite time convergence property. The deficiency in identification of uncertainties and parameter persists until second order filtering is employed. This may lead to corruption of results

[49].

However, super twisting algorithm based second order sliding mode (SOSM) observers possess the same robustness as first order sliding mode and ensure reduction in chattering phenomenon [53]. These observers are utilized for parameters estimation because they make the states observation without filtering. This ensures the identification of uncertainties with just one filtering only, that helps in parameters identification [49], [54].

The other advantages of second order sliding observer include: it may or may not require complete system information and noise distribution for convergence as mandatory in Kalman filter based state/parameter estimation. Moreover, the nonlinear framework of second order sliding mode based technique is efficient, computationally cheap & online implementable as it is free of multiple matrices evaluation and multiplication like in prediction stage of Kalman filter. In addition it does not involve the system to be Jacobian linearized as required in EKF. This linearization can be inaccurate for a system with large nonlinearities for short time period [41]. Similarly SOSM observer is free of transformations, computation of sigma points, Cholesky factor updating, efficient least squares and decompositions as mandatory in UKF and its variants [42]. Therefore, one can implement SOSM observer using low cost embedded system very easily. ■

After going through various fault diagnostic techniques, the following sections will highlight the malfunctions that can occur in gasoline engine.

2.3 Fault Diagnosis in Gasoline Engines

Vehicles with gasoline automotive engines are widely used for transportation purpose in modern era. Figure 2.13 elaborates a subset of the subsystems, sensors and actuators installed in a typical gasoline engine. The mentioned list of sensors are used to precisely monitor engine functions. The actuators are responsible for the execution of the desired tasks. Due to abundant usage of these engines, the demand of flawless engine functioning is also increasing. The demanding sources include environmental protection agencies and end-users. To meet these demands, the above discussed model or model free fault diagnosis techniques have been

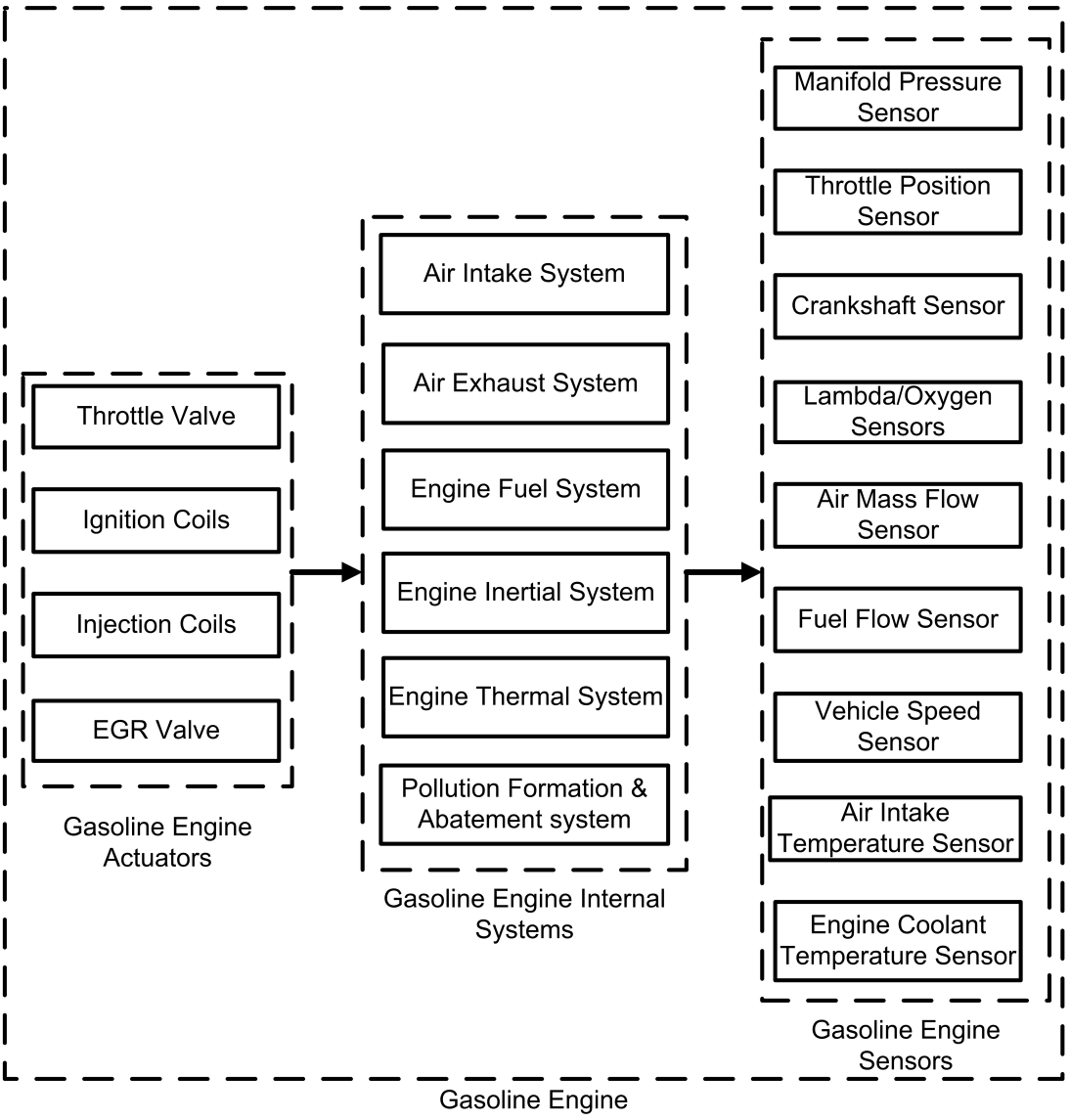

FIGURE 2.13: Automotive gasoline engine; its actuators, subsystems and sensors

widely practiced to monitor various components of gasoline engine [16], [52], [55], [56].

2.3.1 Air Intake System & its Faults

Air Intake System (AIS) is an integral subsystem of a gasoline engine. Primarily, this system is responsible for clean and optimum amount of air for the combustion process. The amount of air that enters the manifold is sensed by an air pressure/flow sensor and the fuel is sprayed from injectors such that air to fuel ratio (AFR) is ensured. If there occurs any fault in AIS, air fuel mixture will either become rich or lean. As a consequence, loss of engine power, harmful exhaust

emissions and retarded fuel efficiency will effect engine performance. Thus, strict monitoring of AIS function must be ensured in order to avoid these problems

In this section malfunctions due to various components involved in AIS of gasoline engine are discussed. These components are air filter, pressure manifold, throttle body, manifold pressure and angular speed sensors. Each of the components if not working properly can cause multiple adverse effects on engine performance. The following discussion will give us an idea about the problems caused by clogged air filter, manifold leakages and reduced throttle body efficiency. Similarly, crankshaft and manifold pressure sensor can also degrade the engine performance, if not working properly. Each subsection sequent will contain a brief overview about the past efforts of researchers to diagnose these faults. After going through the severity of the faults and certain limitations of available diagnosis techniques, these faults are planned to be diagnosed in order to ensure optimum engine performance.

2.3.1.1 Clogged Air Filter

Air filter is supposed to deliver clean air for combustion process. This will help in reducing dust concentration in air intake path. A serious consequence of increase in abrasive dust particle is engine wear and tear. As air filter remains exposed to environmental hazards most of the time, the natural phenomenon of choking degrades the air filter performance with the passage of time. A clogged air filter (as shown in Figure 2.14) will hinder to deliver required amount of air to produce optimum power, especially at high speeds and loads. The choking phenomenon increases the pressure drop across air filter [57], [58]. This negatively affects the pressure dynamics of intake manifold. Figure 2.14 gives us an idea about the clogged and healthy air filter.

Factors effecting air filter performance has been discussed in detail in [57]. The degraded air filter in open loop carburated engine vehicles, affects fuel efficiency significantly. It has been shown in [59] that the fuel economy is increased by 14% when clean air filter is used. However, in modern electronically controlled vehicles, air filter has no significant affects on fuel economy. The closed loop/feed forward action in Engine Control Unit (ECU) maintains the desired AFR despite of choked

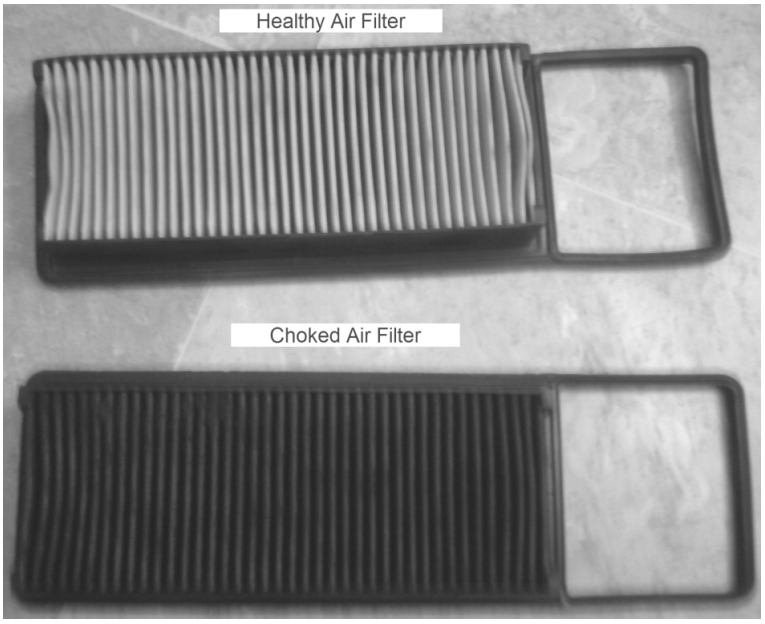

FIGURE 2.14: Healthy and Clogged Air Filters

air filter. On the other hand, clogged air filter influences the driving performance of ECU equipped engines as acceleration/pick up time is increased.

2.3.1.1.1 Clogged Air Filter Diagnosis Methodologies: Keeping in view the adverse effects of clogged air filter on engine performance, its health monitoring becomes mandatory. In the literature, air filter health is mostly diagnosed by measuring pressure drop across it. The filter health degradation is directly related to pressure drop after air filter. This requires installation of additional three pressure sensors [57], [59]. Similarly, a signal based diagnosis of emulated choked air filter has been carried out by [60]. It has been observed that air filter health diagnosis is less practiced in available literature. One of the main reasons is: air filter is either ignored or assumed as clean filter while modeling pressure dynamics of engine air intake path [61], [62], [63].

2.3.1.2 Manifold Leakages and Reduced Throttle Body Efficiency

Among the major components of air intake system, intake manifold and throttle body are primarily responsible for smooth air flow for air fuel mixture. This ensures optimum engine performance. However, the intake manifold behavior is adversely affected by leakages. Similarly, throttle body efficiency is reduced if its effective area is reduced or increased. Figure 2.15 and Figure 2.16 give an idea

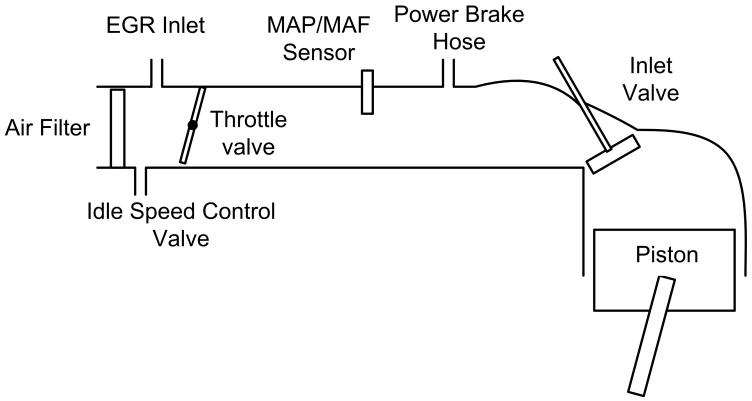

FIGURE 2.15: Intake manifold and its connecting elements

about intake manifold and throttle body respectively. The following discussion about manifold leakages and reduced Throttle Body Efficiency will brief about their effect on engine and how researchers have diagnosed these problems.

2.3.1.2.1 Manifold Leakages: Air leakages in inlet manifold increase the amount of uncontrolled oxygen for combustion process, that may result in high engine rotational speed and unpredictable manifold pressure. This malfunctioning may let end-user experience:

- Hissing Noise
- Engine Stumbling
- Rough/Fast Idling or Stalling
- Poor Gas Mileage
- Hesitation/Poor Pick Up

However, in actual air leakages in manifold force manifold absolute pressure sensor to generate false measurements that can result in AFR deviation. The deviation in AFR may cause emissions to increase. Similarly, an inevitable consequence of manifold leakages is the loss of generated power due to lean air fuel mixture.

FIGURE 2.16: Throttle Valve/Butterfly Valve

These symptoms become visible after air leakage has occurred. The possible causes of manifold leakages may be aging affects of hoses connecting manifold to other components like Exhaust Gas Recirculation (EGR) hose, power brake booster hose. Other causes may include EGR valve leaks, intake manifold gasket leaks, aging of throttle/butterfly valve and other gaskets leaks. Figure 2.15 gives an idea of components attached to AIS, that may result in air leakage. Besides leakage in AIS, components in connection with manifold, if get ruptured, also cause air leakages. For example, any damage to power brake booster can cause air leakage in manifold.

2.3.1.2.2 Defective Throttle Body/Butterfly Valve: Similarly, the second factor that may hamper engine performance is defective throttle valve. Throttle valve is responsible to deliver desired amount of air for combustion process. Manipulating throttle valve controls the power produced by engine. Any malfunction by the actuator will effect the engine performance. One of the main consequences of degraded throttle valve is its loss of effectiveness. This results in Throttle Effective Area (A_E) reduction. This decrease in A_E can be due to deposition of unwanted materials in throttle body or any obstruction in AIS. On the other hand, electronically operated throttle valve can malfunction to decrease A_E if there exists any fault in its electronic circuit. Similarly, bowden cable operated

throttle valve is dependent on cable for its efficiency. Any damage to bowden cable will negatively effect A_E due to decrease in throttle valve performance. Moreover, A_E reduction can be due to the clogged air filter, as it remains exposed to environmental hazardous most of the time.

2.3.1.2.3 Manifold Leakages and Reduced A_E Diagnosis Methodologies: Keeping in view the adverse effects of manifold leakages and decrease in A_E due to throttle malfunction, various researchers have tried to diagnose these AIS faults through various algorithms. Nyberg et al. [55] identified manifold air leakage and throttle faults by proposing a physical model of these faults for turbo charged engine whose parameters were identified by Recursive Least Squares (RLS). The identified parameters helped to check the severity of leakages and decrease in A_E. The authors in [64] presented mathematical model of an internal combustion engine to detect failures in the intake manifold. The proposed fault detection and isolation method performed threshold tests on the directional residuals. The residuals were generated by a combination of a state-dependent Kalman filter, an open-loop observer and an unknown input estimator. In [65], it was proposed to detect air leakage using the with-in cycle crank-angle-based Model. The proposed scheme showed improved fault sensitivity as compared to Mean Value Engine Model (MVEM) based approach. Franchek et al. [66] suggested diagnostic approach for air leakage based on a static air path model, which was adapted online such that the model output matches the measured output during steady state conditions. The resulting changes in the model coefficients created a vector whose magnitude and direction were used for fault detection and isolation. Sangha et al. [16] proposed Radial Basis Function (RBF) neural network based diagnosis scheme for air leakages. MVEM was used to simulate air leaks and other faults to validate the scheme. The authors in [60] proposed classifier fusion approach for diagnosis of automotive systems. The methodology validation was limited to synthetic faults generated by Computer aided multi analysis system in Hardware In Loop Simulations (HILS). Weinhold et al. [67] suggested model based diagnosis of air leakage and A_E blockage. PI observer was employed to generate residuals. Later on these residuals were evaluated to diagnose AIS health. It can be observed

that diagnosis of leakages and A_E reduction is widely practice but an algorithm compliant to OBD-II scanner is still a question.

2.3.1.3 Air Intake System Sensor Faults

Engine fuel efficiency depends on the air to fuel ratio of in-cylinder mixture that is required to be as close to its stoichiometric proportions as possible. The standard stoichiometric ratio can be maintained if AIS performance is ensured. Any malfunction in AIS will affect the amount of oxygen required for complete combustion, thus disturbing stoichiometric proportion. One of the main factors that retards fuel efficiency is malfunctioning of manifold absolute pressure and crankshaft sensor.

2.3.1.3.1 Manifold Pressure Sensor: A faulty MAP sensor may let an end-user experience:

- Exhaust Gases and gas smell.
- Rough Idling.
- Poor Gas Mileage.
- Hesitation/Poor Pick Up.

However, in actual, due to various nature of sensor faults, MAP sensor generate false measurements that can result in:

- Deviation in AFR, that may cause emissions to increase. (Pollution)
- Lean or rich air fuel mixture, that may cause misfire. (Hesitation)

2.3.1.3.2 Crankshaft Sensor: Similarly, a crankshaft sensor is used to measure angular speed. If it has failed or is failing, certain timing problems will arise in engine function. The engine may start normally in some cases, but will cut off after a few minutes (or seconds) of operation. More than likely the engine will be unable to start at all. Since the crankshaft sensor is responsible for engine timing,

the driver may experience engine backfire or irregular angular speed function, if the vehicle starts at all.

These symptoms are visible only after fault in the sensors has occurred. These faults can be due to bias or drift in sensor outputs. Other causes may include loss in effectiveness, damaging of sensors or frozen sensor outputs. In order to avoid such situations early diagnosis of sensor health becomes inevitable. Currently, automotive industry utilizes many experience and lookup tables based techniques to monitor sensor faults. However, in literature, various researchers have attempted to diagnose sensor faults in automotive engine.

2.3.1.3.3 Sensor Faults Diagnosis Methodologies: Sensor fault diagnosis has been carried out with various algorithms. Balaban et al. [68] employed neural network based classifier to figure out different faults in sensors with its application in aerospace systems. Similarly, Singh et al. [69] developed an artificial neural network-based virtual fault detector for detection and identification of faults in Wheatstone bridge-oriented transducers of a computer-based measurement system. In automotives, the authors in [70] discussed sensors fault detection, isolation, and accommodation procedure for public transportation. The approach was to develop analytical redundancy for installed sensors that can diagnose the faults efficiently. Crossman et al. [71], analyzed various signals of vehicle sensors and control module to diagnose its faults. The procedures of pattern recognition were employed to classify different faults. Rizzoni and Min [72] proposed detection filters to diagnose sensor failures in automotive engine control systems. The detection filter utilized analytical redundancy within a dynamical system to isolate the cause and location of abnormal behavior. Hsu et al. [73] suggested a hexadecimal decision table to relate all possible failure patterns to the residual code. The residual code was obtained through simple threshold testing of the residuals, which were the output of a general scheme of residual generators. The proposed diagnostic system was applied to automotive engine sensors and actuators. Nyberg [74] developed a model based fault diagnosis algorithms to detect air intake system faults: sensor faults and manifold leakage. In [60] it was suggested to fuse classifiers for the diagnosis various faults in automotive systems. The authors in

[75] described the hybrid solution, based on artificial neural networks, and the production rule adopted in the realization of sensor fault detection, isolation, and accommodation scheme for automotive applications. It can be observed that AIS sensors fault diagnosis is widely practiced but a model based sensor fault diagnosis compatible to On-Board Diagnostic version-II (OBD-II) standards is still an open problem.

2.4 Conclusion

This chapter explored basic fault diagnosis terminologies and various fault diagnosis techniques. The overview gave an idea and application areas of each fault diagnosis scheme. Keeping in view the advantages of SOSM observer based fault diagnosis technique, it can efficiently diagnose engine health based on the estimation of critical parameters. These critical parameters can be helpful to diagnose the possible discussed faults that can occur in various components of AIS. The adverse effects of these faults have been explored in detail. It can be seen that each fault affects the engine performance negatively and thus needs to be monitored.

It can be observed that model based engine diagnosis are extensively explored but still automotive industry is still struggling to incorporate OBD model based methodologies to monitor gasoline engine health in real time. Currently, lookup table and experience based diagnosis techniques are widely employed in available production vehicles. However, keeping in view the strengths of model based on-board condition monitoring, it is still an open challenging task for automotive industry.

In the coming chapter, mean value engine model will be formulated for model based fault diagnosis scheme. A second order sliding mode observer based parameter estimation scheme will be formulated for air intake system of gasoline engine. Later on, the estimated parameters will be analyzed for gasoline engine health monitoring.

Chapter 3

AUTOMOTIVE ENGINE MODELING

Model based fault diagnostic schemes heavily rely on accurate model of the dynamical system. This chapter will discuss the gasoline engine functions and its mathematical modeling. Various engine parameters like Throttle Discharge Coefficient, Volumetric Efficiency, Combustion Efficiency etc are employed to develop a realistic mean value engine model. These parameters are used to produce actual engine behavior from the mean value engine model developed on ideal physical laws. The attempts to model these engine parameters are also discussed in the chapter. A successful validation of the developed mean value engine model is carried out against a commercial vehicle engine. Later on the validated model will be used for estimation and diagnosis purposes.

3.1 Gasoline Engine

The engine is a device which converts chemical energy into mechanical energy. Chemical energy stored in the fuel is first converted to thermal energy by means of combustion process with air inside the cylinder. This thermal energy then raises the temperature and pressure of the gases within the cylinder of the engine. This high-pressure gas then expands against the mechanical mechanisms of the engine. This expansion is converted by the mechanical linkages of the engine to a rotating crankshaft which is the output of the engine.

The engine under study is naturally aspirated spark ignition internal combustion engine. Its working cycle consists of four strokes with reciprocating basic design. The first stroke sucks fluids inside the cylinder termed as *Intake Stroke*, which is compressed in the second stroke i.e *Compression Stroke*. The third stroke takes place after combustion carried by the ignition of spark plug. The spark plug gives a high-voltage electrical discharge between two electrodes which ignites the air-fuel mixture in the combustion chamber surrounding the plug. This stroke is

responsible for the work done by the engine and is known as *Power Stroke*. Finally, the *Exhaust Stroke* expels all the gases created as result of combustion.

A Spark Ignition (SI) engine is highly complex system that consists of several subsystems and can be modeled by a combination of highly nonlinear algebraic and differential equation. SI engine can be modeled based on its reciprocating nature under *Discrete Event Models (DEM)* and if we neglect discrete cycles of engine and consider all processes of continuous nature then this approach is termed as *Mean Value Engine Modeling*. The choice of model depends on the control objectives, like DEMs are used for engine mis-fire detection and MVEMs used for the control of slow engine processes.

Mean Value or low frequency model neglects discrete events of engine and describes the engine dynamics with limited bandwidth, equivalent to considering the mean behavior of states variables over a few engine cycles. All Mean Value Engine Models are control oriented models, which means input-output behavior of the system is modeled with reasonable precision but low computational complexity and include explicitly all relevant transients effects. MVEMs have been extensively used for engine control strategy development [62].

Most mean value models are having lumped parameters i.e. system description that has no spatially varying variables and that are represented by ordinary differential equation. If location, volume, temperature are to be used as independent variables, then resulting models are represented by Partial Differential Equations (PDE) and PDEs are computationally too demanding.

The subsystems involved in mean value modeling depends on the nature of control tasks as certain subsystems can be neglected in order to make the model relatively simpler and computational friendly. Following are the subsystems that can be modeled in MVEMs

- *Air system*, defines how much air is inducted into cylinder
- *Engine Inertial system*, explains the engine speed.

- *Torque Generation system*, defines how much torque is produced by air/fuel mixture.
- *Fuel system*, defines how much fuel is inducted into cylinder.
- *Engine Thermal system*, dictates dynamic thermal behavior of the engine
- *Pollution Formation system*, models the engine-out emissions.
- *Pollution Abatement system*, models the behavior of catalyst, sensors and other relevant equipment in the exhaust pipe.

Based on our pre-defined objectives, we will be modeling the first three subsystems in order to obtain a Mean Value Engine Model. The formulated model will have output as engine speed in revolutions per minute (RPM) & inlet manifold pressure in kilo pascals (kPa)and input as throttle angle in degrees (°).

The model is based upon the important modeling processes namely throttle body, intake manifold, combustion and rotational dynamics processes. The modeling processes of the above sub-models are carried out by considering few assumptions. One-dimensional steady compressible flow is considered in the throttle body [61]. Filling and emptying approach is employed for capturing the air dynamics in the intake manifold. Otto cycle is utilized for analysis of in-cylinder dynamics [2]. The

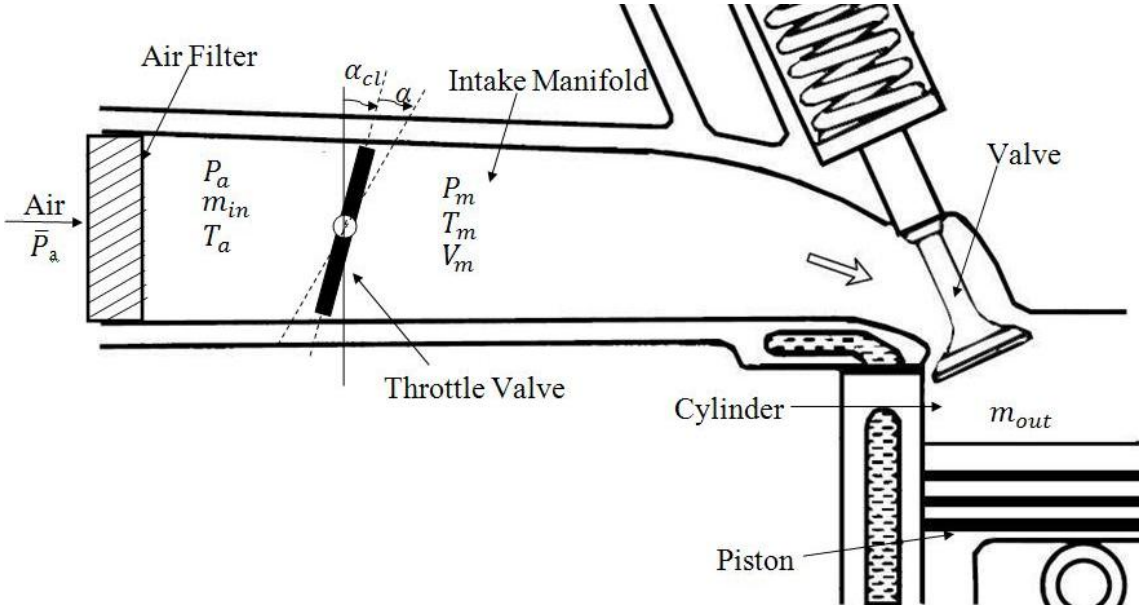

FIGURE 3.1: Components Involved in Engine Modeling

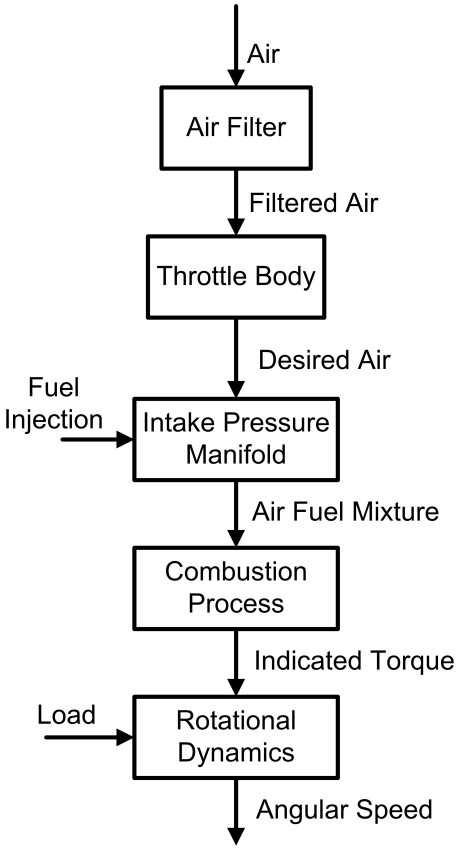

FIGURE 3.2: Block diagram elaborating the component modeling flow.

Newton's Law is applied to calculate the torque and rotational dynamics. The schematic diagram can be seen in Figure 3.1 which shows the air intake system components that are used in engine modeling.

The modeling of each engine component will be performed systematically as elaborated in Figure 3.2. First air filter behavior will be analyzed, then air flow across the throttle body will be defined. Throttle body controls the air flow into the intake manifold. Fuel is added into air to make an air-fuel mixture, intake manifold pressure is obtained. The air-fuel mixture enters the cylinder and becomes a part of combustion process. This process generates indicated torque during expansion of gases against piston in the cylinder. The brake torque is obtained by subtracting the frictional, pumping and load torques from indicated torque. The net torque produces acceleration in the crank shaft. Engine speed is the final output, which is calculated by integrating the acceleration.

3.2 Air Intake System

Among various subsystems of gasoline engine, air intake system hold prime importance. Its prime objective is to deliver proper amount of air accurately and equally to all the cylinders at proper time in the engine cycle. This subsystem comprises of following components to deliver the assigned objective.

- Air filter
- Throttle Valve
- Pressure Manifold

The air, after purifying from dust particles and other unwanted agents through air filter, passes through the butterfly/throttle valve. The effective area of throttle determines air flow through manifold where certain pressure is required to be built up. Each of these components will now be discussed in detail.

3.2.1 Air Filter

Air filter is an important part of the Air intake System, that ensures clean air inflow from the environment. Air filter blocks the dust particle and let the clean air to approach throttle valve. This maximum engine power would be expected to be affected by the intake air restriction imposed by a clogged filter [59]. Effects of air filter on air flow in AIS can be modeled either by pressure drop across it or by measuring its discharge coefficient C_{af}.

3.2.1.1 Pressure Drop Across Air Filter

Air filter can be represented by modeling the pressure drop across it. As a consequence of deposition of pollutants, pressure drop across the air filter increases. This pressure drop is dependent on velocity of air flow [57]. It has linear relationship with filter thickness and exponential relationship with filter porosity [58]. The velocity factor is negligible in our case as the air intake velocity is less than 20-30 cm/s and has no significant effect on pressure drop [57]. Therefore, we can

say that the pressure available after the filter can be expressed by the following expression,

$$P_a = \bar{P}_a - [P_{ini} e^{-\epsilon_{por}\epsilon_{dia}} + c\epsilon_{th}] \qquad Eq\ (3.1)$$

where,

$\bar{P}_a$ is Ambient Pressure in Pascals (Pa).
ϵ_{por} is Filter Porosity in (%).
ϵ_{dia} is Filter pores diameter in millimeters (mm).
ϵ_{th} is Filter fiber thickness in millimeters (mm).
c is proportionality Constant.
P_{ini} is the maximum pressure drop in Pascals (Pa).

The maximum pressure drop (P_{ini}) across the air intake for SI engines is generally 5-7.6 kPa.

The simulations carried out on the above formulated model show typical behavior of engine. Figure 3.3 shows the air filter performance which is dependent on its porosity. Its can be observed that the pressure drop decreases with the increase

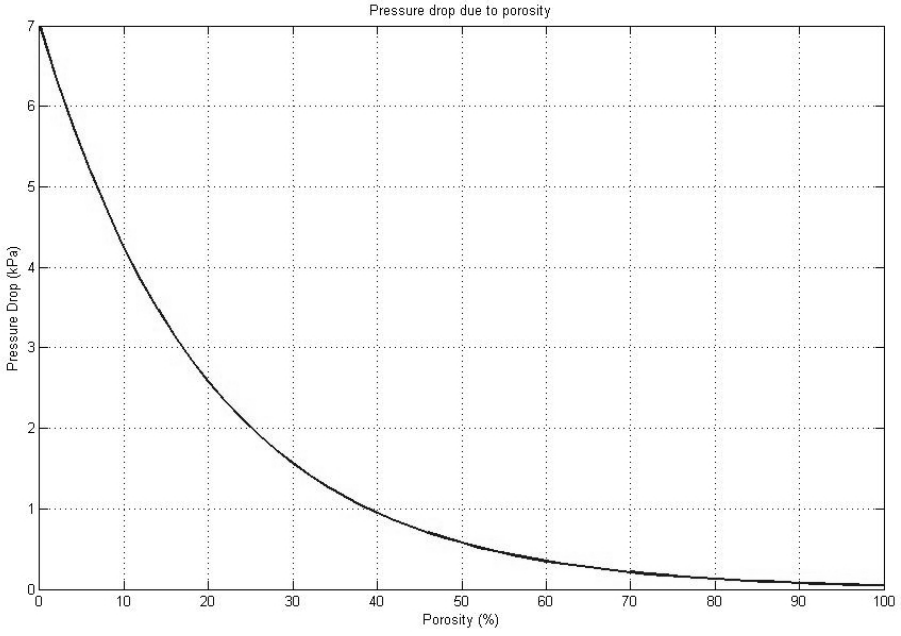

FIGURE 3.3: Decline in pressure due to porosity

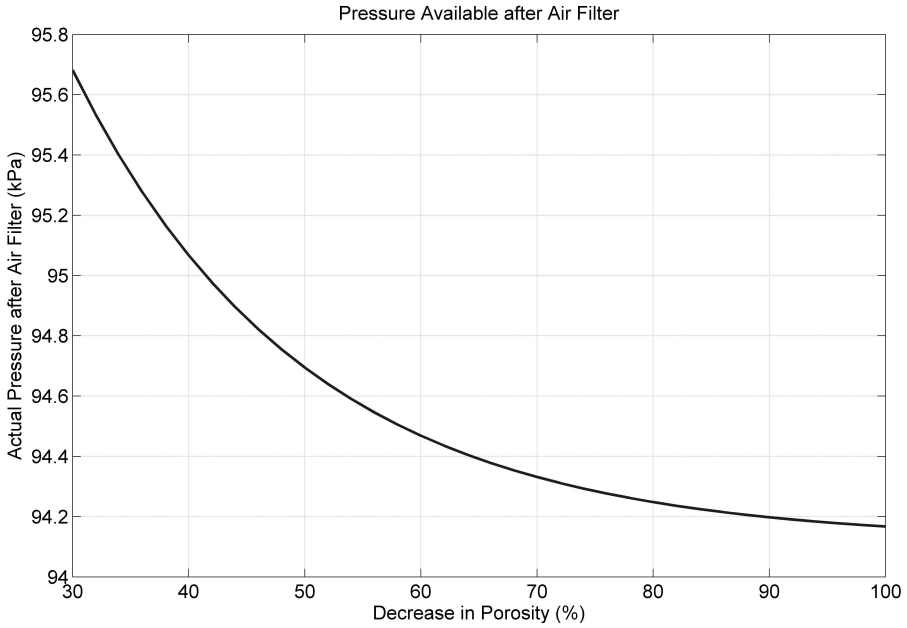

FIGURE 3.4: Pressure available after the air filter

in porosity. As the porosity decreases with time due to pollutants and dust in the environment the pressure available after the air filter is not ambient pressure. The pressure available after the air filter with 90% porosity can be seen in Figure 3.4.

3.2.1.2 Discharge Coefficient of Air Filter C_{af}

Alternately, a realistic modeling of engine can also be carried out by considering the affects of air filter on intake manifold dynamics. It can be visualized in Figure 3.1 that the restrictions in flow can be either due to throttle body or air filter. Generally, throttle discharge coefficient (C_D) is used to measure flow limitations caused by throttle body. Under steady state conditions C_D remains a constant value [76]. Other fluctuations in air flow under steady state operation can be due to air filter behavior. In order to incorporate the effects of air filter health on air flow through inlet manifold, C_{af} has been proposed in this manuscript. Smaller C_{af} means lesser air flow through air intake path components and vice versa. Mathematically, C_{af} can be defined as

$$C_{af} = \frac{\dot{m}_{in_{(actual)}}}{\dot{m}_{in_{(ideal)}}} \qquad Eq\ (3.2)$$

where,

$\dot{m}_{in_{(actual)}}$ Actual Air flow entering the manifold in kg/sec.
$\dot{m}_{in_{(Ideal)}}$ Ideal Air flow entering the manifold in kg/sec.

The actual degraded air flow rate due to air filter is determined experimentally and ideal mass flow rate is given by the flow equation. When the engine is in steady state conditions, none of the flow rates will be equal to zero. Hence this parameter will always be greater than 0 and less than 1.

3.2.2 Throttle Effective Area

Throttle is a butterfly valve mounted at the intake of air path after the air filter. Its function is to control the amount of air flow required by the engine. Car accelerator is connected with throttle plate, the more the accelerator is pressed the more is the throttle angle. The state of the throttle valve is called wide open throttle (WOT) when the pedal is fully pressed, otherwise, it is termed as part open throttle. It is assumed that there is a steady one-dimensional compressible air flow from ambient to past throttle. This flow can be considered as isentropic flow due to its adiabatic and reversible nature in the throttle body. The Effective Throttle Area is the area of throttle pipe through which the air can pass. It is calculated by subtracting the disc (at an angle) area from the total area of throttle pipe. The effective throttle area can be expressed in simple mathematical form as [77]

$$A_E = (1 - cos\alpha)\pi\frac{D^2}{4} \qquad \textit{Eq (3.3)}$$

where,

A_E is the throttle effective area in m^2.
α is the throttle angle in degrees (^{o}).
D is the diameter of inlet pipe in meters (m).

Eq (3.3) is a simple approximation of effective area. However, slightly precise equation can be of the form [78], [79]

$$A_E = (1 - cos(\frac{\alpha + \alpha_{cl}}{\alpha_{cl}}))\pi\frac{D^2}{4} \qquad \textit{Eq (3.4)}$$

where,

α_{cl} is the throttle angle at closed position w.r.t. normal axis.

More accurate and complex equations can be seen in [56], [80].

The selection of expression for calculation of effective area depends upon the level of required accuracy and the type of application. In some cases it may be necessary to use the more exact expression. The accuracy of area plays a pivotal role in the accurate measurement of air flow to an engine cylinder. The throttle angle is either controlled by electric devices or by bowden cable, which gives desired effective area. The engine outputs can be manipulated by the air flow through controlling the effective throttle area.

3.2.3 Manifold Pressure Dynamics

The intake pressure manifold is responsible to deliver air to the engine through pipes to each cylinder. The intake manifold can be visualized in Figure 3.1, it is the part of the air intake system that starts after throttle body and it finally connects to the piston. It is also termed as *receivers/runners*. These receivers are assumed to have fixed volume for which the thermodynamic states (pressure, temperature...) are same all over the volume (lumped parameter approach). The manifold dynamics can be modeled on the basis of filling and emptying of air. The mass and energy of the air serves as inputs and outputs of the receivers. It is assumed that no substantial changes occur in energy and no mass & heat transfers through the walls [61]. Therefore, we can describe such a receiver by

$$\frac{d}{dt}m = \dot{m}_{in} - \dot{m}_{out} \qquad \textit{Eq (3.5)}$$

where,

$\dot{m}_{in}$ is air flow entering the manifold in kg/sec.
$\dot{m}_{out}$ is air flow entering the cylinder/leaving the manifold in kg/sec.

The fluids can be modeled as perfect gases, for which the following expression holds [61], [81],

$$P_m V_m = mRT_m \qquad \textit{Eq (3.6)}$$

where,

V_m is Manifold volume in (m^3).
P_m is Manifold pressure in Pascals (Pa).
T_m is Manifold temperature in Kelvin (K).
R is Specific gas constant in J/kg.K.
m is the mass of the air in kg.

It is assumed that temperature of out-flowing and in-flowing gases from manifold is same i.e. $T_{out} = T_{in}$. Taking the derivatives of *Eq (3.6)* and substituting respectively in *Eq (3.5)* gives us,

$$\frac{d}{dt}P_m = \frac{RT_m}{V_m}[\dot{m}_{in} - \dot{m}_{out}] \qquad \textit{Eq (3.7)}$$

3.2.3.1 Air Flow Across Throttle Body ($\dot{m}_{in}$)

The flow of fluids between two reservoirs is determined by valves. The basis of the fluid flow at the inlet of the manifold i.e.throttle body is one-dimensional compressible flow and is modeled with respect to pressure across the device [80]. Lumped parameter approach is also employed in modeling of fluid in-flow i.e. the temperature and pressure remain homogeneous within flowing body. The intake manifold model can be developed on principles of conservation of mass and energy, ideal gas laws and Dalton‘s law of partial pressure [61], [62], [82].

The modeling of flow through the valve can be done with the following assumptions in view,

- The fluid is compressible
- There is no friction and inertial effects in the flow
- No losses occur in accelerating part up to narrowest point i.e. potential energy isentropically converts into Kinetic Energy
- After the narrowest point, the flow is fully turbulent and it kinetic energy dissipates in thermal energy.

Now the fluid flow across the valve can be determined by *Bernoulli Law* as a function of inlet and outlet pressure.

$$\dot{m}_{in} = A_E \rho_a \sqrt{2C_p(T_a - T_m)} \qquad \textit{Eq (3.8)}$$

where,

C_p is $\frac{\gamma R}{\gamma - 1}$
ρ_a is Air density in kg/m^3.
γ is Ratio of heat capacities.
T_a is ambient temperature in Kelvin.

The flow process in the throttle body is adiabatic process [2]. Based on adiabatic process *Eq (3.8)* can be modified as

$$\dot{m}_{in}(t) = A_E \rho_a \sqrt{2C_p T_a [1 - \frac{P_m}{P_a}]^{\frac{\gamma-1}{\gamma}}} \qquad \textit{Eq (3.9)}$$

The entropy of the fluid flowing across the throttle remains the same, i.e. isentropic process, this phenomena helps us is formulating the air density across the valve as

$$\rho_a = (\frac{P_m}{P_a})^{\frac{1}{\gamma}} \frac{P_a}{RT_a} \qquad \textit{Eq (3.10)}$$

Substituting *Eq (3.10)* in *Eq (3.9)* and simplifying,

$$\dot{m}_{in}(t) = A_E P_a \sqrt{\frac{2\gamma}{((\gamma-1)RT_a)}} \sqrt{(\frac{P_m}{P_a})^{\frac{2}{\gamma}} - (\frac{P_m}{P_a})^{\frac{\gamma+1}{\gamma}}} \qquad \textit{Eq (3.11)}$$

As the fluid passes by narrowest point i.e. choked flow, the above equation can be modified as [61], [62],

$$\dot{m}_{in}(t) = A_E P_a \sqrt{\frac{1}{(RT_a)}} \sqrt{\gamma [\frac{2}{\gamma+1}]^{\frac{\gamma+1}{\gamma-1}}} \qquad \textit{Eq (3.12)}$$

Analytically, the choked flow can be determined by critical pressure if it is greater then manifold pressure i.e. $P_m < P_{cr}$, where

$$P_{cr} = [\frac{2}{\gamma+1}]^{\frac{\gamma}{\gamma-1}} P_a \qquad \textit{Eq (3.13)}$$

As the piecewise switching functions in *Eq (3.11)* and *Eq (3.12)* are unsmooth and the existence of derivatives of such functions is not guaranteed, therefore these functions are not suitable for control, estimation and diagnosis purpose, hence we can replace these functions by a single non-switching nonlinear function as follows [79].

$$\dot{m}_{in} = A_E P_a \sqrt{\frac{1}{(RT_a)}} \sqrt{\gamma (\frac{2}{\gamma+1})^{\frac{\gamma+1}{\gamma-1}} (1 - exp(\frac{P_m}{P_a} - 1))} \qquad \textit{Eq (3.14)}$$

3.2.3.1.1 Throttle Discharge Coefficient C_D: The inflow of air across the throttle body of an automotive engine is represented by the gas equation of isentropically compressible air mass flow through an orifice under ideal conditions given in *Eq (3.14)*. In the real world, ideal conditions hardly exist; therefore, the modeled equation is unable to correctly predict the air mass flow across the throttle valve. To accommodate the assumptions and inaccuracies, a coefficient of discharge is introduced in gas equation. This correction factor is defined as a ratio of actual to the ideal flow rates of air mass. Actual mass flow rate is determined experimentally and ideal mass flow rate is given by the flow equation. When the engine is running, any one of the flow rates would not be equal to zero; hence, C_D

would be well defined within the operating range of engine as,

$$C_D = \frac{\dot{m}_{in_{(actual)}}}{\dot{m}_{in_{(ideal)}}}$$

In steady-state conditions discharge coefficient is nearly a constant number. But at varying input and engine load, it is neither a constant parameter nor a linear variation [83]. Therefore, a number of approaches can be found in literature to analyze the effect of C_D. The coefficient of discharge has been taken as a constant parameter by most researchers in MVEM like in [79], [84], [82]. Other community working on engine has taken discharge coefficient as a varying parameter and developed various expressions that require other engine parameters as input like manifold pressure, throttle valve area, air temperature, engine speed etc [83], [63]. Several authors have attempted to estimate C_D from sliding mode observers [47], [52].

So, the realistic throttle mass flow $\dot{m}_{in}$ can be represented as

$$\dot{m}_{in} = C_D A_E P_a \sqrt{\frac{1}{(RT_a)}} \sqrt{\gamma (\frac{2}{\gamma+1})^{\frac{\gamma+1}{\gamma-1}} (1 - exp(\frac{P_m}{P_a} - 1))} \qquad \textit{Eq (3.15)}$$

As discussed in Section 3.2.1, the air filter effects on air flow in manifold can be modeled by incorporating air filter discharge coefficient C_{af}. Thus, *Eq (3.15)* can be further modified to represent real air flow in manifold as,

$$\dot{m}_{in} = C_D C_{af} A_E P_a \sqrt{\frac{1}{(RT_a)}} \sqrt{\gamma (\frac{2}{\gamma+1})^{\frac{\gamma+1}{\gamma-1}} (1 - exp(\frac{P_m}{P_a} - 1))} \qquad \textit{Eq (3.16)}$$

3.2.3.2 Idle Air Control

Idle Air Control is a type of alternate route of the throttle plate. In the alternate route, there is a valve which controls the amount of air flow into the intake manifold during idle operation. The throttle is typically closed during idle operation [2], [62]. Idle air control is also modeled with *Eq (3.16)* in a manner similar to the throttle body. The effective area for estimation of idle air is equal to $5^o - 10^o$

opening of the throttle plate. For the particular engine is use, this angle in 9.8^o

$$\dot{m}_{in_{idle}} = C_D C_{af} A_E(\alpha = 9.8^o) P_a \sqrt{\frac{1}{(RT_a)}} \sqrt{\gamma(\frac{2}{\gamma+1})^{\frac{\gamma+1}{\gamma-1}}(1 - exp(\frac{P_m}{\bar{P}_a} - 1))} \quad \textit{Eq (3.17)}$$

3.2.3.3 Vacuum Leaks

Vacuum Leaks of intake manifold are also considered. The size of leak depends on the condition of intake manifold. These leaks occur repeatedly during intake stroke due to vacuum in the intake manifold. The vacuum leaks are also modeled with *Eq (3.16)* as a repeated sequence with a leak size of two percent of the total throttle area [62].

$$\dot{m}_{in_{leaks}} = 0.02 C_D C_{af} A_E P_a \sqrt{\frac{1}{(RT_a)}} \sqrt{\gamma(\frac{2}{\gamma+1})^{\frac{\gamma+1}{\gamma-1}}(1 - exp(\frac{P_m}{\bar{P}_a} - 1))} \quad \textit{Eq (3.18)}$$

3.2.3.4 Air Flow Across Engine ($\dot{m}_{out}$)

The air mass induced into the cylinder is due to the reciprocating motion of engine. The intake stroke creates negative pressure and sucks the air inside the piston. The exhaust stroke exhales the combustion mixture. This motion resembles reciprocating pumps or compressors and it can be modeled with the help of speed density equation [61]. A typical formulation for such four stroke engine is given by

$$\dot{m}_{out} = \frac{V_d \omega_e}{4\pi} \rho_m \quad \textit{Eq (3.19)}$$

where,

$\dot{m}_{out}$ is air flow entering the cylinder/leaving the Manifold in kg/sec.
V_d is displaced volume (m^3).
ω_e is engine Speed in rad/sec.
ρ_m is the density air in manifold in kg/m^3.

and according to ideal gas law,

$$\rho_m = \frac{P_m}{RT_m} \qquad \textit{Eq (3.20)}$$

The displacement volume is a fraction of manifold volume and can be expressed as

$$V_d = kV_m \qquad \textit{Eq (3.21)}$$

Thus, an ideal air flow leaving the manifold is given by *Eq (3.19)*. The realistic air flow leaving manifold can be modeled by incorporating volumetric efficiency (η_{vol}) of engine.

Volumetric Efficiency (η_{vol})

One of the most important process that governs power and performance of engine is getting the optimum amount of air into the cylinder during each cycle. More air means more fuel can be converted to output power. Ideally, a mass of air equal to the density of atmospheric air times the displacement volume of the cylinder should be ingested in each cycle. However, because of the short cycle time available and the flow restrictions caused by air filter, intake manifold and intake valves, less than ideal amount of air enters the cylinder. η_{vol} is the measurement of how close the actual volumetric flow rate is to the theoretical volumetric flow rate. Mathematically, it can be defined as [2],

$$\eta_{vol} = \frac{\dot{m}_{out_{(actual)}}}{\dot{m}_{out_{(ideal)}}} \qquad \textit{Eq (3.22)}$$

where,

$\dot{m}_{out_{(actual)}}$ is the actual air mass flow leaving the manifold.
$\dot{m}_{out_{(ideal)}}$ is the ideal air mass flow leaving the manifold.

Under normal operating conditions none of the air flows will be zero. Actual air mass flow rate is determined experimentally and ideal air mass flow rate is given by the speed density equation. Typically, η_{vol} for an engine at wide open throttle remains steady state but it alters with the throttle body movements [2].

The change in η_{vol} effects the pumping efficiency of the engine thus motivating the need for its estimation. In the public literature various attempts have been employed to measure the volumetric efficiency of the engine. A number of authors have considered volumetric efficiency as constant term [47], [62], [56], thus ignoring the dynamics induced by η_{vol} while manipulating the throttle angle. In [2], a mathematical relationship based on displaced volume and air density for its estimation is suggested. Recently, Muller [85] attempted to explain η_{vol} as a function of inlet and exhaust manifold pressure. The author in [79] calculated the volumetric efficiency through modeling of the valve opening and closing. Some researchers [86] utilized parametric and non parametric techniques to measure the η_{vol} through available sensors data. [80] suggested mathematical relation of η_{vol} for its transient and steady state behavior that depends on engine speed, air inflow, and various other engine parameters.

Thus, the real air mass flow entering the engine cylinder or leaving the intake manifold can finally be given as

$$\dot{m}_{out} = \frac{V_d \omega_e}{4\pi} \rho_m \eta_{vol} \qquad \textit{Eq (3.23)}$$

3.2.3.5 Complete Manifold Pressure Dynamics

Finally, by replacing *Eq (3.23)* and *Eq (3.16)* in *Eq (3.5)*, we get manifold pressure dynamics as

$$\dot{P}_m = \frac{RT_m}{V_m}(C_D C_{af} A_E P_a \sqrt{\frac{\gamma}{RT_a}(\frac{2}{\gamma+1})^{\frac{\gamma+1}{\gamma-1}}}(1-exp(\frac{P_m}{P_a}-1))-(\frac{kV_m\omega_e}{4\pi})(\frac{P_m}{RT_m}\eta_{vol})) \qquad \textit{Eq (3.24)}$$

3.3 Torque Generation System

The primary objective of an automotive engine is to produce mechanical power. Its speed determines the amount of torque to be produced. The torque produced depends on mixture and its composition in the cylinder. The mean value engine

torque can be taken as nonlinear function of many variables i.e. fuel mass, air/fuel ratio, engine speed, ignition or injection timing etc.

The phenomenon of torque generation from pressure has been approximated in different way by various authors. Like in [61], the engine torque simplification has been made on *Willans Approximation*, which states that simple relationship between mean fuel pressure and mean effective pressure approximates real engine behavior. Where mean fuel pressure is brake mean effective pressure, that an engine with an 100% efficiency (perfect conversion of fuel thermal energy into mechanical energy) would produce with fuel mass burnt per engine cycle. Brake mean effective pressure is defined as the pressure that has to act on piston during one full expansion stroke to produces the same amount of work as the real engine does in two engine revolutions. In [79], the authors utilized the same concept of torque generation i.e. the total pressure developed as a result of thermal energy released by the fuel minus the pressure generated due to frictional and other losses. [82] emphasized on components engine dynamics other than torque generation. [87] suggested torque generation as function of air/fuel mixture, mass of EGR, spark advance and engine speed. Similarly, [88] discussed the engine dynamics by indicated torque and frictional torque.

Kazmi and Trimizi in [77] have formulated the torque generation model based on Otto cycle. The Otto cycle explains the thermodynamics taking place inside four stroke engine using Pressure Volume (PV) diagram as shown in Figure 3.5. The mean effective pressure has been calculated using Otto cycle derivations and later on, mean effective pressure will utilized for the calculation of generated torque. The generated torque will be further exploited to calculate the angular engine speed.

In mean value engine modeling, angular speed is simply calculated from the torque produced as a consequence of pressure produced in engine cylinders. One can define the relation of torque and engine speed as

$$T_b = J_e \frac{d}{dt}\omega_e \qquad \textit{Eq (3.25)}$$

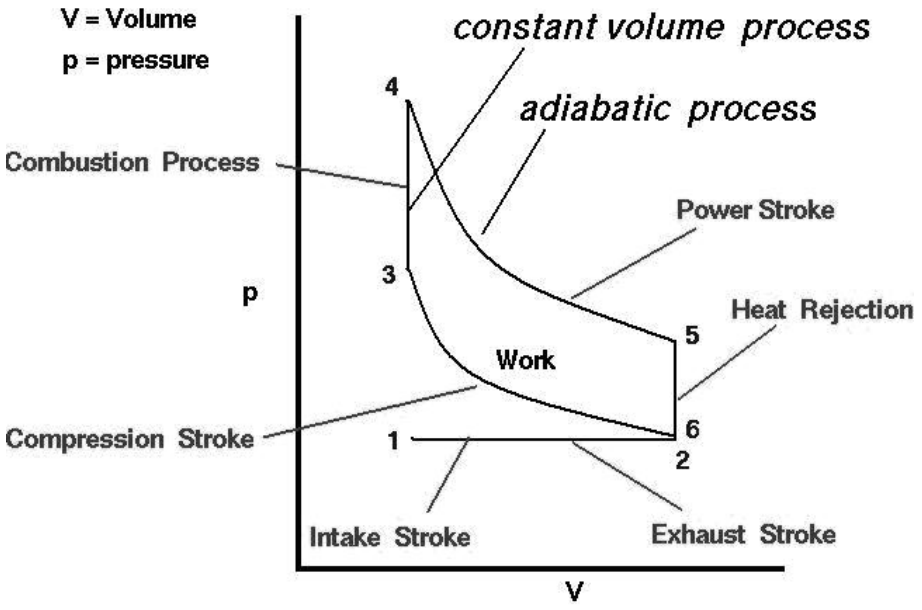

FIGURE 3.5: Pressure Volume diagram of Otto Cycle

where,

$$T_b = T_i - T_f - T_p - T_l \qquad Eq\ (3.26)$$

and,

T_b is Brake torque in Nm

T_i is Indicated torque in Nm

T_f is Frictional torque in Nm

T_p is Pumping torque in Nm

T_l is Load torque in Nm

J_e is Engine inertia in kgm^2

ω_e is Engine angular speed in rad/sec

The angular velocity in rad/sec can be converted in revolution per seconds (RPM) according to following relation.

$$N_e = \omega_e \frac{60}{2\pi} \qquad Eq\ (3.27)$$

where,

N_e = Engine angular speed in RPM.

Now each of the torque contributing in engine angular speed generation will be discussed individually.

3.3.1 Indicated Torque (T_i)

The energy produced inside the combustion chamber due to air-fuel mixture burning during power stroke results in indicated torque. The resultant torque produced exhibits conversion of chemical energy into mechanical energy without any losses. It is a function of mean effective pressure and can be defined as

$$T_i = \frac{V_d}{4\pi}\eta_{th}.mep \qquad \textit{Eq (3.28)}$$

where,

$$\begin{aligned} mep &= \frac{Work/cycle}{SweptVolume} \\ Work/Cycle &= \frac{p_3V_3 - p_6V_6}{\gamma - 1} - \frac{p_5V_5 - p_4V_4}{\gamma - 1} \\ SweptVolume &= V_c c_r \\ \eta_{th} &= [1 - (\frac{V_c}{V_c + V_d})^{\gamma - 1}] \end{aligned}$$

and,

η_{th} is Thermal efficiency

mep is Mean effective pressure in kPa

V_c is Compressed volume in m^3

c_r is Compression ratio

The subscripts of p and V refer to PV diagram shown in Figure 3.5.

Finally, indicated torque is explained as

$$T_i = B_1 \eta_c P_m \qquad \textit{Eq (3.29)}$$

where

$B_1 = \frac{V_d Q \eta_{th} (1-(c_r^{\gamma-1})^{-1})(c_r^{2-\gamma})((c_r^{\gamma-1})-1)}{4\pi AFR(\gamma-1)(c_r-1)c_v T_m}$

and

η_c is Combustion efficiency.

Q is Heat value of fuel in J/kg.

AFR is Air to fuel ratio.

c_v is Specific heat at constant volume in J/m^3K.

T_m is Manifold temperature in Kelvin.

The detailed derivation of the above mention expression can be found in [2].

3.3.1.1 Combustion Efficiency (η_c)

Combustion efficiency plays an important in conversion of chemical energy stored in fuel to mechanical energy. The combustion process time is very brief and not all the fuel molecules may find an oxygen molecule to combine. Similarly, 100% combustion will not occur if the combustion chamber temperature is not favorable for reaction. These reasons may cause incomplete combustion of fuel. Consequently, a small amount of fuel remains unburnt and exits with the exhaust flow [2]. This results in inefficient fuel performance and air pollution if three way catalyst is not employed. The amount of fuel burnt can be explained by *Combustion efficiency*. For SI engines, air and fuel mixtures richer than stoichiometric ratio prevents complete combustion of fuel carbon and hydrogen due to the lack of required oxygen. The combustion efficiency steadily decreases as the mixture becomes richer, provided the engine combustion process remains stable. Mathematically, combustion efficiency can be defined by the ratio of net chemical energy (H_{net}) produced during chemical reaction to the fuel energy (H_{fuel}) supplied in the combustion

chamber [2].

$$\eta_c = \frac{H_{net}}{H_{fuel}}$$

Typically, combustion efficiency is modeled as a function of AFR [2], [89]. Most of the time it is taken as constant value of 0.95-0.98.

3.3.2 Frictional Torque

Friction torque is mainly a function of engine speed, load and engine oil temperature [90]. Friction torque losses may also change with time due to aging of the engine components. This behavior may lead to change engine speed function in an unpredictable fashion. In public literature, various attempts to model SI engine friction are available. The modeling of frictional torque can be carried out as a function of engine speed. Stotsky in [90] delivered a solution to estimate frictional torque through a look-up table. The look-up table defines engine friction torque as a function of engine speed and indicated torque. An empirical function based on engine speed has been developed in [2]. The empirical expression derived in [2] is

$$T_f = 11.72 + 5.69 \times 10^{-5}\omega_e + 2.33 \times 10^{-14}\omega_e^2 \qquad \textit{Eq (3.30)}$$

Similarly, in [1], [79] an empirical relation has been derived for engine dynamics by investigating friction induced by each engine component. These relations require engine characteristics like bore diameter, bearing diameter & width, valve lift, stroke length, oil viscosity etc. The mechanical friction losses of the rubbing engine components can be divided into four component groups:

- Crankshaft: Main bearings, front and rear main bearing oil seals.
- Reciprocating: Piston skirts, piston rings, connecting rod bearings.
- Valve train: Camshafts, cam followers and valve actuation mechanisms.
- Auxiliary Components: Components which are running along with the engine, inducing mechanical friction to the engine.

For each of the component groups, an expression for the losses, expressed in pressures, are drawn up in [1]. The frictional mean effective pressure *fmep* can be taken as

$$fmep = cfmep + rfmep + vfmep + afmep \qquad Eq\ (3.31)$$

where,

cfmep is Crankshaft friction.
rfmep is Reciprocating friction.
vfmep is Valve train friction.
afmep is Auxiliary friction.

Finally, after incorporating the effects of the above mentioned frictional elements formulated in [1], [79], the mathematical form of the frictional mean effective pressure comes out to be

$$T_f = 5.21\omega_e^{-1} + 2.00 + 0.46\omega_e^{.5} + 0.09\omega_e + 2.33\times10^{-14}\omega_e^2 - 3.30\times10^{-6}\omega_e^3 \quad Eq\ (3.32)$$

Remark 3.1. The empirical constants in *Eq (3.30)* and *Eq (3.32)* were identified off-line using least squares methods for the engine used in experimentation. The input to the empirical formula is engine angular speed.

3.3.2.1 Drawbacks of current techniques

It can be observed that current techniques statically model friction torque through engine speed & indicated torque. However, engine modeling reveals that T_f is also dependent on P_m (T_i and T_p calculation requires P_m) besides T_l & ω_e. Moreover, these methodologies require a list of engine parameters like bore diameter, oil viscosity etc, that are not readily available to solve respective expressions.

3.3.3 Pumping Torque

The torque required by engine to perform pumping action i.e. intake and exhaust of gas mixtures, is termed as pumping torque. Mathematically, it is developed from pumping mean effective pressure, that is the sum of the intake and exhaust

pressures. Based on this phenomena the expression for pumping torque comes out to be

$$T_p = \frac{V_d}{4\pi}(P_a - P_m) \qquad \textit{Eq (3.33)}$$

The engine speed can now be obtained from *Eq (3.25)* by employing T_i, T_f and T_p. T_l is the torque contributed by engine components like flywheel, pistons, crankshaft etc. It can be taken constant as 30 $N.m$ under steady state conditions or it can be estimated as in [47], [52] and [91].

3.4 Complete Dynamics of Gasoline Engine

The pressure and angular speed dynamics based two state gasoline engine model can be represented by the states and input given as follows;

$$\begin{bmatrix} P_m \\ \omega_e \end{bmatrix} = \begin{bmatrix} ManifoldPressure \\ EngineAngularSpeed \end{bmatrix} \qquad \textit{Eq (3.34)}$$

$$\alpha = ThrottleAngle \qquad \textit{Eq (3.35)}$$

Finally, the gasoline engine model can be explained as follows;

$$\begin{aligned} \dot{P}_m &= A_1 f(P_m) - A_2 P_m \omega_e \eta_{vol} \\ \dot{\omega}_e &= \frac{1}{J_e}(B_1 \eta_c P_m - T_f - T_p - T_l) \end{aligned} \qquad \textit{Eq (3.36)}$$

where,

$$\begin{aligned} A_1 &= \frac{RT_m}{V_m} A_E(\alpha) P_a C_D C_{af} \gamma_c \\ A_2 &= \frac{V_d}{V_m 4\pi} \\ A_E(\alpha) &= \pi \frac{D^2}{4}.(1 - cos(\frac{\alpha + \alpha_{cl}}{\alpha_{cl}})) \\ \gamma_c &= \sqrt{\frac{1}{(R.T_a)}}.\sqrt{\gamma(\frac{2}{\gamma+1})^{\frac{\gamma+1}{\gamma-1}}} \\ f(P_m) &= 1 - e^{(\frac{P_m}{P_a} - 1)} \end{aligned}$$

$$B_1 = \frac{V_d Q \eta_{th}(1-(c_r^{\gamma-1})^{-1})(c_r^{2-\gamma})((c_r^{\gamma-1})-1)}{4\pi AFR(\gamma-1)(c_r-1)c_v T_m}$$

$$T_p = \frac{V_d}{4\pi}(P_a - P_m)$$

$$T_f = 11.72 + 5.69 \times 10^{-5}\omega_e + 2.33 \times 10^{-14}\omega_e^2$$

TABLE 3.1: MVEM parameters description, nominal values and units

Symbol	Description	Values/Units
P_a	Ambient pressure	101325Pa
T_m	Manifold temperature	325K
T_a	Ambient temperature	298K
α_{cl}	Throttle angle at closed position	9.8°
D	Inlet diameter	0.054m
R	Specific gas constant	287J/kg.K
C_D	Throttle discharge coefficient	0.8
γ	Ratio of heat capacities	1.4
V_d	Displaced volume	$0.001294m^3$
V_m	Manifold volume	$0.001127m^3$
η_{vol}	Volumetric efficiency	0.7
η_c	Combustion efficiency	0.9
AFR	Air to fuel ratio	14.7
J_e	Engine inertia	$0.25kg.m^2$
Q	Heat value of fuel	44kJ/Kg
c_v	Heat capacity at specific volume	$717J/(m^3K)$
c_r	Compression ratio	10

3.5 Simulation Results

In the first phase, the mean value engine model formulated in *Eq (3.36)* will be analyzed through simulations. The values of the MVEM parameters used for simulation are given in Table 3.1. The engine model has the input as throttle angle and the initial load. These two inputs have been manipulated to observe the engine behavior. The outputs of interest are engine angular speed and manifold pressure. Figure 3.6 shows the response with constant load and variable throttle angle. It can be observed that by increasing the throttle angle the engine angular speed increases and the manifold pressure settles at lower values after slight transients die out.

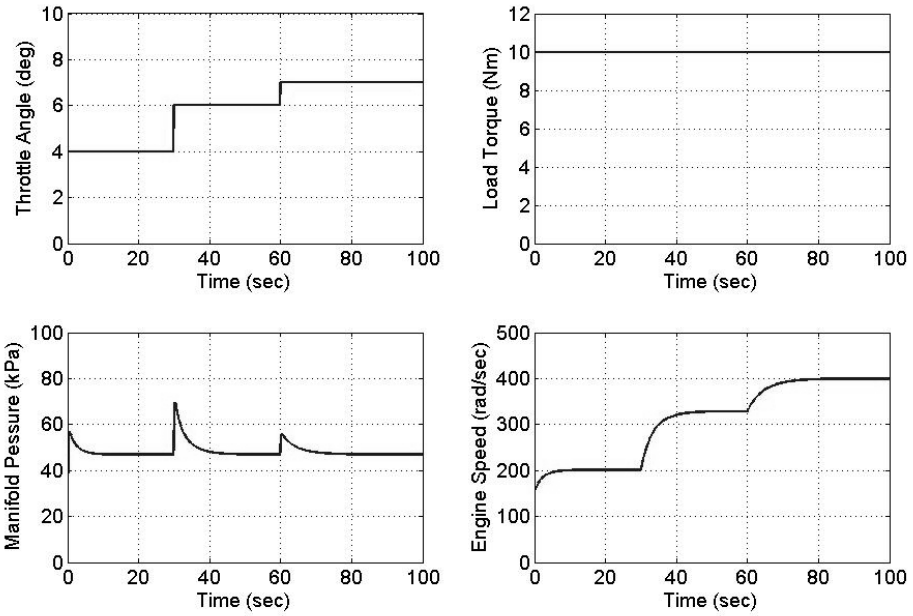

FIGURE 3.6: Engine response with variable throttle angle and constant load

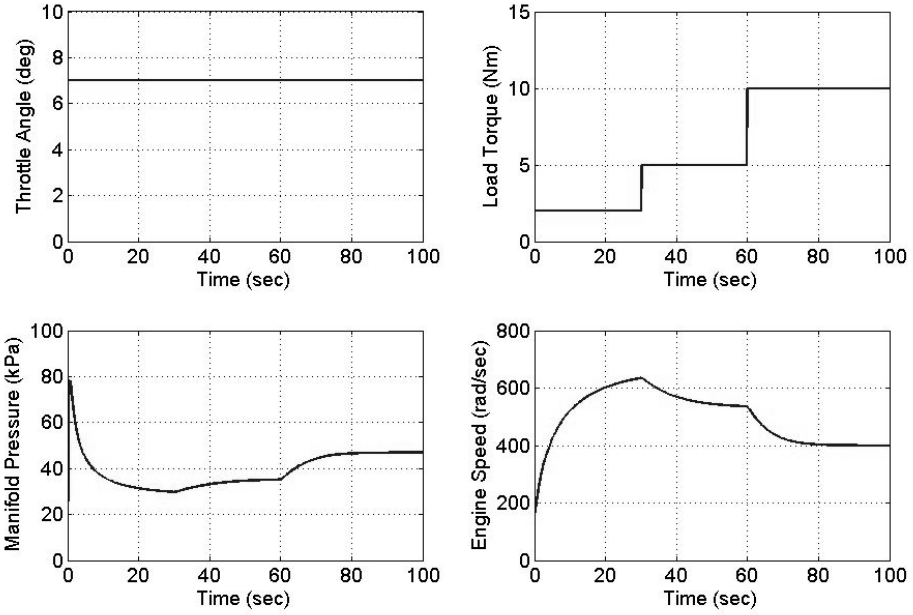

FIGURE 3.7: Engine response with variable load and constant throttle angle

Similarly, in Figure 3.7 the throttle angle is kept constant and load is varied with time. One can observe that due to increase in load engine angular speed declines and manifold pressure increases. These simulation results apparently validate the engine behavior. Further validation will be carried on the actual of 1.3L production vehicle engine.

3.6 MVEM Validation

The rigorous validation of model in *Eq (3.36)* is carried out against a 1.3L gasoline engine of production vehicle. The details regarding experimental setup are discussed in Chapter 5. The inputs and outputs of the engine were accessed by OBD-II data scanning and logging software. The validation procedure involved manipulation of throttle paddle several times. Extra load on engine was induced at 300 sec as vehicle air conditioner is turned on. For the validation purpose, the inputs to the actual engine logged by OBD-II scanner/logger were provided to MVEM in *Eq (3.36)* and the logged outputs were compared with MVEM outputs. The response shown in Figure 3.8 depicts that 1.3L engine and model in *Eq (3.36)* exhibit almost the same response with some acceptable discrepancies due to modeling errors. These errors can be explained on the grounds of structural uncertainties like air by-pass valve. Another factor may include un-modeled couplings between manifold pressure and rotational speed dynamics. Similarly, temperature dynamics are assumed to be constant. Moreover, the engine parameters during simulation were taken constant with nominal values found in literature [2].

However, as MVEM remains accurate in steady state conditions with uniform temperature, the same conditions were ensured during second validation process. The operating temperature of the engine was around 89°C. The throttle valve was kept constant after manipulating it at 110, 170 & 230 seconds and steady state conditions were ensured. The off-line identified parameters of MVEM were used to obtain the desired results. The response of MVEM and 1.3L engine to the same inputs is shown in Figure 3.9. It can be observed that the MVEM in *Eq (3.24)* and *Eq (3.25)* exhibits same response as actual engine in steady state conditions. The error of pressure and angular speed dynamics remain within 5% and 8% respectively. Thus, the verified model can be used for estimation and fault diagnosis scheme.

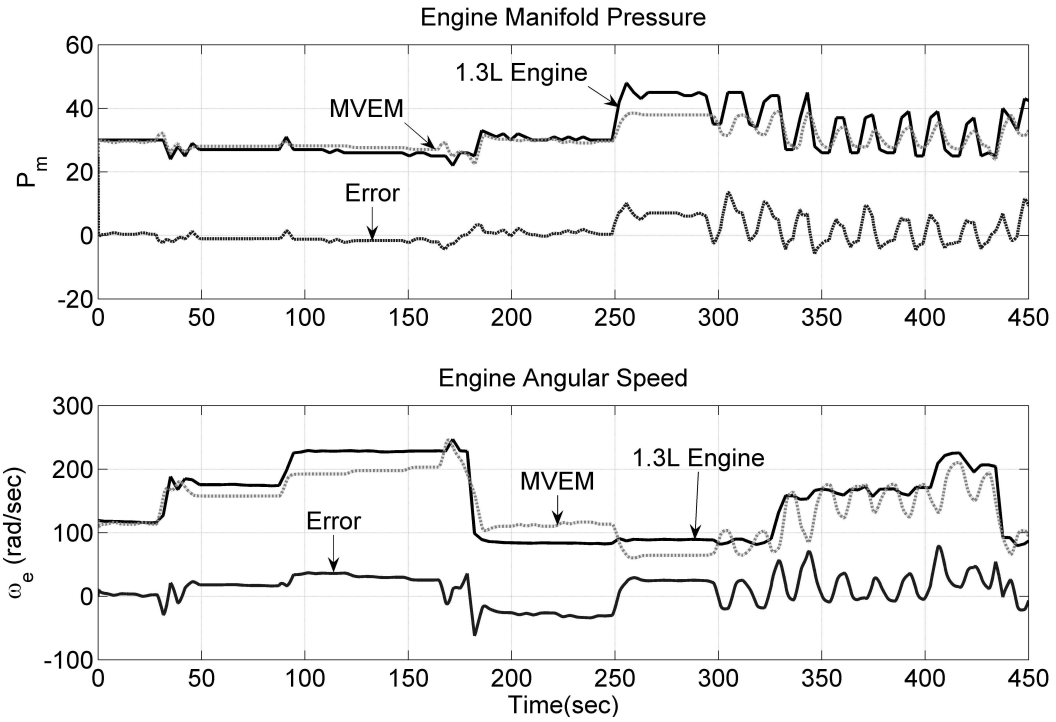

FIGURE 3.8: Rigorous Comparison of the MVEM *Eq (3.36)* and 1.3L commercial engine

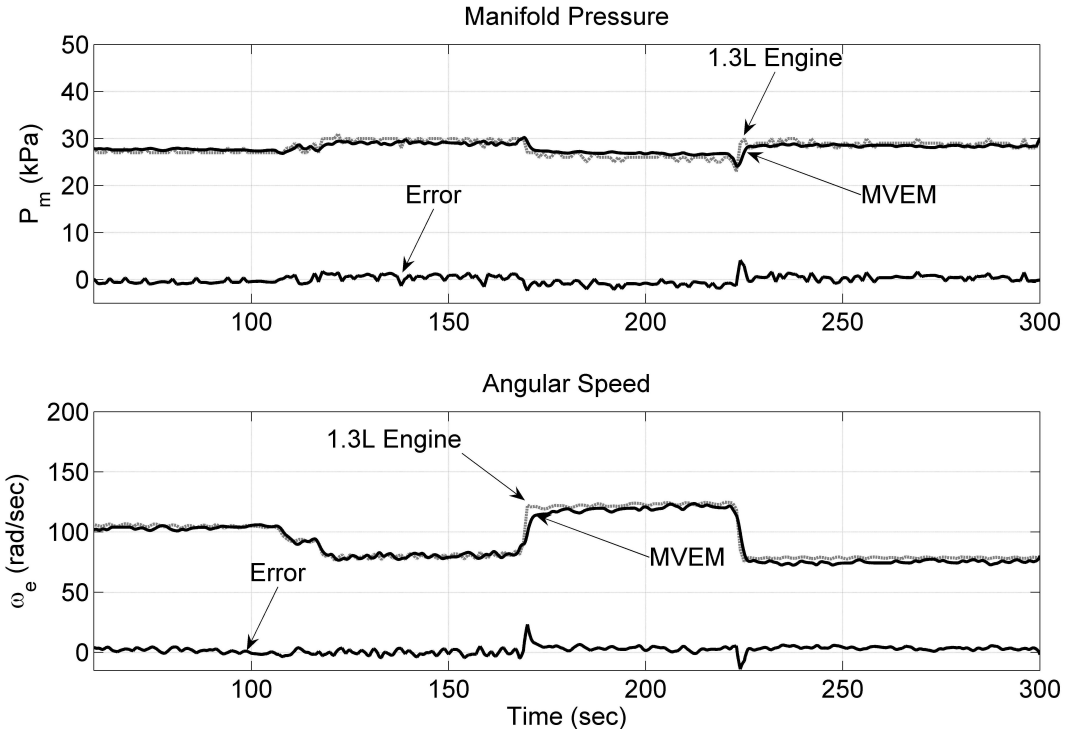

FIGURE 3.9: Validation of MVEM in *Eq (3.36)* with 1.3L production vehicle engine in steady state comparison

3.7 Conclusion

A two state mean value engine model has been formulated in this chapter. Realistic modeling of air intake path is practiced by considering the contributing effects air filter, throttle body and frictional torque. The intake manifold pressure dynamics and angular speed dynamics in *Eq (3.36)* have been successfully validation against a 1300cc production vehicle engine. This validated model can now be utilized in estimation of un-measurable parameters like C_D, C_{af}, η_{vol}, η_c and T_f, as these parameters vary for different operation conditions. Furthermore, these critical parameters can be analyzed for the health diagnosis various components in air intake path.

Chapter 4

GASOLINE ENGINE PARAMETER ESTIMATION

This chapter deals with the estimation of gasoline engine parameters based on the model given in the preceding chapter. Among various engine parameters five critical parameters have been chosen for estimation. These parameters include: Frictional Torque, Combustion Efficiency, Volumetric Efficiency, Throttle Body Discharge Coefficient and Air Filter Discharge Coefficient. These parameters provide credible knowledge about engine performance and can be efficiently used for health monitoring of gasoline engine and its various components. Along-with the estimation scheme, a methodology for the development of virtual sensors for pressure and angular speed is also discussed. These objectives have been achieved by employing a robust Second Order Sliding Mode (SOSM) Observer based estimation scheme. The super twisting based SOSM Observer operates on a highly nonlinear two state pressure and angular speed dynamics. A successful implementation of the estimation scheme is conducted on a production vehicle engine. Initially, the parameters have been estimated under steady state and healthy operating conditions. Later on, these values can be compared with faulty operating values to generate residuals for proficient engine condition monitoring.

4.1 Benefits of Parameter Estimation

There are certain system parameters that directly correspond to system health status. Most of the times, these parameters are measurable by installing sensors to sense the respective phenomena. However, in some cases it is almost impossible to use a sensor to assess particular parameter for health diagnosis. In case of control and diagnosis scheme development, precise values of un-measurable parameters are required to develop an accurate mathematical model of a dynamical system. Sometimes, it is required to create redundancy for the installed sensor in order to

obey strict safety bylaws. These problems can be resolved by employing state-of-art estimation techniques. The significant benefits of parameter estimation are:

- Efficient health monitoring can be done by the estimation of un-measurable critical parameter [74].
- Instead of installing another sensor, virtual sensors can be developed to sense a phenomena in parallel to real sensors (A cheaper solution). This reduces dependance on a single sensor and can also help in sensor health monitoring [92].
- As model based fault diagnosis techniques heavily depends on precise dynamical models, this model precision can be achieved by estimating unknown parameters [47].

Keeping in view the various advantages of parameter estimation, there are certain critical parameters in gasoline engine whose estimation can benefit us in number of ways. Among various engine parameters, following parameters are selected based on their numerous advantages, as discussed below.

4.1.1 Frictional Torque

Frictional torque has been discussed in detail in Section 3.3.2. It plays an important role in the torque based angular speed model accuracy. The available techniques identify frictional torque based on number of readily unavailable parameters like bore diameter, bearing diameter & width, valve lift, stroke length and oil viscosity. This motivates the need of estimating frictional torque from readily available information. It can be seen in *Eq (3.36)* that we can easily identify frictional torque from the pressure sensor and angular speed measurements. To improve fuel efficiency, frictional torque must be reduced if it is monitored properly. Honda used Molybdenum Disulfide coated pistons, ion plating piston rings, piston oil jets and plateau honing cylindrical walls in Intelligent Variable Valve Timing and Electronic Control (i-VTEC) engine to reduce 10% frictional torque as compared to conventional engines [93]. This was only possible due to precise measurement of frictional torque.

4.1.2 Combustion Efficiency

Combustion efficiency (η_c) plays an important role in improving engine performance. Typically, combustion efficiency is modeled as a function of air to fuel ratio (AFR) [2], [89], but availability of AFR remains a question unless a lambda sensor is installed for its measurement. A cheaper solution of judging combustion efficiency can be its estimation by manifold pressure and engine rotational speed (These sensors are mandatory in every OBD-II compliant vehicle engine.). This will also facilitate in monitoring AFR indirectly. Even in modern cars with lambda sensors installed in the exhaust manifold to observe AFR, the estimated combustion efficiency can serve as second indicator for AFR cross-check. Moreover, the computation of combustion efficiency can be helpful in health monitoring of lambda sensors. Various smart concepts like spark advance, dual ignition cylinders, intelligent variable valve control system to control valve timing at variable engine speeds are used to enhance combustion efficiency. This task can only be accomplished with the help of precise estimation of η_c.

4.1.3 Volumetric Efficiency

Volumetric efficiency (η_{vol}) is discussed in detail in Section 3.2.3.4. This parameter explains the actual pumping efficiency of engine. Volumetric efficiency provides an estimate of air being sucked inside from intake manifold and pumped into exhaust manifold. It depends on various engine design parameters such as piston size, piston stroke, and number of cylinders and is strongly influenced by camshaft design. An apparent advantage of estimating volumetric efficiency can be optimization of these engine components for desired performance. Another benefit of estimating η_{vol} is, it will let us know whether there is any leakage in intake manifold or any blockade in air intake path. The leakage will result in low values of η_{vol} and blockade will result in higher values of pumping efficiency. Thus reliable engine fault diagnosis can be ensured.

4.1.4 Throttle Body Discharge Coefficient

Butterfly valve/throttle valve is integral part of air intake path of gasoline engine. The actual air flow across can be modeled by estimating throttle body discharge coefficient (C_D). The estimation of throttle discharge coefficient can be helpful in improving throttle/butterfly valve. Another benefit of estimating C_D is health monitoring of throttle valve. The decrease in values of C_D will result in degraded throttle valve performance. In conventional vehicles, throttle is normally operated by bowden cable, however in modern electronic vehicles drive by wire throttle mechanism is introduced. The proper functioning of both manipulating mechanisms can be ensured if we can precisely estimate C_D.

4.1.5 Air Filter Discharge Coefficient

Another obstruction in air flow but useful component in intake path, is air filter. The values of air filter discharge coefficient (C_{af}) is the measured air amount flowing across the air filter. This coefficient can be useful in improving air filter quality and its assembly designs. On the other hand, although air filter is manufactured from delicate fibreous material and is well protected inside a dust proof body but it still remains exposed to hazards of polluted environment. The air flow across air filter decreases with the increase of clogging due to air pollutants. This clogging phenomenon of air filter can be efficiently monitored by estimating C_{af}.

4.1.6 Virtual Sensors

Virtual sensors measure a phenomena through another inter-related process, thus providing a redundancy in measurements. The sensors under consideration are: Manifold Air Pressure (MAP) Sensor and Crankshaft Sensor. The estimation of pressure ($\bar{P}_m$) from angular speed and rotational speed ($\bar{\omega}_e$) from manifold pressure can help us in the development of virtual sensors. Modern automotive industry employee highly sophisticated sensors. These sensors are heavily relied upon to ensure optimum engine performance. The development of virtual sensors can help in creating redundancy for these sensors and health monitoring of these sensors can be conducted efficiently.

4.2 Pertinent Model Properties

Consider a nonlinear system,

$$\dot{\mathbf{x}} = f(\mathbf{x}, \mathbf{p}, t, u)$$
$$\mathbf{y} = g(\mathbf{x}, \mathbf{p}, t, u) \qquad \textit{Eq (4.1)}$$

where,

$\mathbf{x} \in \Re^n$ are the system states.

$\mathbf{p} \in \Re^p$ are the system parameters.

u $\in \Re^q$ is the input to the system.

$\mathbf{y} \in \Re^l$ are the system outputs.

Before proceeding to the development of estimation scheme, the definition of following terminologies will contribute in better understanding in the coming sections.

4.2.1 Observability

Definition 4.1. The nonlinear system in *Eq (4.1)* is said to be observable if at any unknown initial state $\mathbf{x}(0)$, there exist a finite $t_1 > 0$ such that the knowledge of the input $\mathbf{u}$ and the output $\mathbf{y}$ over $[0, t_1]$ suffices to determine uniquely the initial state $\mathbf{x}(0)$ [94].

In differential geometry, nonlinear system in *Eq (4.1)* is said to be observable if following observability matrix (J_O) does not lose its rank or,

$$rank(J_O) = rank[\frac{\partial f_i}{\partial x_j}] = n \qquad \textit{Eq (4.2)}$$

where, $i = 1, 2, ...n$ and $j = 1, 2, ...n$ [95].

If any system obeys observability criteria then one can design state observer based on the available system outputs.

4.2.2 Identifiability

Definition 4.2. The nonlinear system in *Eq (4.1)* is said to be identifiable w.r.t $\mathbf{p}$ if at any unknown initial parameter $\mathbf{p}(0)$, there exist a finite $t_1 > 0$ such that the knowledge of the input $\mathbf{u}$ and the output $\mathbf{y}$ over $[0, t_1]$ suffices to determine uniquely the initial parameter $\mathbf{p}(0)$.

In differential geometry, nonlinear system in *Eq (4.1)* is said to identifiable with respect to $\mathbf{p}$ if following identifiably matrix (J_I) remains full ranked or,

$$rank(J_I) = rank[\frac{\partial f_i}{\partial p_j}] = n \qquad Eq\ (4.3)$$

where, $i = 1, 2, ...n$ and $j = 1, 2, ...k$ [95].

In simple words, whether the parameters of interest are identifiable or not, this inspection is conducted under identifiability analysis.

4.2.3 Boundedness

Definition 4.3. If for the nonlinear system in *Eq (4.1)*, $\exists\ f^+$ and δf^+ as two positive numbers $\forall\ t \in \Re^+$, $\forall\ \mathbf{x}$ and $u < u^+$ such that following relations are satisfied.

$$|f(\mathbf{x}, p, t, u)| < f^+ \qquad Eq\ (4.4)$$

$$|\frac{df(\mathbf{x}, p, t, u)}{dt}| < \delta f^+ \qquad Eq\ (4.5)$$

Then the system is termed as bounded in nature. ■

Initially, the above mentioned analysis will be performed for pressure and angular speed dynamics. The observability analysis will ensure whether SOSM Observer can be designed for pressure/speed dynamics or not. The identifiability analysis will confirm the whether the parameters of interest are detectable or not. Boundedness of pressure/speed dynamics will be useful for finite time convergence of SOSM Observers.

4.3 Second Order Sliding Mode Observers for Gasoline Engine

Keeping in view the importance of afore-mentioned parameters and attributes of SOSM Observer discussed in Section 2.2.2.4, these parameters can be estimated by super twisting algorithm based SOSM Observer. Figure 2.12 explains SOSM Observer functioning and Figure 4.1 outlines the proposed estimation strategy for gasoline engine pressure and angular speed dynamics. The measurements from engine will serve as inputs to the designed observer and the resultant correcting injectors of these SOSM Observers will deliver us un-measurable parameters.

The SOSM Observer based estimation scheme is not only computationally cheap but also has the potential for online implementation as it involves 'sample by sample' processing of the data acquired from OBD-II scanner (See Chapter 5

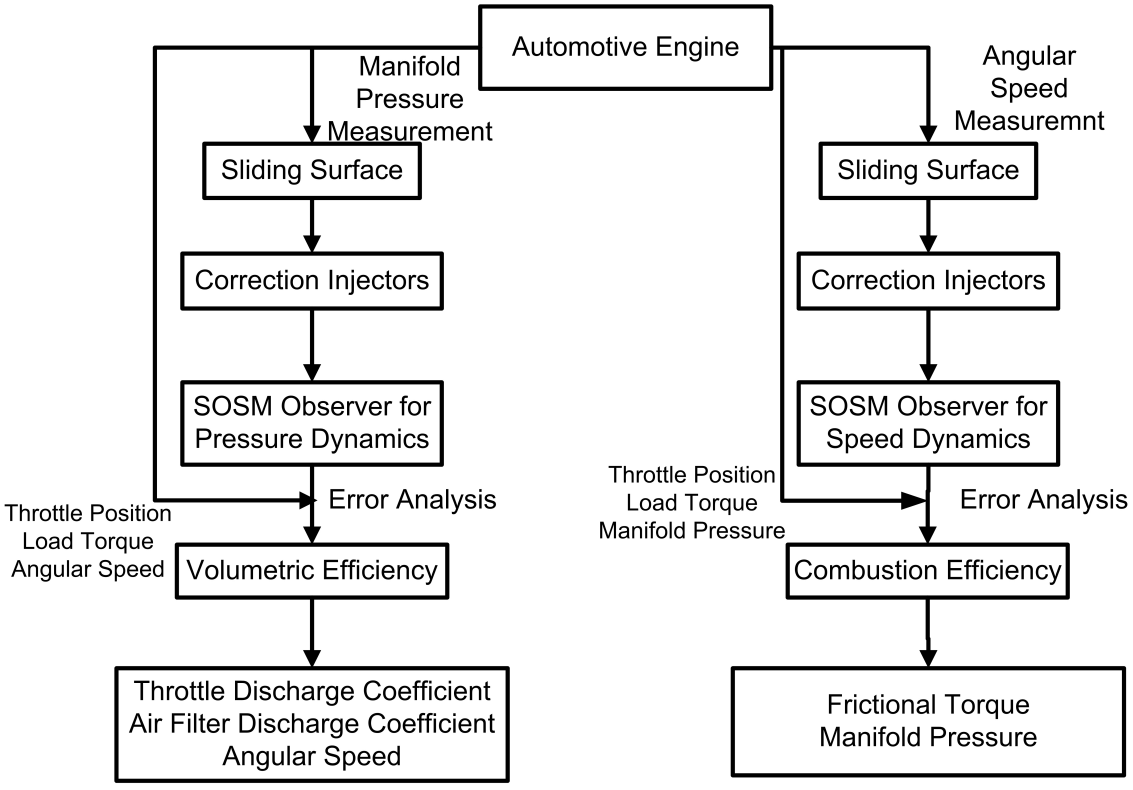

FIGURE 4.1: Proposed second order sliding mode observer based estimation strategy for gasoline engine parameters.

for further details on OBD-II). Unlike other estimation schemes (Line Search, Levenberg Marquardt, Powells Dog Leg), that require a batch of samples for curve fitting to develop empirical relations [96]. Moreover, the suggested scheme remains valid for the production line spread of a single make, as it does not involve curve fitting. ■

Now we will analyze the pressure and angular speed dynamics in detail and then design SOSM Observer for both dynamics. Once the observers are running is second order sliding modes the respective error dynamics will be explored to estimate afore-mentioned parameters.

4.4 Intake Manifold Pressure Dynamics

Consider the following states $\mathbf{x}$, outputs $\mathbf{y}$ and input u, as defined in the context of an engine. (See *List of Symbols* for symbols description.)

$$\mathbf{x} = \begin{bmatrix} \mathbf{x}_1 \\ \mathbf{x}_2 \end{bmatrix} = \begin{bmatrix} x_1 \\ x_2 \\ x_3 \\ x_4 \end{bmatrix} = \begin{bmatrix} P_m \\ \dot{P}_m \\ \omega_e \\ \dot{\omega}_e \end{bmatrix} \qquad \textit{Eq (4.6)}$$

$$\mathbf{y} = \begin{bmatrix} x_1 \\ x_3 \end{bmatrix} = \begin{bmatrix} P_m \\ \omega_e \end{bmatrix} \qquad \textit{Eq (4.7)}$$

$$u = \alpha \qquad \textit{Eq (4.8)}$$

Based on above defined states, output and input, the validated pressure dynamics in *Eq (3.36)* can be written as,

$$\dot{x}_1 = x_2 = A_1.f(x_1) - A_2 x_1 x_3 \eta_{vol} = g_1(\mathbf{x}, t, u) \qquad \textit{Eq (4.9)}$$

Taking time derivative of x_2, we get $\dot{x}_2$ as

$$\dot{x}_2 = \frac{A_1}{P_a}(e^{-(\frac{x_1}{P_a}-1)})\dot{x}_1 - A_2\eta_{vol}(\dot{x}_1 x_3 + x_1 \dot{x}_3) \qquad \textit{Eq (4.10)}$$

By replacing pressure and angular speed dynamics (See *Eq (3.36)*) in *Eq (4.10)* and simplifying, we get

$$\dot{x}_2 = A_7 {\eta_{vol}}^2 - (A_5 + A_6 + A_8)\eta_{vol} + A_4 = g_2(\mathbf{x}, t, u) \qquad Eq\ (4.11)$$

where,

$$A_1 = \frac{RT_m}{V_m} A_E P_a C_D C_{af} \gamma_c \qquad Eq\ (4.12)$$

$$A_2 = \frac{V_d}{V_m 4\pi} \qquad Eq\ (4.13)$$

$$A_3 = A_1 \frac{1}{P_a}(-e^{(\frac{x_1}{P_a}-1)}) \qquad Eq\ (4.14)$$

$$A_4 = A_1 A_3 f(x_1) \qquad Eq\ (4.15)$$

$$A_5 = A_3 A_2 x_1 x_3 \qquad Eq\ (4.16)$$

$$A_6 = A_2 A_1 f(x_1) x_3 \qquad Eq\ (4.17)$$

$$A_7 = (A_2 x_3)^2 x_1 \qquad Eq\ (4.18)$$

$$A_8 = A_2 x_4 x_1 \qquad Eq\ (4.19)$$

$$\gamma_c = \sqrt{\frac{1}{RT_a}} \sqrt{\gamma (\frac{2}{\gamma+1})^{\frac{\gamma+1}{\gamma-1}}} \qquad Eq\ (4.20)$$

$$f(x_1) = (1 - e^{(\frac{x_1}{P_a}-1)}) \qquad Eq\ (4.21)$$

$$A_E = \pi \frac{D^2}{4}(1 - cos(\frac{\alpha + \alpha_{cl}}{\alpha_{cl}})) \qquad Eq\ (4.22)$$

Now these dynamics will be analyzed for

- Observability
- Identifiability
- Boundedness

These analysis will evaluate the eligibility of the pressure dynamics to be used for estimation purpose.

4.4.1 Observability Analysis

For the gasoline engine pressure dynamics in *Eq (4.9)* and *Eq (4.11)* the observability matrix (J_O) in *Eq (4.2)* can be written as,

$$J_O = \begin{bmatrix} \frac{\partial g_1}{\partial x_1} & \frac{\partial g_1}{\partial x_2} \\ \frac{\partial g_2}{\partial x_1} & \frac{\partial g_2}{\partial x_2} \end{bmatrix} = \begin{bmatrix} A_3 - A_2 x_3 \eta_{vol} & 0 \\ \frac{\partial g_2}{\partial x_1} & A_3 - A_2 x_3 \eta_{vol} \end{bmatrix} \qquad Eq\ (4.23)$$

where, $\frac{\partial g_2}{\partial x_1} = \frac{1}{P_a} A_3 x_2 - A_2(A_3 - A_2 x_2 \eta_{vol}) + A_2 x_4 \eta_{vol} + A_2 x_1 \frac{\partial x_4}{\partial x_1}$.

or

$$J_O = \begin{bmatrix} -3.5686 & 0 \\ \frac{\partial g_2}{\partial x_1} & -3.5686 \end{bmatrix} \qquad Eq\ (4.24)$$

The SOSM Observer will be implemented under steady state and idle operating conditions, when engine angular speed is around 80 rad/sec and manifold pressure is around 30 Nm. Under such conditions, J_O for air intake pressure manifold remains full ranked ($rank(J_O) = 2 = n$) as $|J_O|$ is not equal to zero (See *Eq (4.25)*).

$$|J_O| = 12.7352 - 0 \neq 0 \qquad Eq\ (4.25)$$

Hence, SOSM Observer can be designed for intake manifold pressure dynamics, as these dynamics are observable in nature.

4.4.2 Identifiability Analysis

The outlined parameters i.e. throttle discharge coefficient, air filter discharge coefficient and volumetric efficiency can be comfortably estimated by manifold pressure dynamics along with the development of virtual sensor for speed. In order to avoid complicated calculations, a comprehensive and straightforward solution can be adopted if we estimate volumetric efficiency (η_{vol}) from *Eq (4.11)* and all other parameters from *Eq (4.9)* one by one. The parameters other than to be identified can be taken as of constant values estimated earlier. This can be

confirmed by following identifiability analysis of pressure dynamics with respect to parameters of interest.

4.4.2.1 Volumetric efficiency and Throttle Discharge Coefficient

The identifiability analysis of pressure dynamics in $g_1(\mathbf{x}, t, u)$ and $g_2(\mathbf{x}, t, u)$ with respect to η_{vol} and C_D results in following matrix.

$$J_I = \begin{bmatrix} \frac{\partial g_1}{\partial C_D} & \frac{\partial g_1}{\partial \eta_{vol}} \\ \frac{\partial g_2}{\partial C_D} & \frac{\partial g_2}{\partial \eta_{vol}} \end{bmatrix} = \begin{bmatrix} \frac{A_9}{f(x_1)} & -A_2 x_1 x_3 \\ \frac{\partial g_2}{\partial C_D} & 2A_7\eta_{vol} - (A_5 + A_6 + A_8) \end{bmatrix} \qquad Eq\ (4.26)$$

where,

$$\frac{\partial g_2}{\partial C_D} = \frac{A_9}{f(x_1)}[-\frac{1}{P_a}A_2 x_1 x_3 e^{(\frac{x_1}{P_a}-1)} + A_2 f(x_1) x_3]$$
$$A_9 = \frac{RT_m}{V_m} A_E C_{af}(\alpha) P_a \gamma_c f(x_1)$$

or

$$J_I = \begin{bmatrix} 1.3677 \times 10^6 & 2.1929 \times 10^5 \\ -1.4641 \times 10^6 & -2.4078 \times 10^6 \end{bmatrix} \qquad Eq\ (4.27)$$

During steady state and idle operations of gasoline engine, the above identifiability matrix remains full ranked as seen in *Eq (4.28)*.

$$|J_I| = -2.1922 \times 10^{12} - (-3.2106 \times 10^{11}) \neq 0 \qquad Eq\ (4.28)$$

Hence, it can be concluded that the parameters C_D and η_{vol} can be estimated/identified from pressure dynamics.

4.4.2.2 Volumetric Efficiency and Air Filter Discharge Coefficient

The identifiability matrix in *Eq (4.3)* for pressure dynamics with respect to η_{vol} and C_{af} comes out as follows,

$$J_I = \begin{bmatrix} \frac{\partial g_1}{\partial C_{af}} & \frac{\partial g_1}{\partial \eta_{vol}} \\ \frac{\partial g_2}{\partial C_{af}} & \frac{\partial g_2}{\partial \eta_{vol}} \end{bmatrix} = \begin{bmatrix} \frac{A_{10}}{f(x_1)} & -A_2 x_1 x_3 \\ \frac{\partial g_2}{\partial C_{af}} & 2A_7\eta_{vol} - (A_5 + A_6 + A_8) \end{bmatrix} \qquad Eq\ (4.29)$$

where,

$$\frac{\partial g_2}{\partial C_{af}} = \frac{A_{10}}{f(x_1)}[-\frac{1}{P_a}A_2 x_1 x_3 e^{(\frac{x_1}{P_a}-1)} + A_2 f(x_1) x_3] \quad \textit{Eq (4.30)}$$

$$A_{10} = \frac{RT_m}{V_m} A_E C_D(\alpha) P_a \gamma_c f(x_1) \quad \textit{Eq (4.31)}$$

or

$$J_I = \begin{bmatrix} 1.3677 \times 10^6 & 2.1929 \times 10^5 \\ -5.8563 \times 10^5 & -2.4078 \times 10^6 \end{bmatrix} \quad \textit{Eq (4.32)}$$

It can be observed that under steady state and idle operating conditions of gasoline engine, the above matrix does not lose its rank (See *Eq (4.33)*) and hence C_{af} turn out as identifiable variable along with η_{vol}.

$$|J_I| = -2.1922 \times 10^{12} - (-1.2842 \times 10^{11}) \neq 0 \quad \textit{Eq (4.33)}$$

4.4.2.3 Volumetric Efficiency and Engine Angular Speed

The third pair of parameters i.e $(\eta_{vol}, \bar{\omega}_e)$ that can be estimated from pressure dynamics results in following identifiability matrix,

$$J_I = \begin{bmatrix} \frac{\partial g_1}{\partial \bar{\omega}_e} & \frac{\partial g_1}{\partial \eta_{vol}} \\ \frac{\partial g_2}{\partial \bar{\omega}_e} & \frac{\partial g_2}{\partial \eta_{vol}} \end{bmatrix} = \begin{bmatrix} -A_2 \eta_{vol} x_1 & -A_2 x_1 x_3 \\ \frac{\partial g_2}{\bar{\omega}_e} & 2A_7 \eta_{vol} - (A_5 + A_6 + A_8) \end{bmatrix} \quad \textit{Eq (4.34)}$$

where,

$$\frac{\partial g_2}{\bar{\omega}_e} = \eta_{vol}^2 x_1 2(A_2 x_3) - \eta_{vol}(A_3 A_2 x_1 + A_2 A_1 f(x_1) + A_2 x_1 \frac{\partial x_4}{\bar{x}_3})$$

or

$$J_I = \begin{bmatrix} -1.3705 \times 10^3 & -2.1929 \times 10^5 \\ 8.4577 \times 10^4 & -2.4078 \times 10^6 \end{bmatrix} \quad \textit{Eq (4.35)}$$

$$|J_I| = 3.3 \times 10^9 - (-1.85 \times 10^{10}) \neq 0 \quad \textit{Eq (4.36)}$$

It can be observed that under steady state and idle conditions, the resultant J_I in *Eq (4.34)* does not lose its rank as it can be seen in *Eq (4.36)*. Hence, the above analysis certifies that η_{vol} can be estimated and sensor redundancy can be created by designing virtual sensor for the measurement of engine angular speed. ■

Based on the above identifiability analysis, the inlet manifold pressure dynamics can be written as:

$$\begin{aligned} \dot{x}_1 &= x_2 \\ \dot{x}_2 &= f_1(\mathbf{x}, t, u) + \xi_1(\mathbf{x}, t, u) \end{aligned} \qquad \textit{Eq (4.37)}$$

where, the initially known nonlinear dynamics of pressure manifold are:

$$f_1(\mathbf{x}, t, u) = A_4 \qquad \textit{Eq (4.38)}$$

and the dynamics to be estimated are:

$$\xi_1(\mathbf{x}, t, u) = A_7 {\eta_{vol}}^2 - (A_5 + A_6 + A_8)\eta_{vol} \qquad \textit{Eq (4.39)}$$

4.4.3 Boundedness Analysis

An Engine Control Unit (ECU) equipped gasoline engine is operating under bounded input ($\alpha < 90°$), the pressure dynamics will always remain bounded. This characterizes the system as Bounded Input and Bounded Output (BIBO) system. Therefore, the uncertain function $\xi_1(\mathbf{x}, t, u)$ defined in *Eq (4.39)* and its time derivative will always remain bounded by positive numbers ξ_1^+ and $\delta\xi_1^+$ respectively. The boundedness of the pressure dynamics will help to ensure convergence of the designed SOSM Observer.

4.4.4 SOSM Observer for Manifold Pressure Dynamics

After analyzing the pressure dynamics in detail, an observer based on [97] is proposed to estimate of the state vector $\mathbf{x}_1$ and extract unknown variables.

$$\begin{aligned}\dot{\hat{x}}_1 &= \hat{x}_2 + z_1 \\ \dot{\hat{x}}_2 &= f_1(\hat{\mathbf{x}}, t, u) + z_2 \\ \hat{y}_1 &= \hat{x}_1 \end{aligned} \qquad \textit{Eq (4.40)}$$

where $\hat{\mathbf{x}}_1$ represents the corresponding observer states and z_1, z_2 are the observer injectors based on super twisting algorithm. These injectors aim to eliminate the error between the estimated states and the actual states i.e. $(e_1 = x_1 - \hat{x}_1)$ & $(e_2 = x_2 - \hat{x}_2)$. These injectors are defined as,

$$\begin{aligned} z_1 &= \lambda_1 |e_1|^{1/2} sign(e_1) + \upsilon_1 \\ \dot{\upsilon}_1 &= \alpha_1 sign(e_1) \end{aligned} \qquad \textit{Eq (4.41)}$$

and

$$\begin{aligned} z_2 &= 0 && if\, e_1 \neq 0 \,\&\, \dot{e}_1 \neq 0 \\ z_2 &= \lambda_2 |z_1|^{1/2} sign(z_1) + \upsilon_2 && if\, e_1 = 0 \,\&\, \dot{e}_1 = 0 \\ \dot{\upsilon}_2 &= \alpha_2 sign(z_1) \end{aligned} \qquad \textit{Eq (4.42)}$$

The state x_1 is available for measurement from the sensor installed in the engine inlet manifold. The gains λ_1, α_1 are the observer gains. The above second order sliding mode observer inherits anti-peaking structure, where e_1 and e_2 reach the sliding manifold one by one in a recursive fashion [97].

4.4.4.1 Convergence and Error Dynamics Analysis

The error dynamics before converging to the surface i.e. $e_1 = 0$ comes out to be

$$\dot{e}_1 = e_2 - z_1$$
$$\dot{e}_2 = F_1(\mathbf{x}, \hat{\mathbf{x}}, t, u) \qquad \textit{Eq (4.43)}$$

where

$$F_1(\mathbf{x}, \hat{\mathbf{x}}, t, u) = f_1(\mathbf{x}, t, u) - f_1(\hat{\mathbf{x}}, t, u) + \xi_1(\mathbf{x}, t, u)$$

In order to analyze the convergence of the proposed observer in *Eq (4.40)* for inlet pressure manifold, $\exists\, \alpha < 90°$, $\forall\, t \in \Re^+$ and $\forall\, \mathbf{x}_1\ \exists\, k_1$ and k_2, such that Assumption 1 is satisfied.

Assumption 1. *There exist two positive constants k_1 and k_2 such that*

$$|f_1(x_1, x_2, t, u)| - |f_1(\hat{x}_1, \hat{x}_2, t, u)| \leq k_1|e_1|$$
$$\frac{d|f_1(x_1, x_2, t, u)| - |f_1(\hat{x}_1, \hat{x}_2, t, u)|}{dt} \leq k_2|e_2| \qquad \textit{Eq (4.44)}$$

Based on BIBO behavior of pressure dynamics (See Section 4.4.3) and Assumption 1, $\forall\, t \in \Re^+$, $\forall\, \mathbf{x}_1, \hat{\mathbf{x}}_1$, u we have

$$|F_1(\mathbf{x}, \hat{\mathbf{x}}, t, u)| < k_1|e_1| + \xi_1^+ \qquad \textit{Eq (4.45)}$$
$$\frac{d|F_1(\mathbf{x}, \hat{\mathbf{x}}, t, u)|}{dt} < k_2|e_2| + \delta\xi_1^+ \qquad \textit{Eq (4.46)}$$

Theorem 4.4. *If the condition Eq (4.45) holds for inlet manifold pressure dynamics in Eq (4.38), and the parameters of the proposed observer in Eq (4.40) are selected according to following criteria [97]:*

$$\alpha_1 > \sqrt{k_1}\dot{e}_{1_o} + \xi_1^+$$
$$\lambda_1 > \frac{4\alpha_1}{\sqrt{\alpha_1 - \xi_1^+}} \qquad \textit{Eq (4.47)}$$

Then $\hat{\boldsymbol{x}}_1$ will converge to $\boldsymbol{x}_1$ in finite time.

Remark 4.5. The choice of α_1 and λ_1 depends on the uncertainty bound and the initial state estimation error ($\dot{e}_{1_o}$) in the worst case. As $F_1(.)$ is bounded for engine pressure dynamics, therefore sufficiently large values of α_1 is chosen to satisfy *Eq (4.47)*.

The constants k_1 and k_2 can be chosen as explained in convergence proof given by [97].

When e_1 converges to sliding manifold, the dynamics of e_2 becomes

$$\dot{e}_2 = F_1(\mathbf{x}, \hat{\mathbf{x}}, t, u) - z_2 \qquad \textit{Eq (4.48)}$$

The constants α_2, λ_2 in z_2 can be chosen in a similar way as discussed for α_1, λ_1 in z_1 and convergence of e_2 will be ensured in similar fashion.

After the second order sliding mode has been achieved, the term e_1 approaches to zero.

$$\dot{e}_1 = e_2 - \bar{z}_1 \qquad \textit{Eq (4.49)}$$

$$0 = e_2 - \bar{z}_1 \qquad \textit{Eq (4.50)}$$

When e_1 approaches to zero, $\dot{e}_1$ also vanishes and from *Eq (4.43)* we are left with,

$$\bar{z}_1 = x_2 - \hat{x}_2 \qquad \textit{Eq (4.51)}$$

where

$$x_2 = A_9 C_D - A_2 \eta_{vol} x_1 x_3 \qquad \textit{Eq (4.52)}$$

or

$$\bar{z}_1 = A_9 C_D - A_2 \eta_{vol} x_1 x_3 - \hat{x}_2 \qquad \textit{Eq (4.53)}$$

As the convergence of e_1 is achieved, the convergence of e_2 is also guaranteed. Under convergence i.e. $e_2 = 0$ and $\dot{e}_2 = 0$ the following sliding mode dynamics from *Eq (4.48)* will be available.

$$\dot{e}_2 = F_1(\mathbf{x}, \hat{\mathbf{x}}, t, u) - \bar{z}_2 \qquad \textit{Eq (4.54)}$$

or

$$0 = \xi_1(\mathbf{x}, t, u) - \bar{z}_2 \qquad \textit{Eq (4.55)}$$

or

$$\bar{z}_2 = \xi_1(\mathbf{x}, t, u) \qquad \textit{Eq (4.56)}$$

where,

$$\xi_1(\mathbf{x}, t, u) = A_7 {\eta_{vol}}^2 - (A_5 + A_6 + A_8)\eta_{vol} \qquad \textit{Eq (4.57)}$$

or

$$\bar{z}_2 = A_7 {\eta_{vol}}^2 - (A_5 + A_6 + A_8)\eta_{vol} \qquad \textit{Eq (4.58)}$$

Remark 4.6. It may be kept in mind that $\bar{z}_1$ and $\bar{z}_2$ are the low pass filtered versions of switching functions z_1 and z_2 respectively. These first order low pass filters are employed to cater for switching of discontinuous injectors in estimation results. The time constant of low pass filters can be chosen as 0.2 seconds for reduced phase lags.

4.4.4.2 Estimation of Parameters from Pressure Dynamics

4.4.4.2.1 Estimation of η_{vol} and C_D: It can be observed that the only unknown in *Eq (4.58)* is η_{vol}, that can be calculated as in *Eq (4.59)*.

$$\eta_{vol} = \frac{(A_5 + A_6 + A_8) \pm \sqrt{(A_5 + A_6 + A_8)^2 + 4A_7\bar{z}_2}}{A_7} \qquad \textit{Eq (4.59)}$$

Once η_{vol} has been estimated it can lead to computation of C_D from *Eq (4.53)* as follows [50].

$$C_D = \frac{(\bar{z}_1 + \hat{x}_2 + A_2\eta_{vol}x_1x_3)}{A_9} \qquad \textit{Eq (4.60)}$$

4.4.4.2.2 Estimation of C_{af}: Similarly, C_{af} can be estimated as follows along with the estimation of η_{vol} by *Eq (4.59)*.

$$C_{af} = \frac{(\bar{z}_1 + \hat{x}_2 + A_2\eta_{vol}x_1\omega_e)}{A_{10}} \qquad \textit{Eq (4.61)}$$

For the estimation of C_{af}, C_D is taken as constant value. The constant value can be taken as found during the evaluation of estimation process for the first pair (η_{vol}, C_D).

4.4.4.2.3 Identification of $\bar{\omega}_e$: The third pair of parameters to be estimated is (η_{vol}, $\bar{\omega}_e$). η_{vol} can be estimated again by *Eq (4.59)* and $\bar{\omega}_e$ can be calculated as follows.

$$\bar{x}_3 = \bar{\omega}_e = \frac{1}{\eta_{vol}A_2x_1}(A_9 - (\bar{z}_1 + \hat{x}_2)) \qquad \textit{Eq (4.62)}$$

We can also say that *Eq (4.62)* provides us sensor redundancy by facilitating with virtual rotational speed sensor [92].

The A_i in above equations are defined in *Eq (4.12)* - *Eq (4.22)*. The estimation of η_{vol} involves an initial value to calculate $C_D/C_{af}/\bar{\omega}_e$, but later on the value of $C_D/C_{af}/\bar{\omega}_e$ is updated with estimated value from *Eq (4.60)*/*Eq (4.61)*/ *Eq (4.62)*. The recursive estimation of parameters involves iterative calculations. For the calculation of $C_D/C_{af}/\bar{\omega}_e$, η_{vol} is replaced in *Eq (4.60)*/*Eq (4.61)*/*Eq (4.62)* by *Eq (4.59)* and vice versa. The new value of $C_D/C_{af}/\bar{\omega}_e$ can be updated as: $C_D/C_{af}/\bar{\omega}_e(k+1) = \epsilon.C_D/C_{af}/\bar{\omega}_e(k)$, where $|\epsilon| < 1$ is guaranteed for manifold pressure dynamics. Hence, the convergence and stability of $C_D/C_{af}/\bar{\omega}_e$ estimation is ensured.

Remark 4.7. *Eq (4.58)* will have two solutions for η_{vol} in general; however we will not be interested in negative values as they have no physical significance.

4.5 Engine Angular Speed Dynamics

Now we will proceed with the analysis of engine angular speed dynamics. Based on states, output and input defined in *Eq (4.6)*, these dynamics given in *Eq (3.36)* can be written as,

$$\dot{x}_3 = x_4 = \frac{1}{J_e}(B_1 x_1 - T_f - T_p - T_l) = g_3(\mathbf{x}, t, u) \qquad \textit{Eq (4.63)}$$

Similarly, by taking the derivative of x_4, higher order angular speed dynamics can be written as,

$$\dot{x}_4 = \frac{1}{J_e}(\eta_c B_1 x_2 + \frac{V_d}{4\pi} x_2 - \dot{T}_f - \dot{T}_l) = g_4(\mathbf{x}, t, u) \qquad \textit{Eq (4.64)}$$

where T_f and T_l can be taken as exogenous inputs and their derivatives can be ignored due to unavailability of required information.

Before we proceed with the development of estimation scheme, the observability, identifiability and boundedness analysis will be performed on above angular speed dynamics. These analysis will reveal whether we can design SOSM Observer based parameter estimation scheme for speed dynamics or not.

4.5.1 Observability Analysis

For the above defined angular speed dynamics, the observability matrix in *Eq (4.2)* can be derived as,

$$J_O = \begin{bmatrix} \frac{\partial g_3}{\partial x_3} & \frac{\partial g_3}{\partial x_4} \\ \frac{\partial g_4}{\partial x_3} & \frac{\partial g_4}{\partial x_4} \end{bmatrix} = \begin{bmatrix} -5.69 \times 10^{-5} - 4.66 \times 10^{-14} x_3 & 0 \\ \frac{\partial g_4}{\partial x_3} & -5.69 \times 10^{-5} - 4.66 \times 10^{-14} x_4 \end{bmatrix} \qquad \textit{Eq (4.65)}$$

or

$$J_O = \begin{bmatrix} -5.69 \times 10^{-5} & 0 \\ \frac{\partial g_4}{\partial x_3} & -5.69 \times 10^{-5} \end{bmatrix} \qquad \textit{Eq (4.66)}$$

Under steady state and idle operating conditions of gasoline engine, J_O for angular speed dynamics remains full ranked ($rank(J_O) = 2 = n$) as $|J_O|$ is not equal to zero (See *Eq (4.67)*).

$$|J_O| = 3.2376 \times 10^{-9} - 0 \neq 0 \qquad \textit{Eq (4.67)}$$

Hence, a SOSM Observer can be formulated for angular speed dynamics, as these dynamics are observable in nature.

4.5.2 Identifiability Analysis

The parameters outlined earlier i.e. combustion efficiency (η_c) and frictional torque (T_f) can be efficiently estimated using angular speed dynamics. Similarly, these dynamics provide solid ground to develop virtual sensor for manifold pressure measurement ($\bar{P}_m$). A systematic estimation procedure can be outlined if we estimate η_c from *Eq (4.64)* and other entities ($T_f, \bar{P}_m$) from *Eq (4.63)*. This practice can provide us simpler mathematical calculations along with better understanding. The estimation/identification of these parameters can be ensured by following identifiability analysis.

4.5.2.1 Combustion Efficiency and Frictional Torque

For angular speed dynamics, the identifiability matrix (J_I) in *Eq (4.3)* with respect to η_c and T_f comes out as

$$J_I = \begin{bmatrix} \frac{\partial g_3}{\partial \eta_c} & \frac{\partial g_3}{\partial T_f} \\ \frac{\partial g_4}{\partial \eta_c} & \frac{\partial g_4}{\partial T_f} \end{bmatrix} = \begin{bmatrix} \frac{1}{J_e}(B_1 x_1) & \frac{1}{J_e} \\ \frac{1}{J_e}(B_1 x_2) & 0 \end{bmatrix} \qquad \textit{Eq (4.68)}$$

or

$$J_I = \begin{bmatrix} 2.3480 \times 10^3 & 4 \\ 5.3839 \times 10^4 & 0 \end{bmatrix} \qquad \textit{Eq (4.69)}$$

Under steady state and idle operating conditions, when the manifold pressure is around 30 kPa and angular speed is around 80 rad/sec, η_c and T_f remain identifiable as the matrix in *Eq (4.68)* does not lose its rank (See *Eq (4.70)*).

$$|J_I| = 2.1536 \times 10^5 - (0) \neq 0 \qquad \textit{Eq (4.70)}$$

Hence, the pair of frictional torque and combustion efficiency remain identifiable from angular speed dynamics.

4.5.2.2 Combustion Efficiency and Manifold Pressure

With respect to η_c and $\bar{P}_m$, for the angular speed dynamics in *Eq (4.63)* and *Eq (4.64)*, the identifiability matrix in *Eq (4.3)* is given as follows.

$$J_I = \begin{bmatrix} \frac{\partial g_3}{\partial \eta_c} & \frac{\partial g_3}{\partial \bar{P}_m} \\ \frac{\partial g_4}{\partial \eta_c} & \frac{\partial g_4}{\partial \bar{P}_m} \end{bmatrix} = \begin{bmatrix} \frac{1}{J_e}(B_1 x_1) & \frac{1}{J_e}(\eta_c B_1 + \frac{V_d}{4\pi}(P_a)) \\ \frac{1}{J_e}(B_1 x_2) & \frac{1}{J_e}(\eta_c B_1 + \frac{V_d}{4\pi}(P_a))[A_1 A_3 - A_2 x_3 \eta_{vol}] \end{bmatrix} \qquad \textit{Eq (4.71)}$$

or

$$J_I = \begin{bmatrix} 2.3480 \times 10^3 & 411.9476 \\ 5.3839 \times 10^4 & 2.0354 \times 10^3 \end{bmatrix} \qquad \textit{Eq (4.72)}$$

Under steady state and idle operating conditions, the mentioned parameters remain identifiable as *Eq (4.71)* does not loose its rank (See *Eq (4.73)*).

$$|J_I| = 4.77 \times 10^6 - (2.2179 \times 10^7) \neq 0 \qquad \textit{Eq (4.73)}$$

Hence it can be concluded that η_c remains identifiable from engine angular speed dynamics along with the development of virtual sensor ($\bar{P}_m$) for manifold pressure measurement. ■

After analyzing the speed engine rotational dynamics in detail analysis, these dynamics can be written as:

$$\begin{aligned} \dot{x}_3 &= x_4 \\ \dot{x}_4 &= f_2(\mathbf{x}, t, u) + \xi_2(\mathbf{x}, t, u) \end{aligned} \qquad \textit{Eq (4.74)}$$

where, the initially known linear rotational dynamics are:

$$f_2(\mathbf{x}, t, u) = B_2 \qquad \textit{Eq (4.75)}$$

where,

$$B_2 = \frac{1}{J_e}(\frac{V_d}{4\pi}x_2) - \dot{T}_l$$

and the dynamics to be estimated are:

$$\xi_2(\mathbf{x}, t, u) = \frac{1}{J_e}(\eta_c B_1 x_2) \qquad \textit{Eq (4.76)}$$

4.5.3 Boundedness Analysis

As ECU equipped gasoline engine is operating under closed loop and bounded input ($\alpha < 90°$), the angular speed dynamics will always remain bounded. This characterizes the system as Bounded Input and Bounded Output (BIBO) system. Therefore, the uncertain function $\xi_2(\mathbf{x}, t, u)$ defined in *Eq (4.76)* and its time derivative will always remained bounded by positive numbers ξ_2^+ and $\delta\xi_2^+$ respectively (See Definition 4.3). The bounded nature of rotational speed will guarantee the convergence of SOSM Observer in future.

4.5.4 SOSM Observer for Engine Rotational Dynamics

After analyzing angular speed dynamics in detail, a similar observer can be defined as follows in order to estimate $\mathbf{x}_2$ and extract unknown variables from these dynamics.

$$\begin{aligned}
\dot{\hat{x}}_3 &= \hat{x}_4 + z_3 \\
\dot{\hat{x}}_4 &= f_2(\hat{\mathbf{x}}, t, u) + z_4 \\
\hat{y_2} &= \hat{x_3}
\end{aligned} \qquad \textit{Eq (4.77)}$$

where $\hat{\mathbf{x}}_2$ represents the observer states and z_3, z_4 are the observer injectors. These injectors can be calculated with the same methodology, that was followed to design

z_1 and z_2 in *Eq (4.41)* and *Eq (4.42)*. The aim of these injectors is to eliminate the error defined as $(e_3 = x_3 - \hat{x}_3)$ & $(e_4 = x_4 - \hat{x}_4)$. The state x_3 is available for measurement from the sensor installed inside the engine housing that can be accessed from OBD II kit. The above second order sliding mode observer inherits anti-peaking structure, where e_3 and e_4 reach the sliding manifold one by one in a recursive way [97].

4.5.4.1 Convergence and Error Dynamics Analysis

The states and parameters involved in ECU controlled engine angular speed dynamics are bounded in nature as discussed in Section 4.5.3. Similarly, k_1 and k_2 for angular dynamics can be calculated to satisfy Assumption 1 and Theorem 4.4 holds for angular speed dynamics. Thus, the convergence of designed observer is also ensured [97].

The error dynamics before converging to the surface i.e. $e_3 = 0$ comes out to be

$$\dot{e}_3 = e_4 - z_3 \qquad \textit{Eq (4.78)}$$

$$\dot{e}_4 = F_2(\mathbf{x}, \hat{\mathbf{x}}, t, u) \qquad \textit{Eq (4.79)}$$

where

$$F_2(\mathbf{x}, \hat{\mathbf{x}}, t, u) = f_2(\mathbf{x}, t, u) - f_2(\hat{\mathbf{x}}, t, u) + \xi_2(\mathbf{x}, t, u)$$

The observer gains pair (α_3, λ_3) and (α_4, λ_4) can be chosen with the same procedure defined in *Eq (4.47)*. As the convergence of e_3 is achieved, the dynamics of e_4 before converging to sliding manifold comes out to be

$$\dot{e}_4 = F_2(\mathbf{x}, \hat{\mathbf{x}}, t, u) - z_4 \qquad \textit{Eq (4.80)}$$

After the second order sliding mode has been achieved, we are left with $e_3 = 0$ and $\dot{e}_3 = 0$.

$$\dot{e}_3 = e_4 - \bar{z}_3 \qquad \textit{Eq (4.81)}$$

or

$$0 = e_4 - \bar{z}_3 \qquad \textit{Eq (4.82)}$$

or

$$\bar{z}_3 = x_4 - \hat{x}_4 \qquad \textit{Eq (4.83)}$$

where

$$x_4 = \frac{1}{J_e}((x_1 B_1 \eta_c) - T_f - T_p - T_l) \qquad \textit{Eq (4.84)}$$

From above, the dynamics during second order sliding mode can be written as,

$$\bar{z}_3 = \frac{1}{J_e}((x_1 B_1 \eta_c) - T_f - T_p - T_l) - \hat{x}_4 \qquad \textit{Eq (4.85)}$$

As the convergence of e_3 is achieved, the convergence of e_4 is also guaranteed. Under convergence of e_4 the following sliding mode dynamics from *Eq (4.80)* will be available.

$$\dot{e}_4 = F_2(t, \mathbf{x}, \hat{\mathbf{x}}, u) - \bar{z}_4 \qquad \textit{Eq (4.86)}$$

or,

$$0 = \xi_2(t, \mathbf{x}, \hat{\mathbf{x}}, u) - \bar{z}_4 \qquad \textit{Eq (4.87)}$$

where,

$$\xi_2(t, \mathbf{x}, \hat{\mathbf{x}}, u) = \frac{1}{J_e}(\eta_c B_1 x_2) \qquad \textit{Eq (4.88)}$$

or,

$$\bar{z}_4 = \frac{1}{J_e}(\eta_c B_1 x_2) \qquad \textit{Eq (4.89)}$$

4.5.4.2 Estimation of Parameters from Speed Dynamics

4.5.4.2.1 Estimation of η_c and T_f: The first pair of parameters to be estimated from engine speed dynamics is (η_c, T_f). It can be observed that the only unknown in *Eq (4.89)* is engine combustion efficiency (η_c), it can be easily calculated as follows [76].

$$\eta_c = \frac{\bar{z}_4 J_e}{B_1 x_2} \qquad \textit{Eq (4.90)}$$

Once η_c has been estimated it can lead to the identification of T_f from *Eq (4.85)* as,

$$T_f = -J_e(\bar{z}_3 + \hat{x}_4) + (x_1 B_1 \eta_c) - T_p - T_l \qquad \textit{Eq (4.91)}$$

4.5.4.2.2 Estimation of η_c and $\bar{P}_m$: The second pair of parameters to estimated from engine angular speed dynamics is (η_c, $\bar{P}_m$). η_c can be estimated by *Eq (4.90)* and then supplied to *Eq (4.85)* for the development of virtual sensor for manifold pressure $\bar{P}_m$. The respective virtual sensor is given below [92],

$$\bar{x}_1 = \bar{P}_m = \frac{1}{B_3}(J_e(\hat{x}_4 + \bar{z}_3) + B_4) \qquad \textit{Eq (4.92)}$$

where,

$$B_4 = \frac{V_d P_a}{4\pi} + T_l \qquad \textit{Eq (4.93)}$$

4.6 Experimental Evaluation of Estimation Scheme

The estimation method formulated in the previous sections was tested and implemented for computing parameters of a 1.3L production vehicle gasoline engine. The details of the experimental setup are discussed in Chapter 5. It was asserted in the previous sections that pressure dynamics were used to develop three independent SOSM Observer based estimation schemes for the following pairs of parameters.

- C_D and η_{vol}
- C_{af} and η_{vol}
- $\bar{\omega}_e$ and η_{vol}

Similarly, the angular speed dynamics were used to develop two independent SOSM Observer based identification schemes for the following pairs of parameters.

- T_F and η_c
- $\bar{P}_m$ and η_c

By independent estimation schemes, it is meant that for each pair of parameters an independent SOSM observer based estimation scheme will execute to deliver results. The evaluation of each SOSM Observer based estimation scheme will be conducted against an independent set of experimental data. A systematic procedure was outlined to estimate the above mentioned parameters. The outlined steps are

1. Data will be acquired from gasoline engine and will be supplied to SOSM Observer.
2. SOSM Observer gains will be selected to ensure its convergence.
3. After convergence, the observer injectors will be used to estimate desired parameters.

The experiment was conducted under steady state and idle condition. Steady state condition means that the throttle valve was kept constant through out the experiment. Idle condition means that the experiment was performed in neutral gear. This scheme allows to estimate nominal values of the mentioned parameters. In future work, this practice can help to identify normal and faulty behavior of the engine under controlled environment. As, any deviation from nominal values will help in the identification of faults.

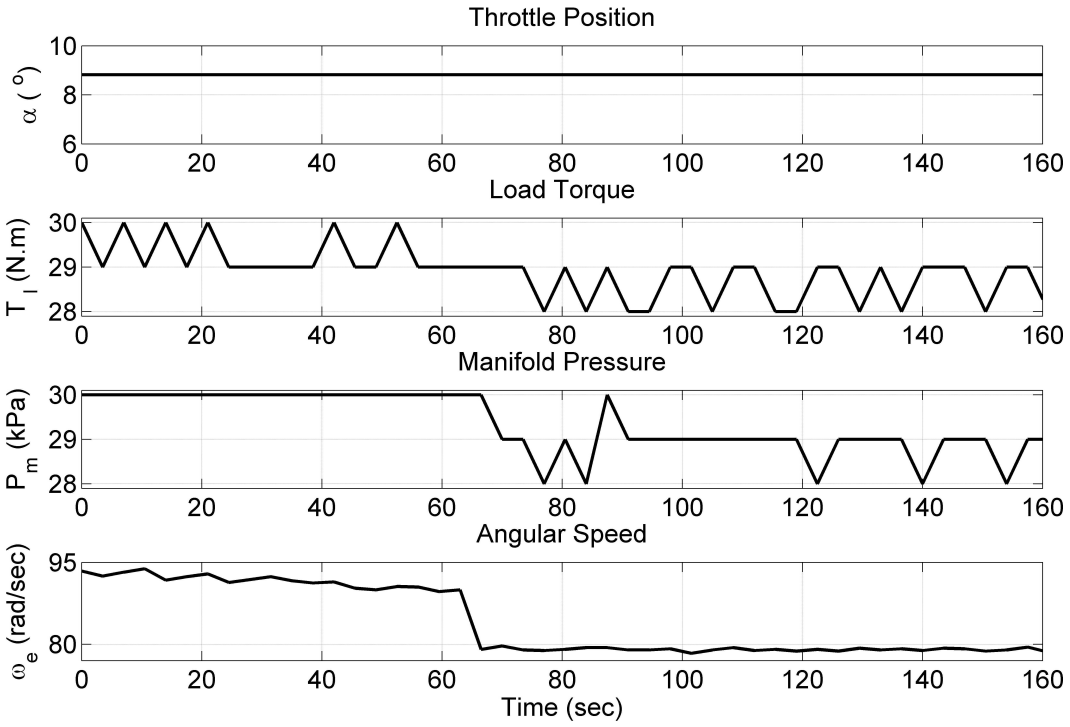

FIGURE 4.2: Measurements of α, T_l, P_m and ω_e taken from OBD-II scanner/logger for the estimation scheme.

4.6.1 Throttle Discharge Coefficient and Volumetric Efficiency Estimation Results

In the first step, the input data required for SOSM Observers was acquired from engine via OBD-II kit as shown in Figure 4.2. It can be observed that under steady state conditions, throttle value remained at 8.8^o. The nominal load on engine is contributed by: rotating engine components mass i.e. crank shaft, fly wheel and power train components engaged. As no extra load was induced, load torque remained around 29-30 Nm. With these inputs to the engine, the pressure and rotational speed can be visualized under steady state conditions too. The slight drop in engine speed at 65 seconds was due to introduction of minor disturbance in air intake path. It can be observed that the measurements are corrupted with acquisition noise and engine behavior even in steady state conditions. The same trends will be observed in the estimation results.

The data set (Figure 4.2) acquired from OBD-II kit serves as input for proposed estimation scheme. SOSM Observer based on pressure dynamics convergence was achieved, in the first phase. The initial conditions and SOSM Observer parameters

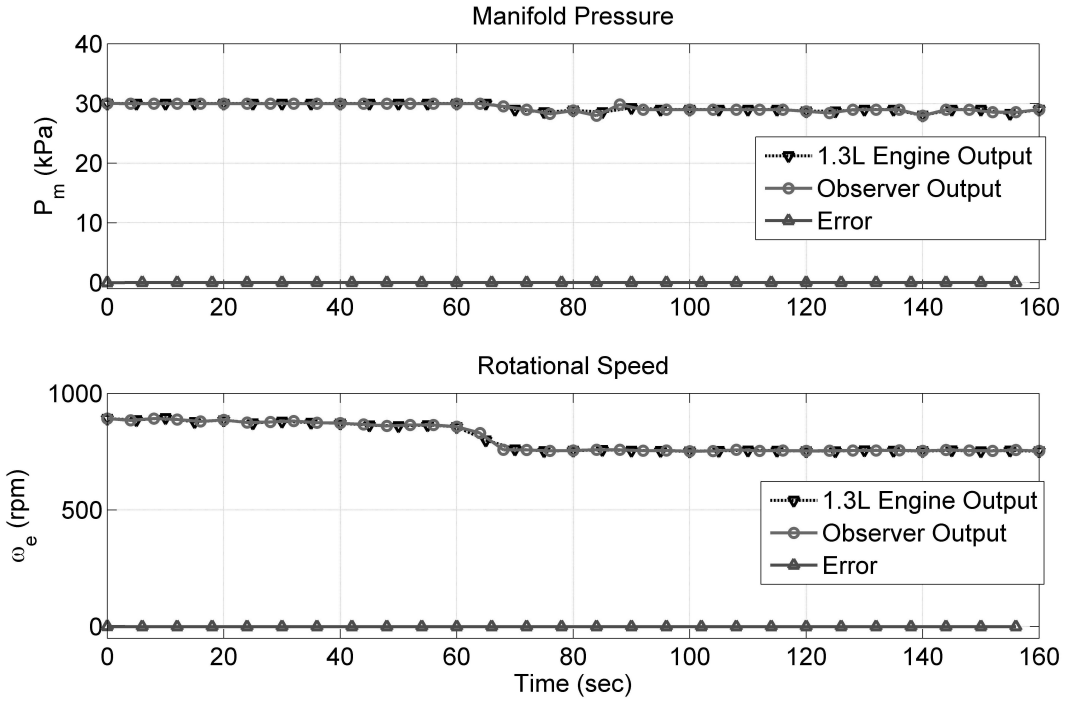

FIGURE 4.3: The convergence of robust SOSM Observers to 1.3L engine pressure and angular speed dynamics.

were chosen as given in Table 4.1. These observer parameters were tuned according to Theorem 4.4 by following Remark 4.5 to acquire desired results. The first result in Figure 4.3 shows the 1.3L engine & SOSM observer output and the convergence error. It can be seen that throughout the experiment, SOSM observer efficiently tracked the actual values of pressure and speed. The tracking error remained near to zero almost.

Remark 4.8. The robustness of the observer can be visualized after t=65s in Figure 4.3. Even with variations in engine behavior, the designed observer tracked the engine outputs efficiently.

TABLE 4.1: SOSM Observer parameters for C_D and η_{vol} estimation.

Parameter	Value
$\hat{x}_1(0)$	30 kPa
$\hat{x}_2(0)$	0
α_1	1.5
λ_1	1.6
α_2	20
λ_2	160

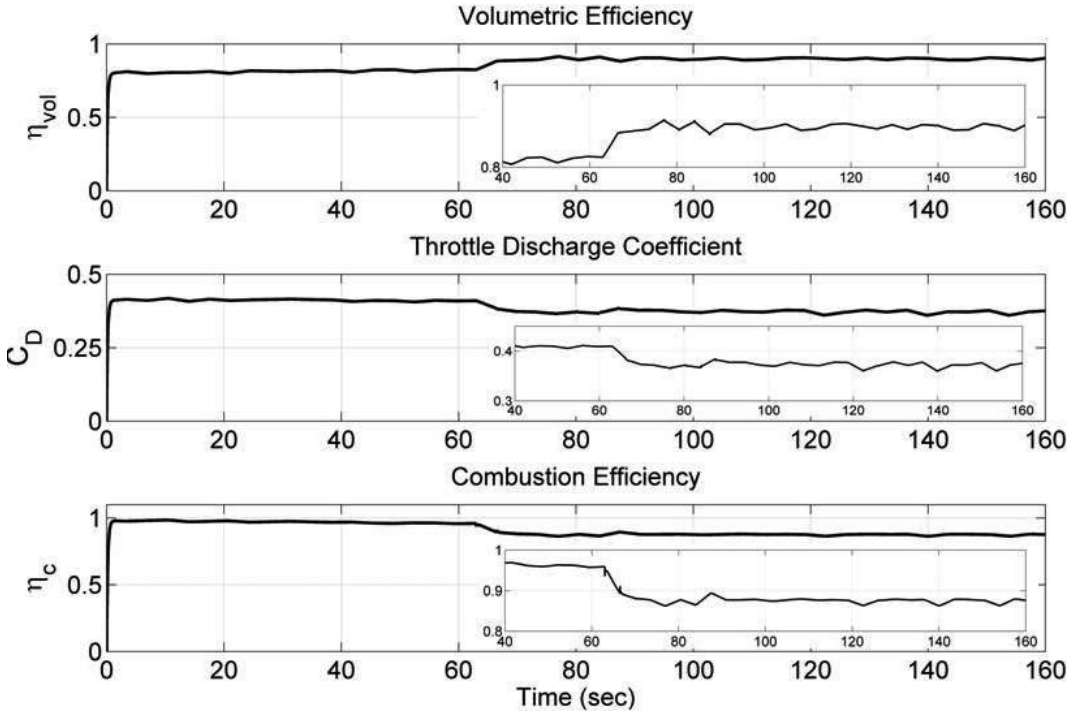

FIGURE 4.4: Estimated volumetric efficiency, throttle discharge coefficient and Combustion efficiency.

Once the observer was successfully running in second order sliding modes, the computed injection signals were used for parameter estimation. The observer in *Eq (4.40)* for pressure dynamics was used to estimate η_{vol} and C_D. In the first phase, η_{vol} was computed through the injector $\bar{z}_2$ as shown in *Eq (4.59)*. The estimated η_{vol} was then fed back in *Eq (4.60)* to compute C_D.

First two results in Figure 4.4 shows the filtered version of estimated values of η_{vol} and C_D under steady state conditions. It can be seen that η_{vol} converged in 0.6 seconds after second order sliding mode was achieved and any change afterwards was adopted in fraction of seconds. This convergence delay of 0.6 seconds was due to reachability phase and will not induce any unwanted issues for its application in fault diagnosis strategies. The estimated value of η_{vol} corresponds to true value that is between .75 and .90, as discussed in [2]. Similarly, C_D converged to the value of $0.4 - 0.5$ which corresponds to its true value as claimed in [47], [52].

4.6.2 Frictional Torque and Combustion Efficiency Estimation Results

The second observer in *Eq (4.77)* designed for rotational speed dynamics was utilized to estimate η_c and T_f. The same data as shown in Figure 4.2 was supplied for estimation purpose. The convergence of SOSM Observer for angular speed dynamics can be seen in second result of Figure 4.3. The initial conditions and SOSM Observer parameters were chosen as given in Table 4.2 and were tuned as discussed for preceding estimation results. η_c was calculated by using uncertainty estimated in $\bar{z}_4$ by *Eq (4.90)*. The estimated η_c was then used for the calculation of T_f through *Eq (4.91)*.

The last result in Figure 4.4 shows the filtered version of estimated values of η_c under steady state conditions. Under normal combustion process, the estimated combustion efficiency η_c converges to the value of 0.95. This value strengthens the claim that under normal combustion process combustion efficiency remained between $0.95 - 0.98$ [2], [89]. The variations shown in zoomed view in Figure 4.4 are due to measurement noise and engine response as shown in Figure 4.2.

Figure 4.5 demonstrates frictional torques calculated from the expressions found in [1], [2] and estimated by the proposed SOSM Observer. The first result in Figure 4.5, corresponds to frictional torque calculated by $T_F = 5.21\omega_e^{-1} + 2.00 + 0.46\omega_e^{.5} + 0.09\omega_e + 2.33 \times 10^{-14}\omega_e^2 - 3.30 \times 10^{-6}\omega_e^3$ [1]. The constants in the expression were identified off-line using least squares methods and are dependent on lubricant viscosity, piston assembly friction, reciprocating crankshaft and valve train motion. The mentioned final expression requires engine angular speed as

TABLE 4.2: SOSM Observer parameters for η_c and T_f estimation.

Parameter	Value
$\hat{x}_3(0)$	93 rad/sec
$\hat{x}_4(0)$	0
α_3	2
λ_3	19.6
α_4	10
λ_4	1700

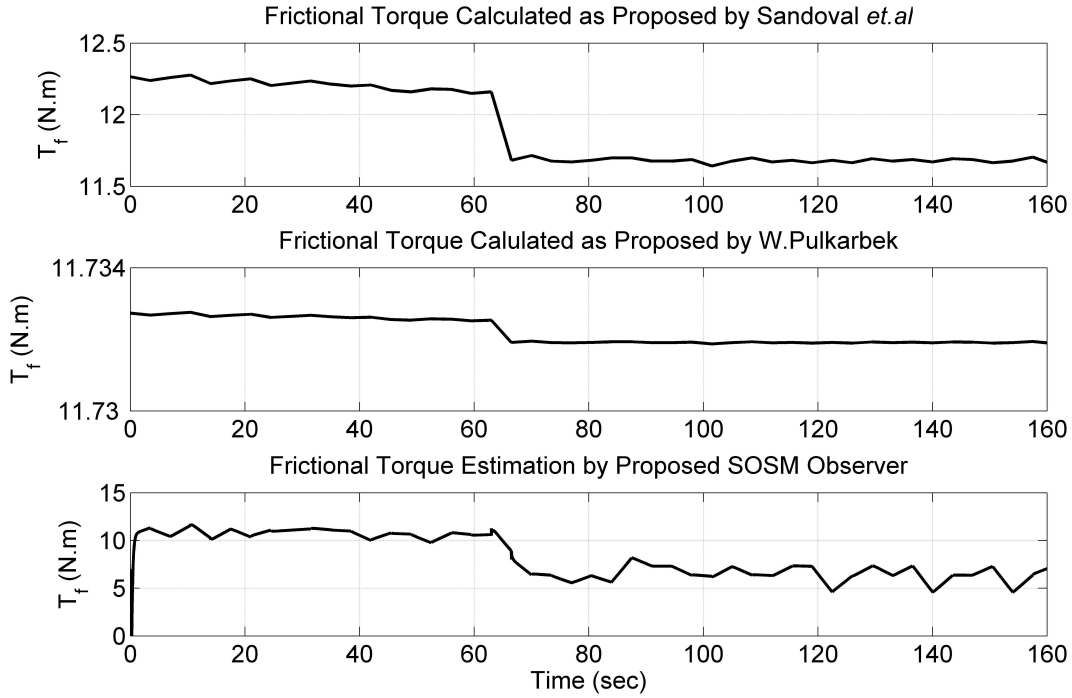

FIGURE 4.5: Frictional torque calculated by [1], [2] and estimated by *Eq (4.91)*, respectively.

input. The second result is of the empirical expression derived in [2], $T_F = 11.72 + 5.69 \times 10^{-5}\omega_e + 2.33 \times 10^{-14}\omega_e^2$. The empirical constants were identified off-line using least squares methods for the engine used in experimentation. The input to the empirical formula is again engine angular speed. The third result is of T_f estimated by SOSM observer using P_m and ω_e. It can be inferred that the magnitude and trend of the proposed estimator for frictional torque correspond to results produced by expressions found in literature [1] and [2]. The slight difference is due to the fact that first two techniques consider ω_e as input and the proposed technique takes P_m, ω_e and T_l as input. The variations in estimation results are due to engine response and measurement noise as shown in Figure 4.2. The similar variations are also observed in estimated parameters in Figure 4.4.

4.6.3 Air Filter Discharge Coefficient and Volumetric Efficiency Estimation Results

Another experiment was conducted to estimated air filter discharge coefficient (C_{af}) along with gasoline engine volumetric efficiency (η_{vol}) from manifold pressure dynamics. The same set of measurements were taken from the same gasoline

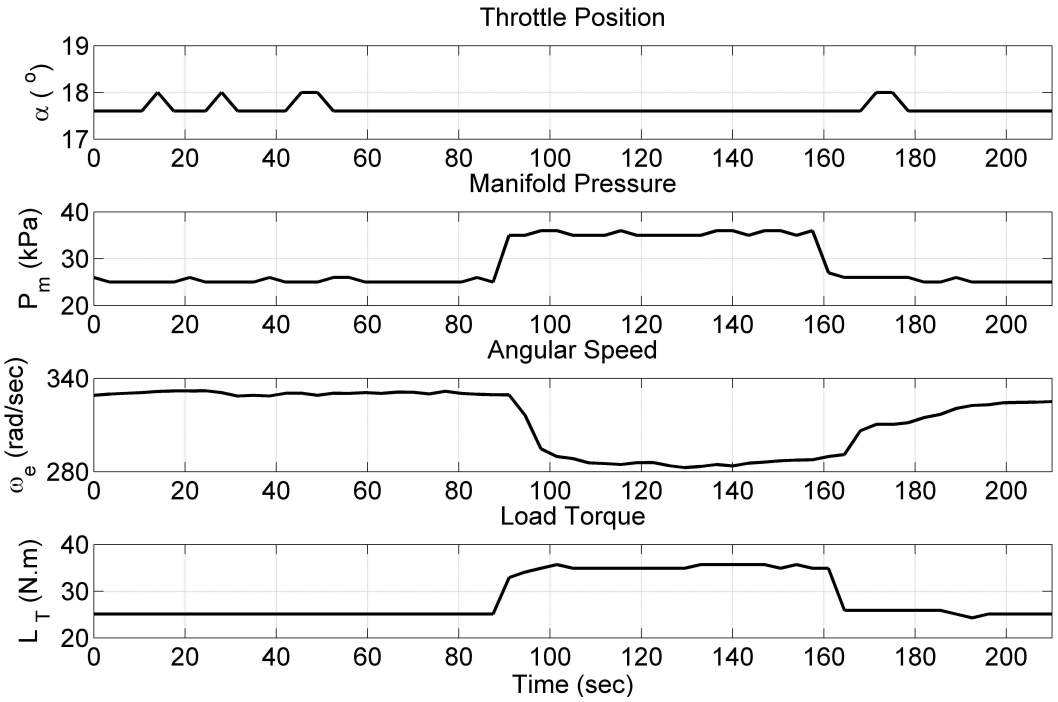

FIGURE 4.6: Input data acquired from OBD-II Scanner/Logger for C_{af} estimation.

engine as shown in Figure 4.6. However, the throttle angle was kept at 18^o and the experiment was conducted in neutral gear. The loads on the engine were increased at 88 seconds by turning on air conditioner, fan, lights and scree vipers. Clean air filter was used for experimentation. The respective measurements of α, P_m, ω_e and T_l were acquired from OBD-II kit and supplied to estimation scheme.

In the second phase of estimation scheme evaluation, convergence of SOSM Observer designed in *Eq (4.40)* was achieved. The initial conditions and SOSM Observer parameters were taken as given in Table 5.2. It can be observed in first

TABLE 4.3: SOSM Observer parameters for C_{af} estimation.

Parameter	Value
$\hat{x}_1(0)$	25 kPa
$\hat{x}_2(0)$	0
α_1	10
λ_1	40
α_2	10
λ_2	190

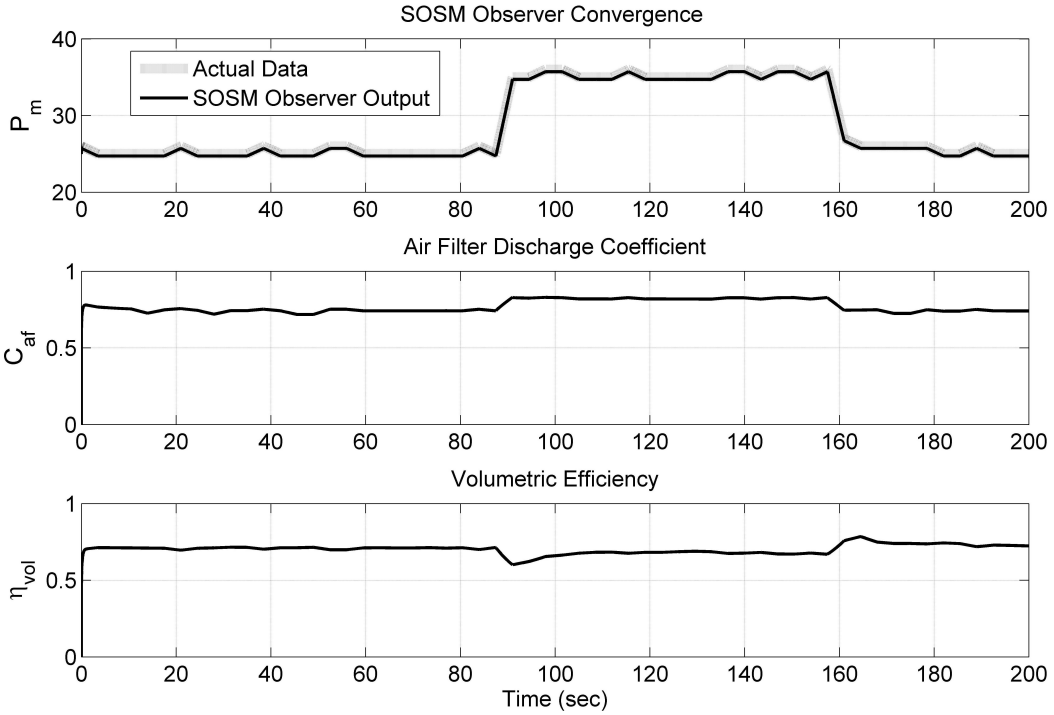

FIGURE 4.7: SOSM Observer convergence and estimated results of C_{af} and η_{vol}.

result of Figure 4.7 that the SOSM Observer successfully tracked the intake manifold pressure through out the experiment. Once the convergence has been achieved, *Eq (4.59)* and *Eq (4.61)* were employed to estimate volumetric efficiency and air filter discharge coefficient respectively. Second and third results in Figure 4.7 demonstrate the estimated values of C_{af} and η_{vol} respectively. For healthy/clean air filter the value of C_{af} converges to 0.8 with in one second and η_{vol} efficiency converges to 0.75 which corresponds to the previous estimated values.

4.6.4 Virtual Sensors for Angular Speed and Manifold Pressure Measurement

Another important outcome of the proposed methodology is the redundancy of the sensors installed in gasoline. These sensors include: manifold pressure and crankshaft sensor. This redundancy is achieved by designing virtual sensors. In this experiment, measurements from pressure sensor were used to develop virtual sensor/estimator for angular speed using *Eq (4.62)*. Similarly crankshaft sensor measurements were used to build virtual sensor/estimator for manifold pressure sensor by employing *Eq (4.92)*.

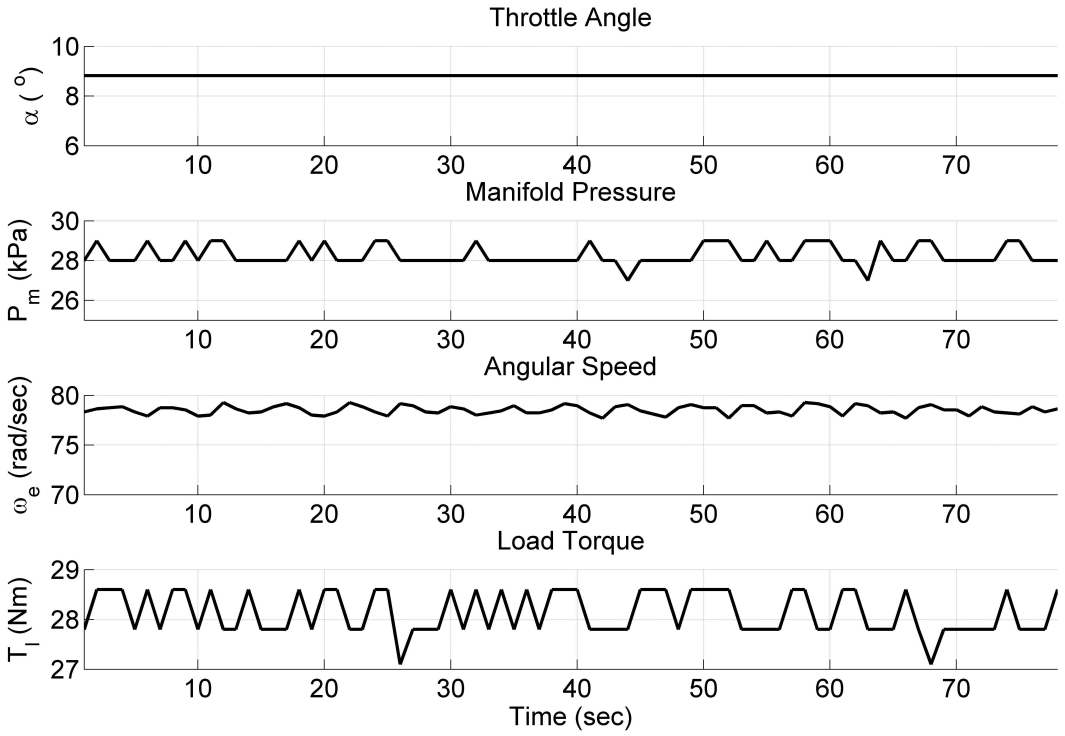

FIGURE 4.8: Input data acquired from OBD-II Scanner/Logger for proposed virtual sensors evaluation.

In the first phase of experimental evaluation, the sensors measurements were acquired from OBD-II kit as shown in Figure 4.8. The acquired data was supplied to the SOSM observer in *Eq (4.40)* to estimate angular speed from pressure dynamics. Similarly, the same data was supplied to SOSM Observer in *Eq (4.77)* for the estimation of manifold pressure from engine angular speed. The convergence of both designed observers for angular speed and manifold pressure estimation is shown in Figure 4.9. The initial conditions and injector parameters for the designed SOSM Observers are given in Table 4.4 and Table 4.5.

TABLE 4.4: SOSM Observer parameters for ω_e virtual sensor.

Parameter	Value
$\hat{x}_1(0)$	30 kPa
$\hat{x}_2(0)$	0
α_1	200
λ_1	18
α_2	550
λ_2	1527

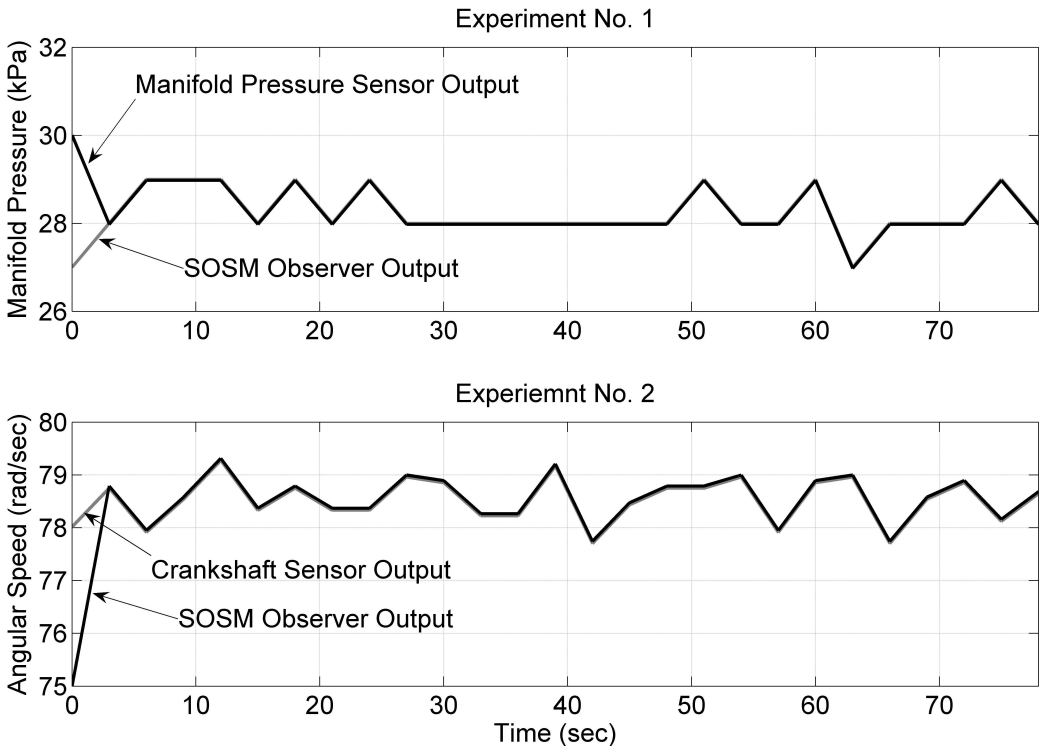

FIGURE 4.9: SOSM observers convergence for virtual sensor experiments.

TABLE 4.5: SOSM Observer parameters for P_m virtual sensor.

Parameter	Value
$\hat{x}_1(0)$	75 rad/sec
$\hat{x}_2(0)$	0
α_1	1
λ_1	1.5
α_2	1
λ_2	135

Figure 4.10 shows the measurements from actual sensors installed inside production vehicle engine and virtual sensors. It can be observed that virtual sensors efficiently track actual sensors as the measurements are with less than 8% error of the actual sensors readings. These minor delays in estimation results are due to reachability phase and do not influence the effectiveness of suggested fault diagnostic methodology. ■

The sequence of instantaneous values of all parameters acquired from *Eq (4.59)*, *Eq (4.60)*, *Eq (4.62)*, *Eq (4.61)*, *Eq (4.90)*, *Eq (4.91)* and *Eq (4.92)* would represent sampled version of their continuous-time nonlinear representations. The

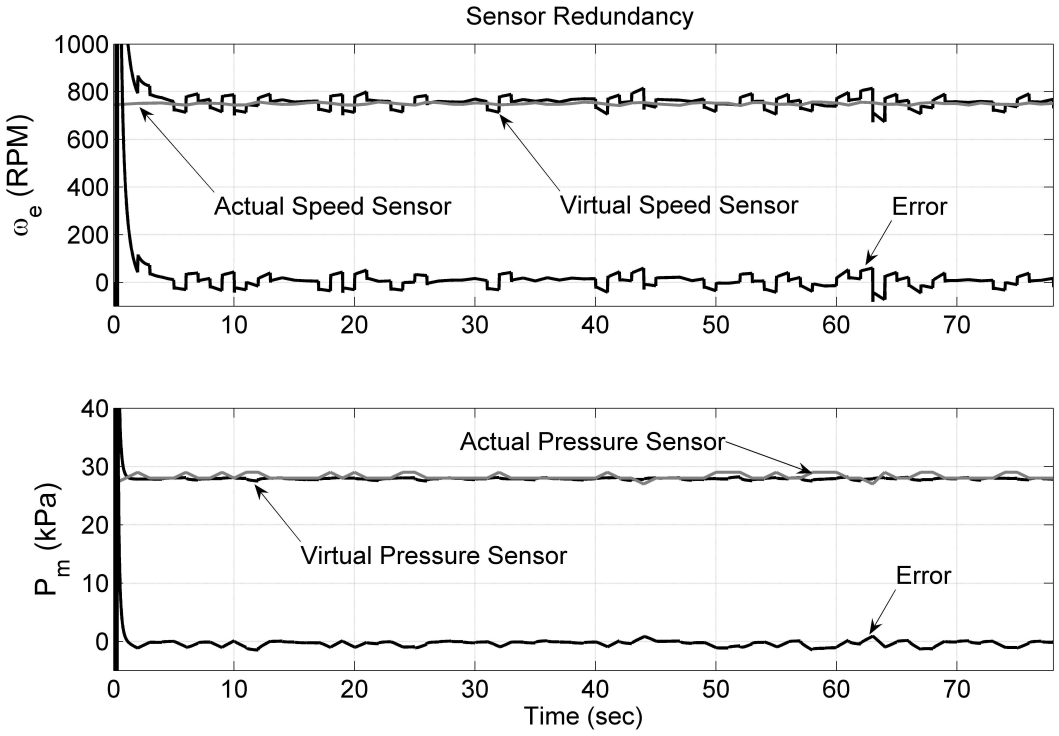

FIGURE 4.10: Measurements by actual and virtual Crankshaft and Pressure sensors, serving as redundancy.

smaller the sample time, each parameter will converge to its continuous time representation. Therefore, a reasonable sampling time 0.01 sec was used to evaluate the observers in all these experiments.

4.7 Conclusion

A second order sliding mode observer based parameter estimation scheme has been proposed for gasoline engine parameters. These critical parameters are unmeasurable in nature as no sensor can be installed to measure them. Similarly, virtual sensors for manifold pressure and angular speed are also devised from the suggested scheme. A successful evaluation of the presented scheme was conducted on 1.3L production vehicle engine. The parameters were estimated under normal operating conditions. The experimental results of estimation schemes were verified by the values of respective parameters found in literature. This practice gave an idea about the nominal operating values of these critical parameters. In the coming chapter these parameters will be explored for the diagnosis of gasoline engine health by estimating listed parameters under both healthy and faulty conditions.

Chapter 5

EXPERIMENTAL EVALUATION OF GASOLINE ENGINE FAULT DIAGNOSIS SCHEME

This chapter includes second order sliding mode observer based strategies for gasoline engine health monitoring. The presented strategies are based on the parameters estimated in preceding chapter. Among various sub systems of gasoline engine, the prime focus of fault diagnosis methodology in this thesis is air intake system. The prime responsibility of this system is to ensure strict proportions of air and fuel in air-fuel mixture in combustion chamber. The components of air intake system are air filter, intake manifold, throttle body, manifold pressure sensor and crankshaft sensor. Each of these components must be strictly monitored to ensure desired engine performance and fuel efficiency. This condition monitoring task can be achieved by estimating critical engine parameters. These critical parameters are observed under both healthy and defective operating engine conditions to generate residuals. These residuals are then evaluated to diagnose various air intake system faults. The presented scheme is successfully applied to a production vehicle engine. It is worth mentioning that on board diagnostic system of the vehicle is unable to diagnose these faults. Thus, adding to the importance and credibility of the presented scheme.

5.1 Experimental Setup

This section elaborates the experimental setup used for the validation of estimation and fault diagnosis scheme. The experimental setup comprises of an On-Board Diagnostic version II (OBD-II) compliant production vehicle engine equipped with engine control unit (ECU) and data acquisition/logging devices. The details of these experimental components are discussed below.

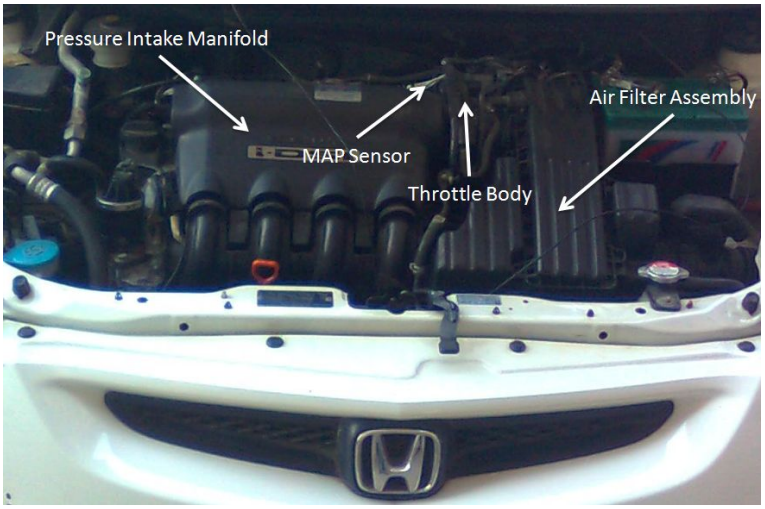

FIGURE 5.1: Honda i-DSI® engine experimental setup

5.1.1 Engine Rig

The production vehicle engine rig used in the experimentation can be seen in Figure 5.1. This engine is equipped with twin spark plugs and 2 valves per cylinder. Each spark plug has independent coil. The low friction designed engine has compact combustion chambers and the cam mechanism is chain driven. Other specifications can be seen in Table 5.1. The intelligent dual sequential ignition (i-DSI) makes the engine more fuel efficient with optimum performance, as fuel is ignited according to engine angular speeds. The engine is equipped with ECU which is compliant to OBD-II standards. This engine was selected for validation process as it meets all the bylaws outlined by environmental protection agencies in OBD-II document. However, some of the faults that effect engine performance and cause emissions are not taken care in the existing on-board diagnostic system. Thus, motivating the need to develop credible fault diagnostic methodology.

Attribute	**Specifications**
Variant	1.3 S
Type	i-DSI, 4-cylinder chain drive
Fuel Supply System	PGM-FI (Programmed Fuel Injection)
Engine Displacement (cc)	1339
Bore/Stroke (mm)	73.0 × 80.0
Compression ratio	10.4
Maximum power	63 kW (84 hp) @ 5700 rpm
Maximum torque	119 Nm (88 lb ft) @ 2800 rpm

TABLE 5.1: Honda i-DSI ® Engine Specifications.

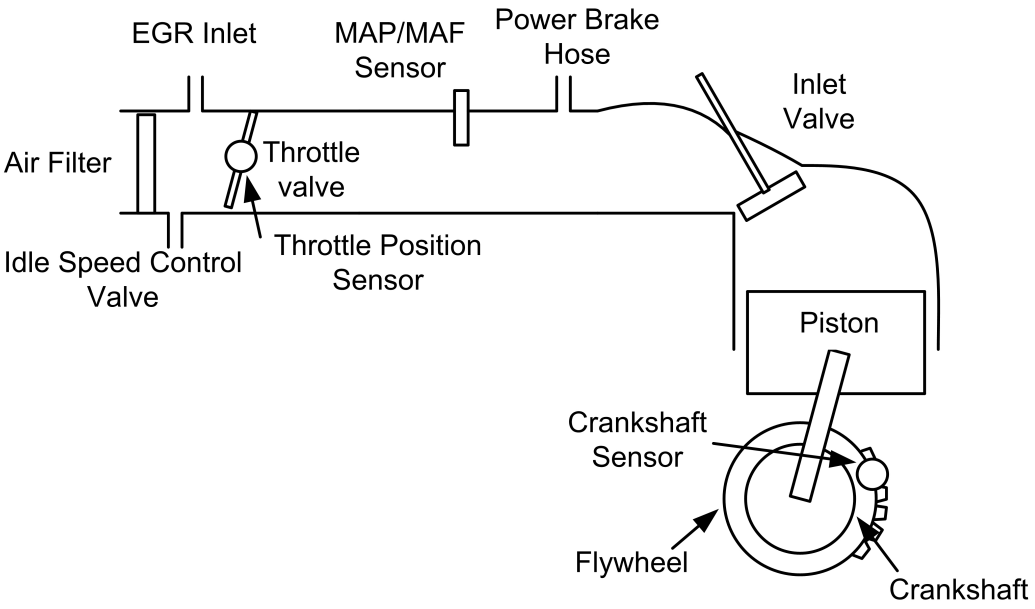

FIGURE 5.2: Schematic diagram of air intake system

This production vehicle engine has various sub systems, which play vital role in its performance. Among these sub systems, air intake system holds prime importance as it is responsible to maintain strict proportions of air and fuel in air fuel mixture. Any fault in air intake path or in its components will result in poor engine performance, degraded efficiency and emissions. Keeping in view the importance of air intake system, the parameter estimation based fault diagnosis scheme has been proposed in the last chapter to look after operations of air intake path and its components.

The schematic overview of air intake system is given in Figure 5.2. The hardware components of interest involved in air intake system are:

- Air Filter Assembly and Air Filter
- Bowden Cable Operated Throttle/Butterfly Valve
- Intake Pressure Manifold
- Sensors

- Manifold Pressure Sensor
- Crankshaft Sensor
- Throttle Position Sensor

Some of these components can be seen in Figure 5.1 in actual.

5.1.2 Engine Control Unit

The engine used for testing and evaluation of fault diagnosis scheme is equipped with Engine control unit(ECU)/engine control module (ECM). It is an embedded electronic device and its prime responsibility is to ensure optimum engine performance and fuel efficiency. This digital device reads signals from the sensors installed to measure respective phenomena and based on engine behavior it issues commands to actuators to execute necessary actions. The ECU comprises of a micro-controller, digital inputs/outputs, analog inputs/outputs, memory devices to store fuel maps and signal conditioning modules. These hardware components coordinate with each other through a built-in firmware.

Figure 5.3 gives an idea about the engine control unit. It can be seen that all sensors in the vehicle share their measurements with ECU. Among these sensors, some sensors are installed at air intake path like Manifold Air Pressure (MAP) sensor, Intake Air Temperature (IAT), etc. Some sensors are installed in air exhaust path like oxygen sensor. Similarly, crankshaft sensor is installed around fly wheel to measure engine angular speed. Based on the engine performance observed through sensors, ECU issues commands to injector and ignition system to ensure optimum performance.

One of the major tasks of ECU is to monitor and announce system health with the help of on-board diagnostics. Whenever there occurs a fault in the engine electronic system, ECU shifts to sub-optimal control strategy and announces the fault through Malfunction Indicator Light (MIL). Once the MIL is turned on the respective information can be acquired and analyzed for the fault rectification.

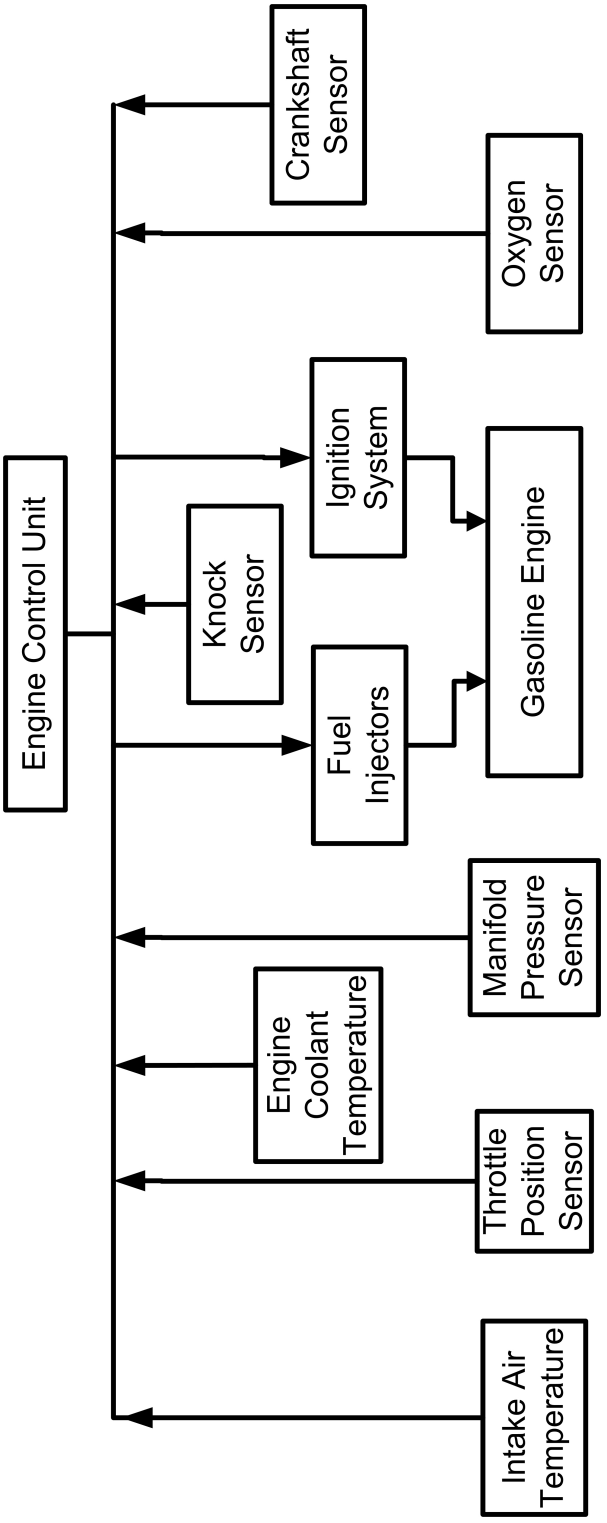

FIGURE 5.3: Schematic diagram of engine control unit

5.1.3 Sensors

The electronic vehicle engine shown in Figure 5.1 is heavily equipped with state of the art sensors. These sensors are heavily relied upon to monitor each of the vehicle subsystem precisely. Among number of sensors in electronic engine, the sensors involved in air intake system can help to monitor its health. Like, manifold absolute pressure (MAP) sensor is used to measure pressure inside the intake manifold. The pressure is sensed due to change in electrical resistance as the silicon chip in the sensor flexes with variable pressure. The rotational speed of the engine is measured by hall effect based crankshaft sensor. Similarly, throttle valve manipulations can be measured by the installed throttle position sensor (TPS). The throttle position is sensed due to change in magnetic field using a hall effect sensor. Another sensor in intake path is air intake temperature (IAT) sensor, its responsibility is to monitor the temperature of the air flowing through the intake path. As, the SOSM Observer based fault diagnostic (FD) is based on two state mean value engine model, therefore the sensors of interest will be MAP sensor, crankshaft sensor and TPS.

5.1.4 Data Acquisition

Each sensor installed in the engine is communicating with ECU. Sensor measurements can be acquired from ECU using OBD-II scanner. OBD-II cable is used to connect OBD-II scanner with ECU through the OBD-II connector. This connector is an essential and legal requirement in electronic fuel injection (EFI) engines. According to OBD-II bylaws, this connector is required to be within 2 feet (0.61 m) of the steering wheel. The scanner/logger is connected to laptop where the sensors data is displayed on graphical user interface, which can be analyzed and saved according to user requirements. The whole communication network is exchanging the information using ISO 9141-2 protocol. By using OBD-II data acquisition devices one can acquire measurements from MAP sensor in kilo Pascals (kPa), Crankshaft sensor in revolutions per minute (RPM) and TPS in degrees. Another requirement of SOSM Observer based fault diagnosis is load torque. The available OBD-II scanner/logger provides estimated values of load torque based on its static

and directly proportional relationship with manifold pressure. The load torque is measured as percentage of maximum available torque given in Table 5.1 i.e. 119 Nm [98].

5.2 Proposed Fault Diagnosis Evaluation Scheme

After going through the experimental setup details, the proposed fault diagnosis can now be understood more comprehensively. Among various air intake system faults, the following ones are planned to be monitored as they effect the engine performance negatively and still remain undiagnosed by the current on-board diagnostic system.

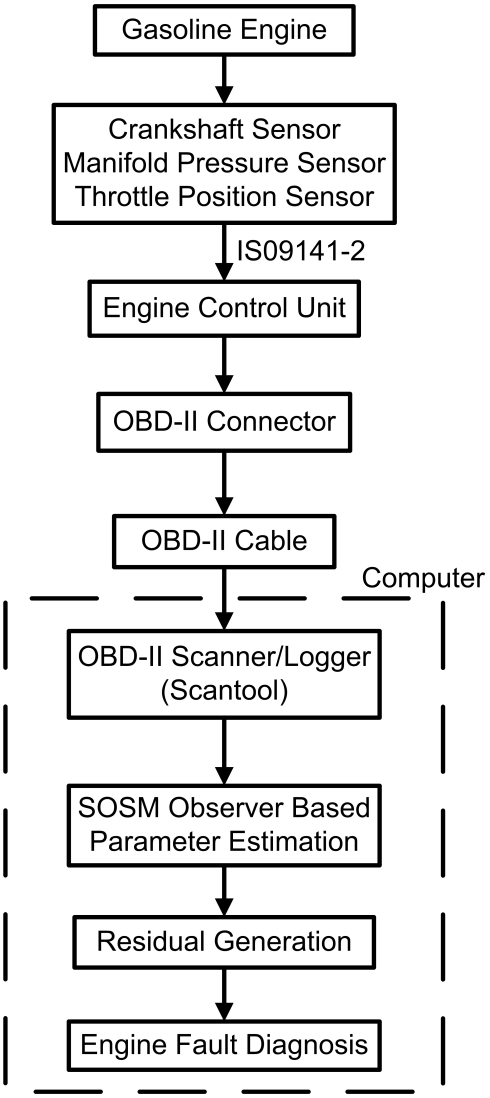

FIGURE 5.4: Experimental evaluation procedure for proposed fault diagnosis scheme.

1. Clogged Air Filter (System Fault)
2. Air Leakages in Intake Pressure Manifold (System Fault)
3. Loss of Effectiveness of Throttle Valve (Actuator Fault)
4. Defected Crankshaft Sensor (Sensor Fault)
5. Defected Manifold Pressure Sensor (Sensor Fault)

These faults can be efficiently monitored by the parameters outlined in Chapter 4. The estimated value of each parameter can reveal the health status of air intake path and its components. Like,

- Air filter discharge coefficient (C_{af}) can monitor air filter health.
- Throttle discharge coefficient (C_D) and volumetric efficiency (η_{vol}) can keep check on throttle body efficiency and pressure manifold leakages.
- Virtual MAP sensor ($\bar{P}_m$) can keep a watch on actual MAP sensor working.
- Virtual crankshaft sensor ($\bar{\omega}_m$) can observe actual crankshaft sensor working.

Figure 5.4 outlines discrete steps for the health monitoring of gasoline engine air intake system. These steps will be ensured for the detection of afore-mentioned faults. The steps are:

1. Gasoline engine will be operated in idle and steady state conditions.
2. Measurements from MAP Sensor, Crankshaft Sensor and TPS will be logged with the help of ODB-II scanner/logger as explained earlier.
3. SOSM Observer convergence will be achieved by selecting suitable gains of α_i, λ_i (i=1...4). The selected gains must satisfy *Eq (4.47)* .
4. The correcting injectors in *Eq (4.41)* and *Eq (4.42)* will be used to estimate the critical parameters.

5. The identified parameters will be compared with their nominal operating values to generate residuals.

6. The residuals will be evaluated to diagnose the respective fault in the air intake system.

The idle and steady state operating conditions are ensured so that the proposed health monitoring can be conducted. Under transient behavior it would become difficult to differentiate between the nominal and faulty values of the estimated parameters. The experimental procedure has been finalized after conducting number of experiments and those experimental procedure were finalized which helped in credible fault diagnosis. This practice is termed as *Active Diagnosis* [81]. In actual active diagnosis means that the system is manipulated is such a way that the hidden faults are exposed for diagnosis.

Remark 5.1. The residuals are evaluated based on thresholding techniques. The thresholds are identified after conducting fault diagnosis experiments. These thresholds can be made adaptive to the operating conditions but as the *active diagnosis* is under practice, fixed thresholds can deliver the acceptable results.

Remark 5.2. For the experimental evaluation of the parameter estimation based engine fault diagnosis, it has been assumed that only one of the afore-mentioned faults will occur at a time.

Now the diagnosis methodology for each of the afore-mentioned air intake system faults will be discussed in details alongwith its experimental results.

5.3 Air Filter Health Monitoring

Air filter effects on engine performance have been discussed in Section 2.3.1.1. Intake manifold pressure dynamics in *Eq (3.24)* can be exploited to monitor its health. These dynamics are used to develop SOSM Observer given in *Eq (4.40)*. The resultant injectors can be used to estimate air filter discharge coefficient (C_{af}) as follows.

$$C_{af} = \frac{(\bar{z}_1 + \hat{x}_2 + A_2 \eta_{vol} x_1 \omega_e)}{A_{10}} \qquad \textit{Eq (5.1)}$$

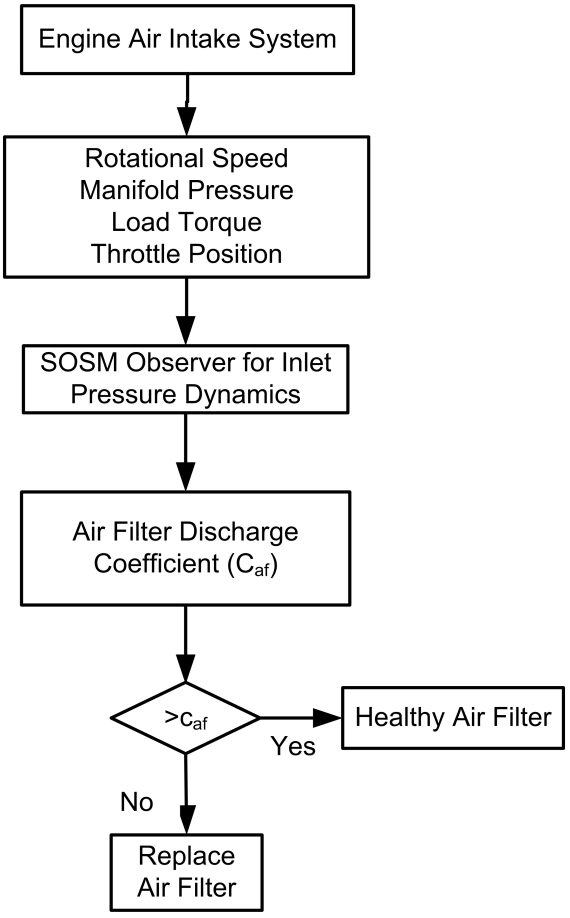

FIGURE 5.5: Air filter fault Diagnosis Methodology

C_{af} provides solid grounds to monitor air filter health, as it measures the hindrance in air flow through air intake path caused by air filter. Figure 5.5 outlines the steps necessary to classify air filter as clogged or healthy.

5.3.1 Data Acquisition & Experimentation

The measurements acquired from OBD-II scanner are used as input for SOSM Observer. Figure 5.7 shows the ECU equipped engine variables i.e. Manifold pressure (P_m), angular speed (ω_e), throttle angle (α) and load torque (T_l). It can be observed that under steady state conditions, throttle valve remained at 18^o. Extra loads on engine were induced at $88s$. With these inputs to the engine, the manifold pressure and angular speed can be seen as well. It can be observed that the measurements are corrupted with acquisition noise and engine behavior even in steady state conditions. The similar trends will contribute in estimation results.

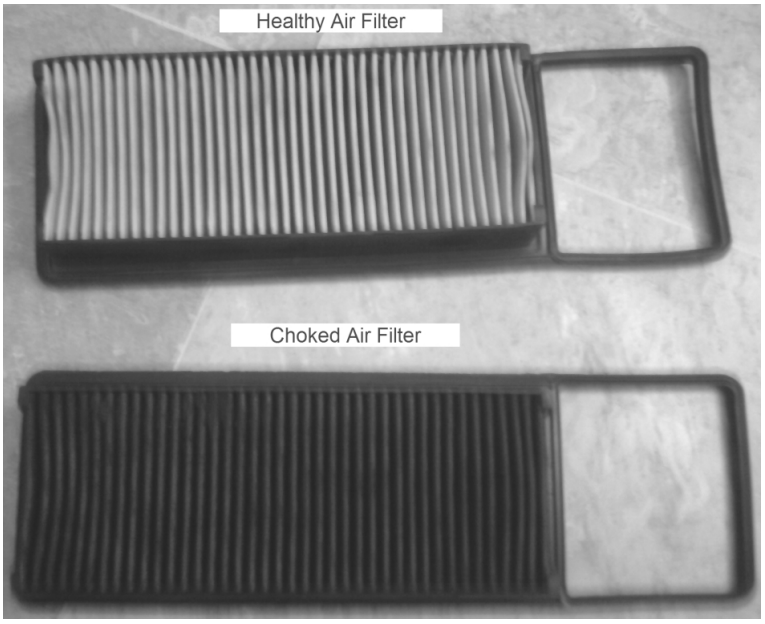

FIGURE 5.6: Clogged and healthy air filters used for experimentation.

Figure 5.6 shows the healthy and clogged air filter used in the diagnosis procedure. It was observed that at low angular speeds and low loads, both air filters provided sufficient amount of air required by engine to carry out normal operations. So, it was not possible to diagnose air filter health at low operating speeds. An experiment was conducted in steady state conditions at higher angular speeds and loads. The throttle angle was kept at 18^o and loads were induced by turning on air conditioner, headlights, screen wipers and fan.

5.3.2 Fault Diagnosis Results

The acquired data sets (Figure 5.7) served as input for proposed estimation and diagnosis scheme. In the first phase, observers convergence was achieved. Figure 5.8 shows the P_m of 1.3L engine & observers output and the convergence error for both air filters. It can be seen that throughout the experiments, SOSM Observers efficiently tracked the actual values of manifold pressure. The estimators error remained near to zero. The SOSM Observer gains and initial conditions were chosen as given in Table 5.2. While tuning observer parameters for the demonstrated results, initially the conditions on α_1 and λ_1 given in *Eq (4.47)* were ensured according to Remark 4.5. Later on, these gains were manipulated to get healthy values of the parameters as found in the literature. The same SOSM Observer

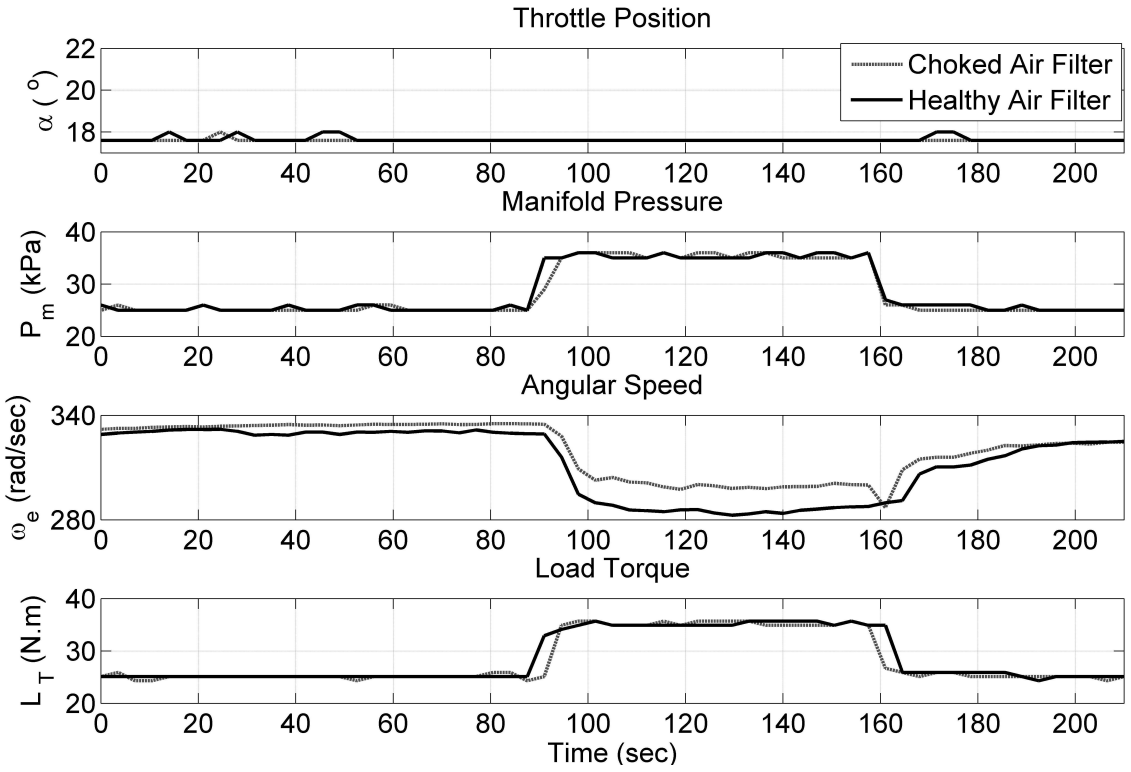

FIGURE 5.7: Data acquired when both clogged and healthy air filter were used for diagnostic experiment.

gains were used for faulty conditions, thus revealing abnormal values of the same parameters.

Figure 5.9 depicts the estimated parameters. It can be observed that η_{vol} remained around 0.7 for both air filters. The value of C_{af} differed in case of healthy & clogged air filter. C_{af} remained around 0.3 for clogged air filer and for healthy air filter it remained around 0.9. The rise in C_{af} and decline in η_{vol} at $88s$ was due to increase of air demand to cater for high loads. As the engine was operating under ECU commands being issued according to lookup maps working on engine speed, η_{vol} was maintained around 0.7 by ECU for both air filters. However, the

TABLE 5.2: SOSM Observer parameters for C_{af} estimation.

Parameter	Value
$\hat{x}_1(0)$	25 kPa
$\hat{x}_2(0)$	0
α_1	10
λ_1	40
α_2	10
λ_2	190

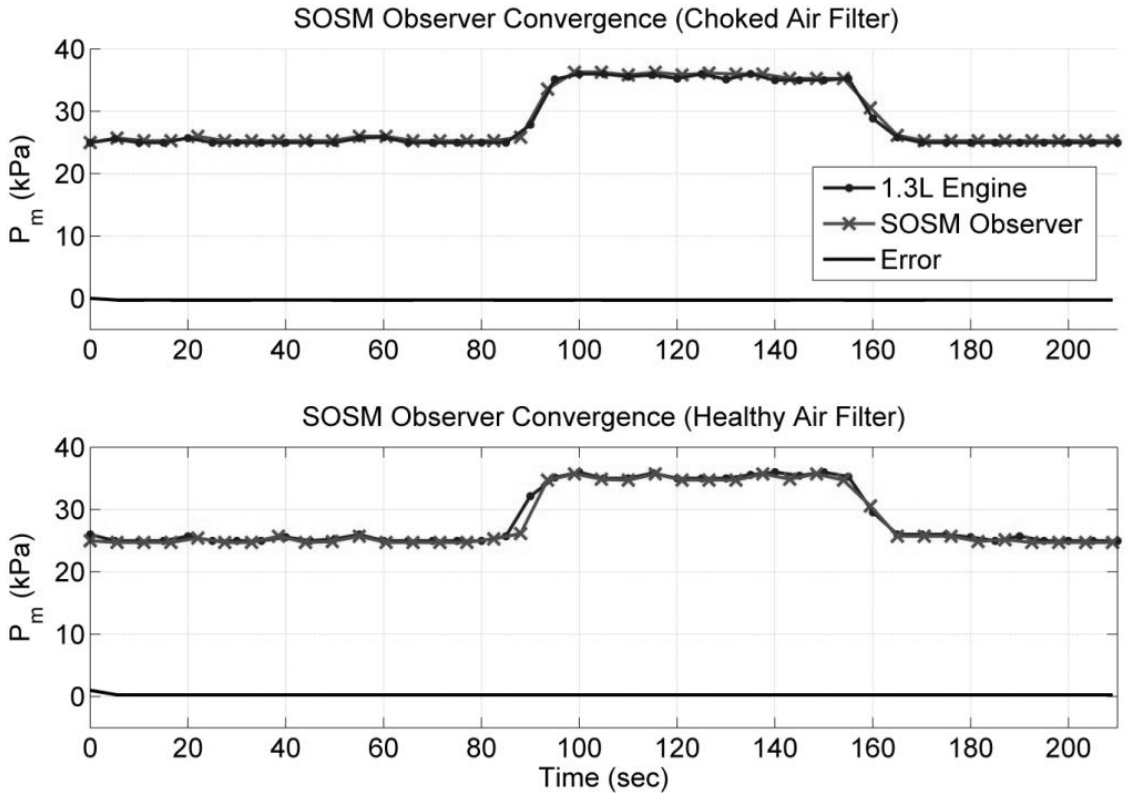

FIGURE 5.8: Observer Convergence for Air Filter Experiment

interruption in air flow due to air filter remained the same even in ECU control. This uncertain hindrance in air flow was modeled under $\bar{z}_1$ by the designed SOSM Observer. Later on, C_{af} was calculated based on $\bar{z}_1$. That is why, C_{af} varied in both cases as it is the measure of obstruction in air flow due to air filter. After the experimental evaluations, it can be observed that a value below $c_{af} < 0.30$ of C_{af} indicates air filter replacement and a value closer to '1' refers to healthy air filter. Thus classification of healthy and clogged air filter is ensured.

5.4 Monitoring of Manifold Leakages and Throttle Body Efficiency

Keeping in view the effects of air leakages and reduced throttle body efficiency on engine performance in Section 2.3.1.2, a diagnostic methodology is devised to cater for these problems. For this purpose, the proposed health monitoring methodology is shown in Figure 5.10. It is proposed that following relations of volumetric efficiency (η_{vol}) and throttle discharge coefficient (C_D) can be efficiently

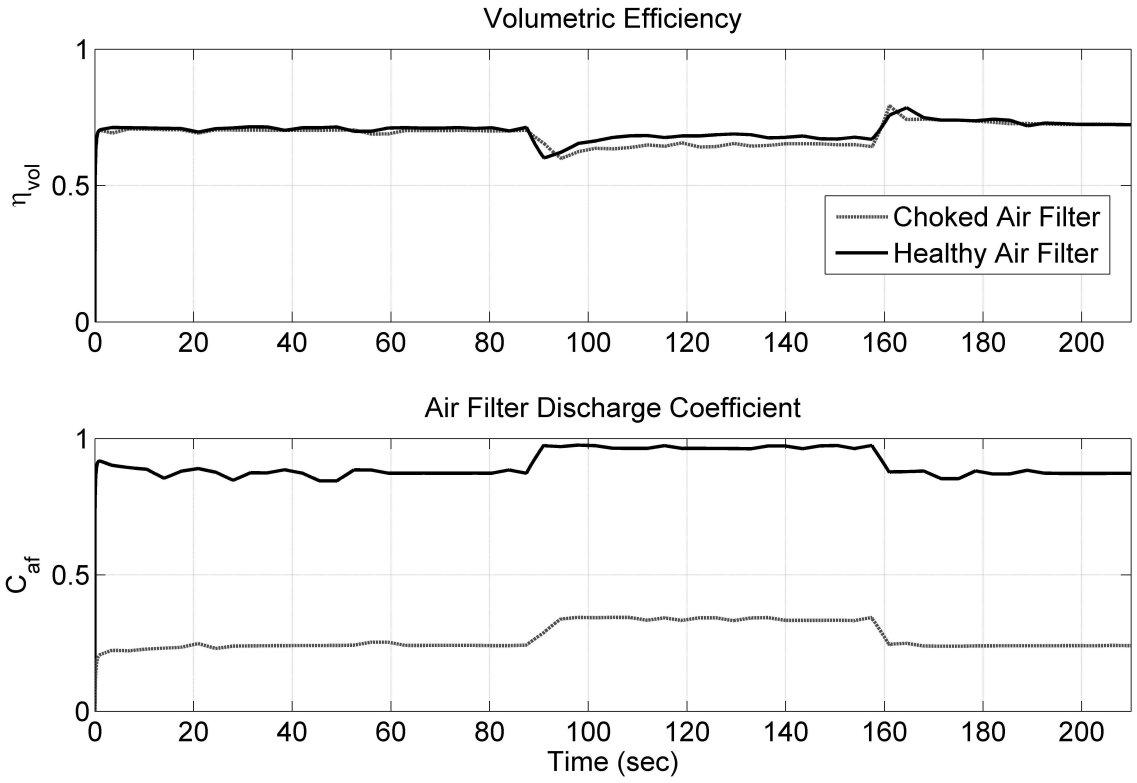

FIGURE 5.9: Air filter parameter estimation results

used to monitor these faults.

$$\eta_{vol} = \frac{(A_5 + A_6 + A_8) \pm \sqrt{(A_5 + A_6 + A_8)^2 + 4A_7\bar{z}_2}}{A_7} \qquad Eq\ (5.2)$$

$$C_D = \frac{(\bar{z}_1 + \hat{x}_2 + A_2\eta_{vol}x_1x_3)}{A_9} \qquad Eq\ (5.3)$$

These parameters are estimated using pressure and angular speed dynamics given in *Eq (3.36)*. The engine pressure dynamics are observed through the SOSM Observer in *Eq (4.40)*. The estimation of η_{vol} and C_D is performed with the help of Manifold pressure (P_m), angular speed (ω_e), throttle angle (α) and load torque (T_l) being acquired from OBD-II scanner/logger. Once these parameters are estimated, their values can be compared with their normal operating ranges. Any deviation in their nominal values will help to generate respective residuals R_{C_D} and $R_{\eta_{vol}}$ defined as

$$R_{C_D} = C_{D_{nominal}} - C_{D_{actual}} \qquad Eq\ (5.4)$$

$$R_{\eta_{vol}} = \eta_{vol_{nominal}} - \eta_{vol_{actual}} \qquad Eq\ (5.5)$$

The thresholds constant are C_1 and C_2. These constants can ideally be zero but practically 10% values of C_1 & C_2 can provide sufficient tolerance to detect faults. These generated residuals will indicate the respective fault and its severity. Furthermore, for the isolation of manifold leakages and reduced throttle body efficiency the signs of residual will be analyzed. Negative values of R_{C_D} and positive values of $R_{\eta_{vol}}$ will indicate leakages in manifold. Similarly, positive values of R_{C_D} and negative values of $R_{\eta_{vol}}$ will specify reduced throttle body efficiency. Therefore, the above discussed faults in air intake system can be efficiently diagnosed by the proposed methodology.

5.4.1 Manifold Leakage Detection

The first experiment involves the detection and identification of air leakage in manifold. Figure 5.12 shows the data acquired from OBD-II scanner. It can be observed that throttle angle remained at 9.8^o (Idle Position) throughout the experiment. The leakages were introduced according to the Table 5.3 as shown in Figure 5.11. As the air flow increases due to leakages, the surge in angular speed can be visualized as well. However, manifold pressure and load torque are solemnly effected due to manifold air leakages. The oscillatory behavior of angular speed and manifold pressure depicts the ECU control action trying to cater these manifold leakages. Initially, it was noticed during the experimentation that minor leakages were successfully controlled by the ECU control action. However, as the leakage diameter was increased ECU was unable to maintain the engine performance as seen in the acquired data. On the other hand, exhaust emissions started to increase and engine stumbled with the increase in leakages. One can observe peaks at 180 seconds in the data acquired from OBD-II scanner/logger. These peaks are due to manual experimentation as precise setup for introducing manifold leakages in production vehicle was not available. The air leakages in pressure manifold were introduced with the help of power brake hose. This hose connects intake manifold with brake drum. The hose diameter is $5mm$ and it was removed for the experiment. Initially, the approximate diameter of leakage was kept at $2mm$ to introduce leakages and gradually it was increased to $5mm$ with time as shown in Figure 5.11.

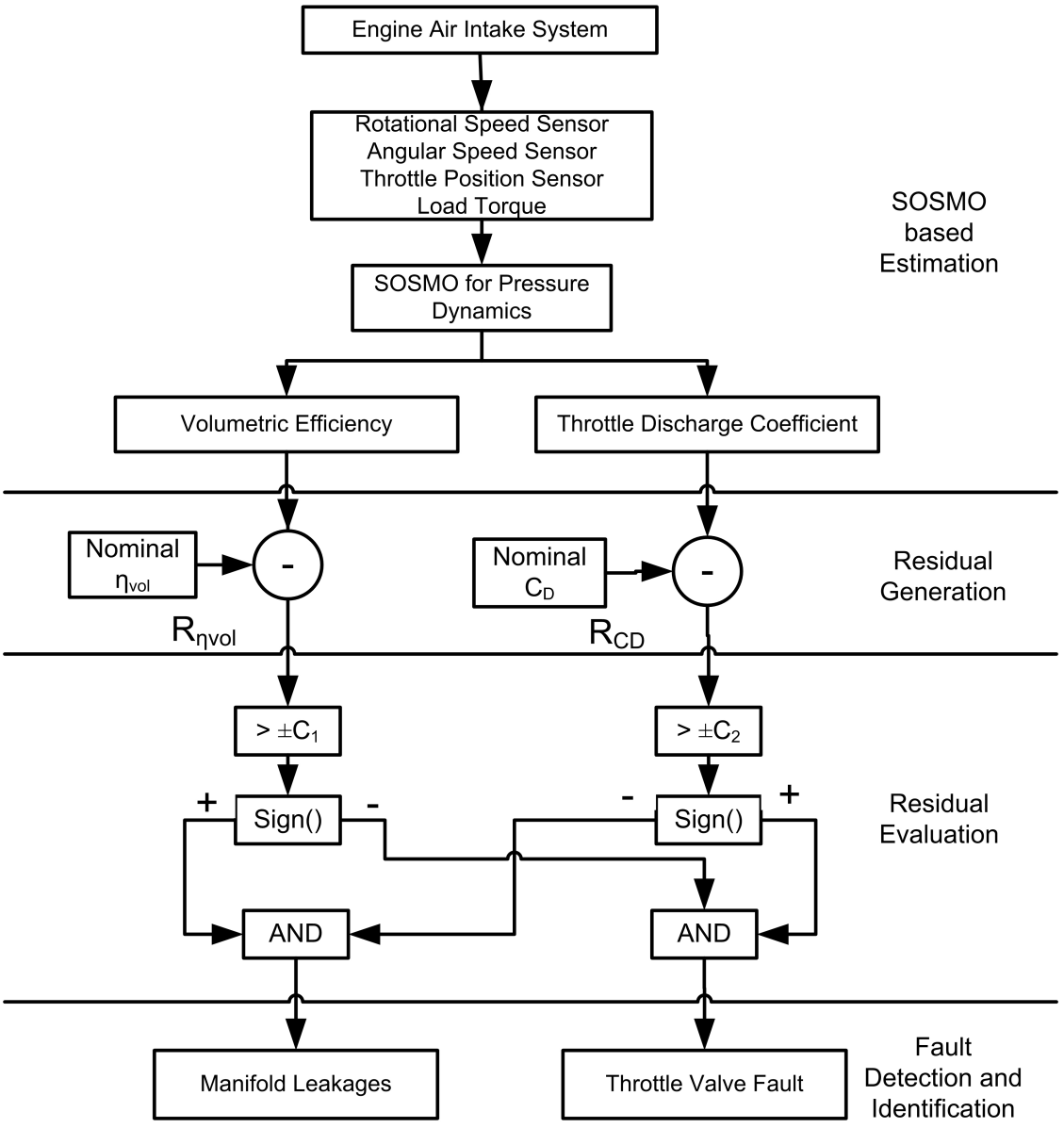

FIGURE 5.10: Manifold leakage and reduced throttle body efficiency monitoring methodology.

5.4.1.1 Manifold Diagnosis Results

The obtained data was given to the designed SOSM Observer in *Eq (4.40)*. The parameters of the designed SOSM Observer are enlisted in Table 5.4. Again the tuning of observer parameters for the demonstrated results was carried out according to Theorem 4.4 through Remark 4.5. Later on, these gains were manipulated to get healthy values of the parameters as found in the literature. The same SOSM

Leakage Diameter (Approx)	Time of Leakage Introduction
2mm	182 seconds
3mm	357 seconds
4mm	679 seconds
5mm	959 seconds

TABLE 5.3: Increase in Manifold Leakage Area with time.

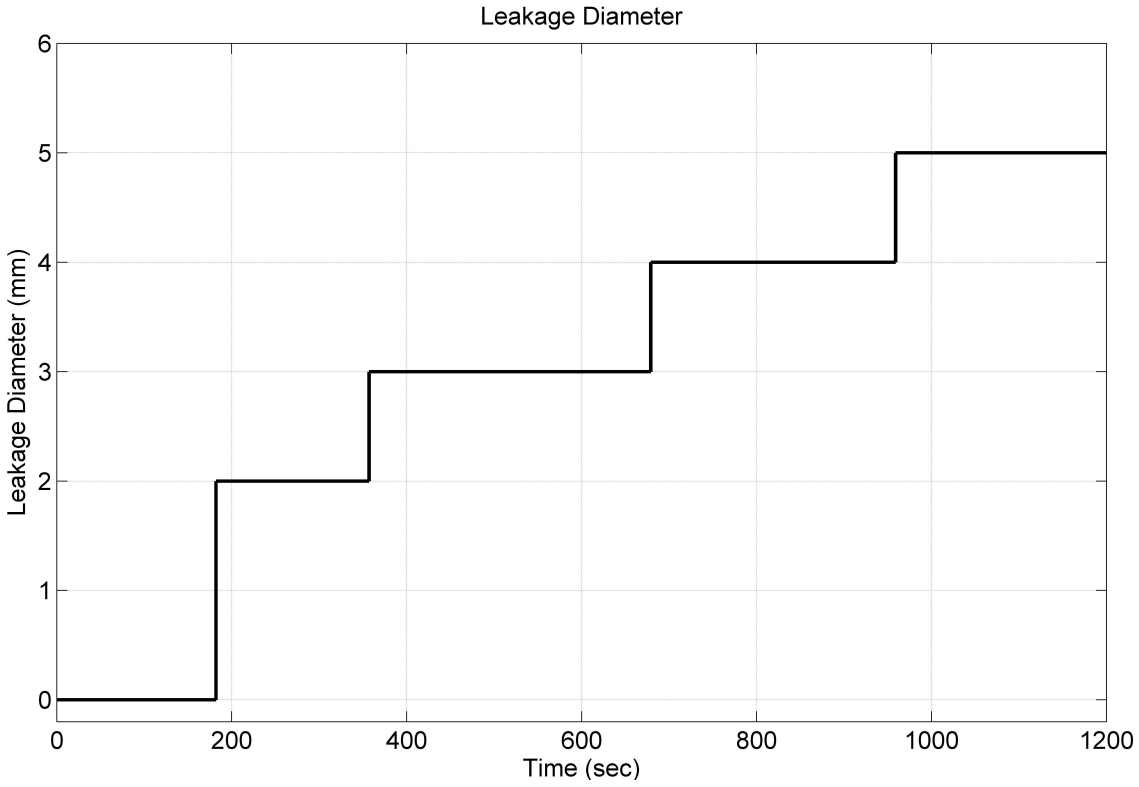

FIGURE 5.11: Introduction of leakages in pressure manifold with time.

Observer gains were then used in faulty conditions, thus revealing abnormal values of the same parameters.

The observer convergence in the presence of leakage in intake manifold is displayed in first result of Figure 5.13. It can be observed that the convergence is achieved within one second as the convergence error remained near to zero through out the experiment. The slight tracking error seen in Figure 5.13 is due to demonstration of results such that the responses can be distinguished, however in actual the error is near to zero.

After the SOSM Observer convergence was achieved, the computed injector signals z_1 and z_2 were used for the estimation of un-measurable critical parameters C_D and η_{vol}. It can be observed that under normal operating conditions (before 182

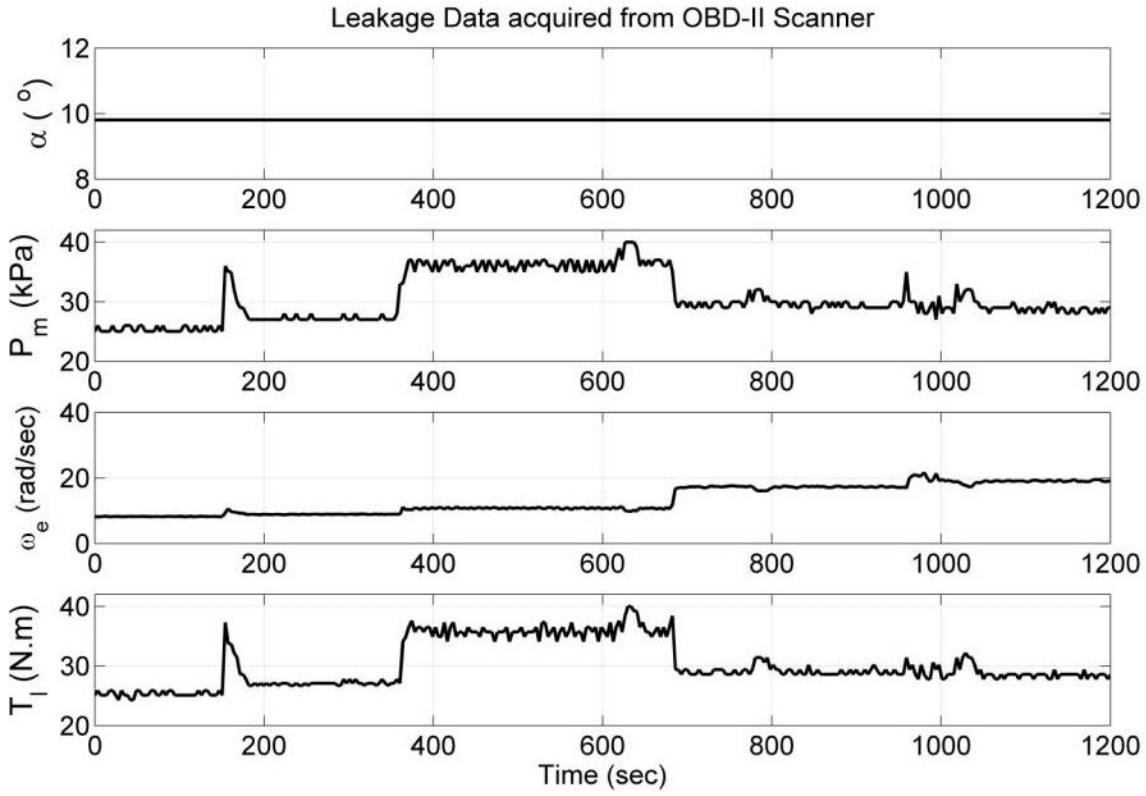

FIGURE 5.12: Experimental data for Manifold Leakages

seconds), the values of the estimated parameters corresponded to their actual values as discussed in [50]. However, as the leakages were introduced, uncontrolled air flow increased in pressure manifold. In other words, the pumping efficiency of the engine reduced as it was unable to pump all of the available air. The same trends can be observed in estimated parameters. The increase in C_D indicates the increase in air flow through intake manifold. Similarly, the decrease in η_{vol} shows the decrease in pumping capacity of engine due to increase in air flow in the manifold.

The nominal operating values of estimated parameters (values before 182 seconds

Parameter	**Value**
$\hat{x}_1(0)$	26 kPa
$\hat{x}_2(0)$	0
α_1	1
λ_1	1.5
α_2	30
λ_2	140

TABLE 5.4: SOSM Observer parameters for manifold leakage detection.

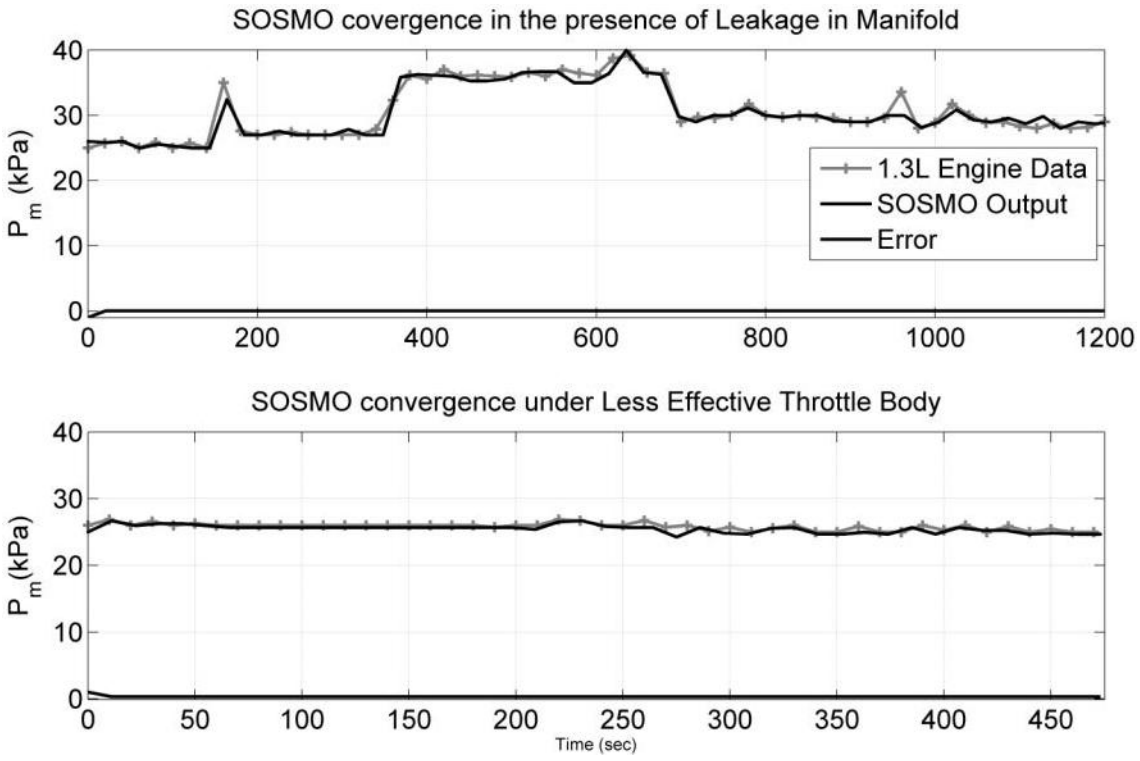

FIGURE 5.13: Observer Convergence for Manifold Leakages and reduced throttle body efficiency.

in Figure 5.14) and faulty operating values (values after 182 seconds in Figure 5.14) are used to generate residuals. These residuals are generated according to *Eq (5.4)* and *Eq (5.5)*. The residuals generated due to deviation in nominal values of estimated parameters can be visualized in Figure 5.15. The detection and identification of air leakage can be performed easily based on these residuals. Decrease in R_{C_D} and increase in $R_{\eta_{vol}}$ represent leakage in manifold and respective magnitudes can be further analyzed to quantify the severity of the air leakages.

Remark 5.3. It can be visualized that when the leakage area was increased at 679 seconds in Figure 5.12, the pressure sensor started to generate false readings. One possible reason can be the location of installed sensor, which is at 6 inches away from the leakage in manifold (One can visualize the leakage location in Figure 5.2, the leakage was introduced near power brake hose). The performance of the engine started to decline and ECU was unable to detect and announce malfunctioning of engine as malfunction Indication Light (MIL) remained off through out the experiment.

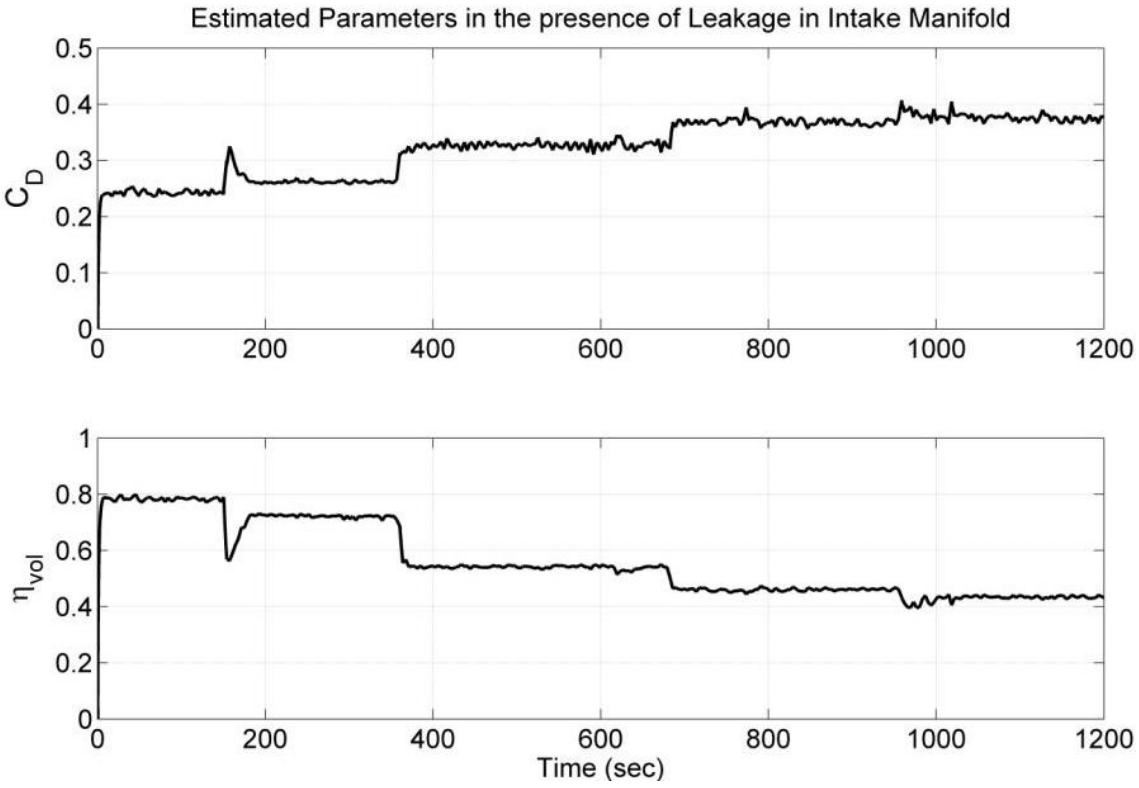

FIGURE 5.14: Estimated values of C_D and η_{vol} from pressure manifold dynamics in the presence of leakages.

5.4.2 Reduced Throttle Body Efficiency

The second experiment involved the detection and identification of reduced throttle body efficiency (throttle valve fault). Figure 5.16 depicts the data acquired from OBD-II scanner and logger. It can be visualized that throttle angle remained at 16.4^o throughout the experiment instead of 9.8^o. The reduction in A_E at 9.8^o did not allow much provision to emulate throttle body fault. Therefore, the idling throttle angle was kept at higher values as it facilitated with large effective throttle area (A_E) that can be blocked to emulate reduced throttle body efficiency. The efficiency was reduced by decreasing A_E according to Table 5.5 as shown in Figure 5.17. This reduction in A_E represents throttle body fault. As the required amount of air is reduced due to blockage of A_E, decrease in angular speed can be visualized as well. The decrease in rotational speed is due to reduced power produced as lesser amount of air fuel mixture was available in combustion chamber. This data was then supplied to SOSM Observer and its convergence was achieved as shown in second result of Figure 5.13. The SOSM Observer parameters were

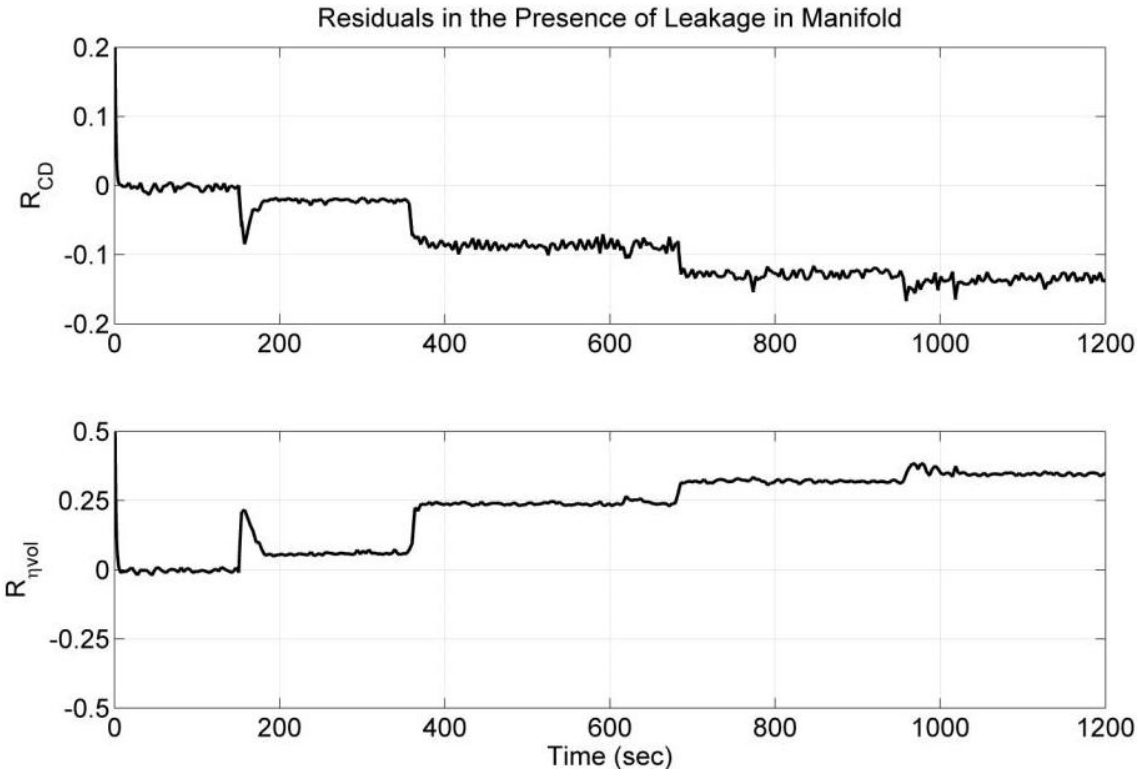

FIGURE 5.15: Resultant residuals in the presence of manifold leakages

chosen as shown in Table 5.6. The tuning of SOSM Observer gains was performed as discussed in preceding experiments.

Reduced A_E in %	**Time of Blockade Introduction**
10%	115 seconds
22%	196 seconds
48%	280 seconds
60%	350 seconds

TABLE 5.5: Decrease in Effective Throttle Area

5.4.2.1 Throttle Body Fault Diagnosis Results

Once the second order sliding mode was achieved, the respective parameters were estimated. Figure 5.18 shows estimated C_D and η_{vol} in the presence of throttle fault. It can be noticed that due to decrease in A_E, the air flow in air intake system decreases as C_D is reduced. The other outcome of blocked A_E was the engine started pumping more of the available air, thus its pumping efficiency increased as shown in Figure 5.18. The nominal values of estimated parameters when engine was working normally till 115 seconds, were used to generate residuals. These residuals were evaluated for detection and identification of throttle fault. The

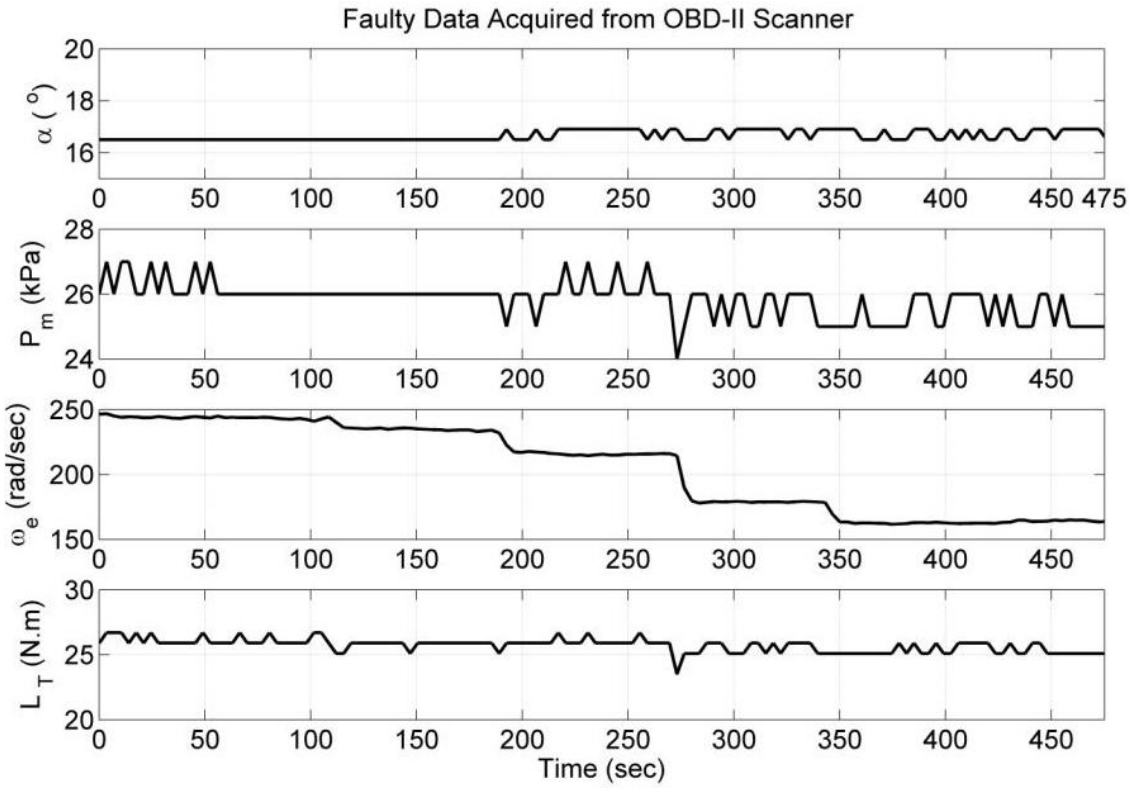

FIGURE 5.16: Experimental data for reduced throttle body efficiency attained by blocking throttle effective area.

Parameter	Value
$\hat{x}_1(0)$	25 kPa
$\hat{x}_2(0)$	0
α_1	5
λ_1	30
α_2	3
λ_2	80

TABLE 5.6: SOSM Observer parameters for throttle fault detection

increase in R_{C_D} and decline in $R_{\eta_{vol}}$ actually represented engine behavior in the presence of A_E blockage as discussed earlier. The magnitude of the respective residuals can be further analyzed for the severity of A_E blockage.

Remark 5.4. It is interesting to note that due to blockage in A_E, the engine performance started to decline as diagnosed and shown in Figure 5.16. However, ECU was unable to detect the respective fault as MIL was off throughout the experiment.

Remark 5.5. It can be observed that under high speeds (Figure 5.16), the estimated parameters (C_D & η_{vol} in Figure 5.14 and Figure 5.18) possess different nominal

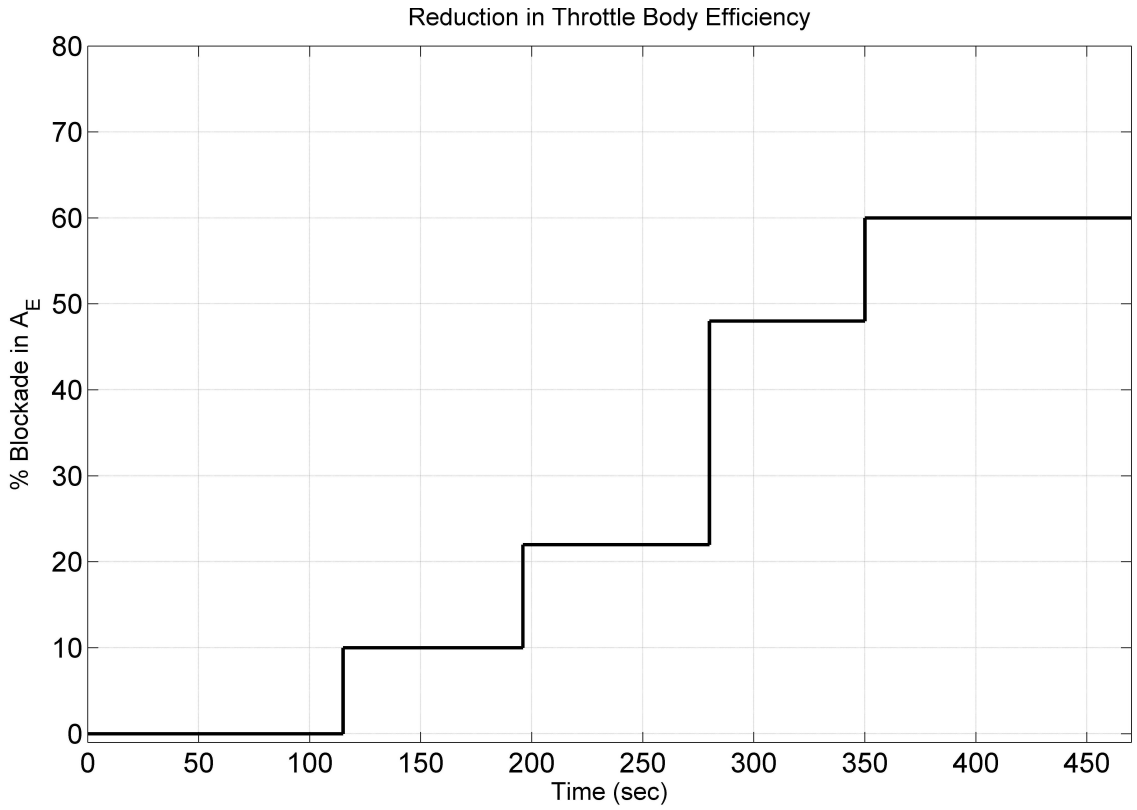

FIGURE 5.17: Decrease in Effective Throttle Area due to blocking throttle effective area.

operating values as compared to values in low speeds (Figure 5.12) [50]. Thus the results strengthens the motivation for estimation scheme as these parameters have different values at different operating conditions.

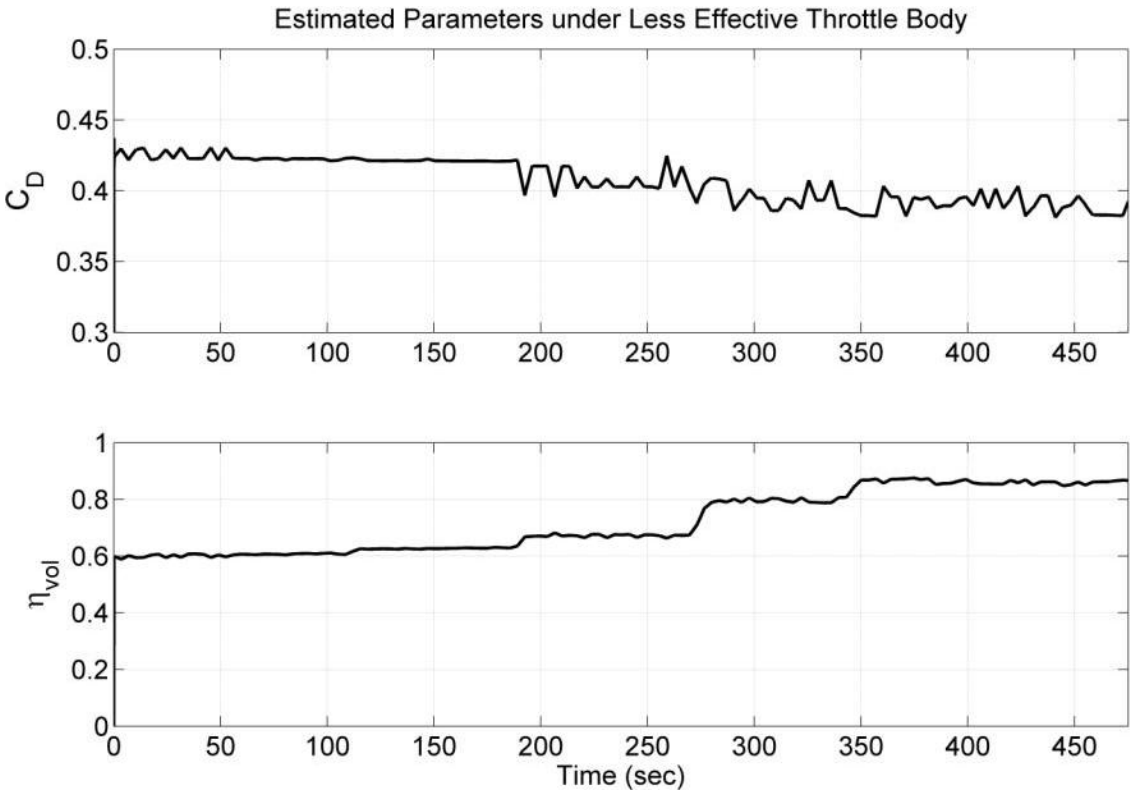

FIGURE 5.18: Estimated C_D and η_{vol} (Reduced A_E)

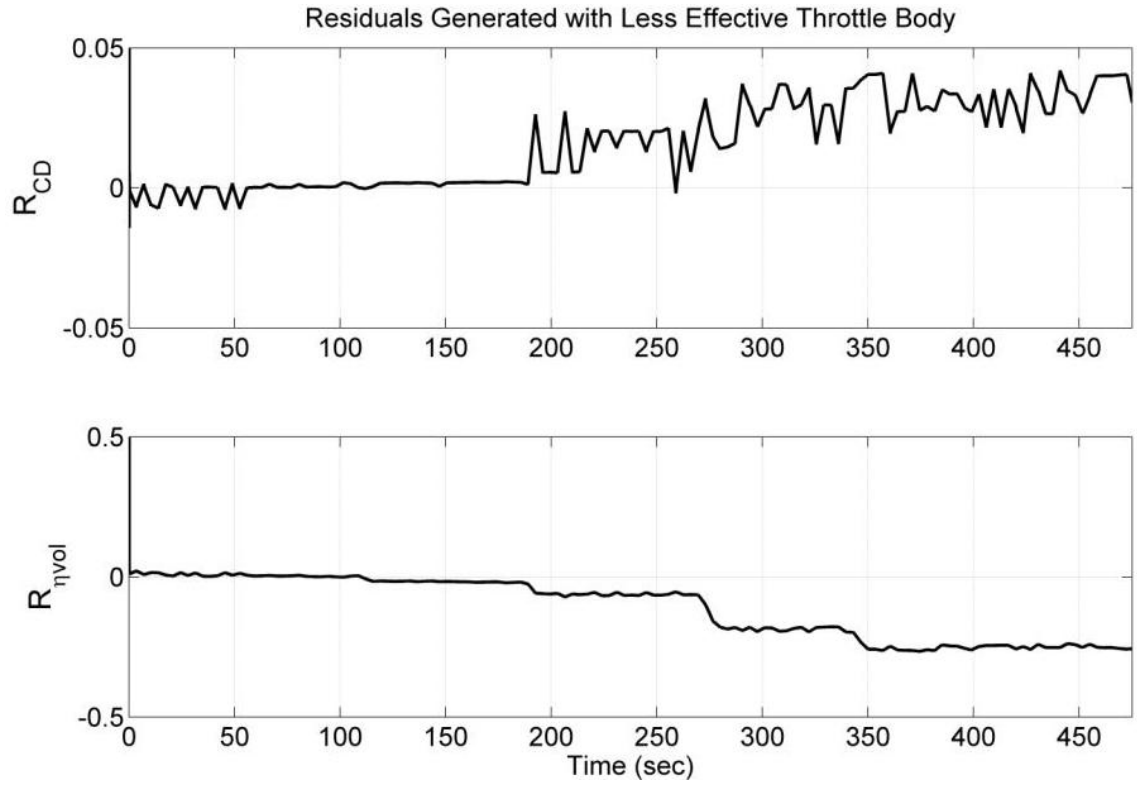

FIGURE 5.19: Residuals (Reduced A_E)

5.5 Sensor Fault Diagnosis Scheme

The last and major outcome of the proposed scheme is the fault diagnosis of the installed sensors in air intake system. Figure 5.20 describes the fault diagnosis methodology for pressure and angular speed sensor. The SOSM Observer designed in *Eq (4.40)* used measurements from manifold pressure sensor to watch engine angular speed through *Eq (4.62)*. Similarly, SOSM Observer designed in *Eq (4.77)* utilized measurements from crankshaft sensor to monitor manifold pressure using *Eq (4.92)*.

These estimated values were compared with the actual sensor measurements to generate residuals. In healthy circumstances, the following residuals should remain within a bound (Thresholding).

$$r_1 = P_m - \bar{P}_m \qquad Eq\ (5.6)$$

$$r_2 = \omega_e - \bar{\omega}_e \qquad Eq\ (5.7)$$

These thresholds are defined under c_p for pressure sensor and c_w for crankshaft sensor. Ideally, c_p and c_w can be zero but in actual 10% values of these constants can provide sufficient tolerance. Under faulty condition, the residuals will exceed the defined bound and sensor fault can be detected well in time. All the sensor faults: bias, drift, scaling, freeze and drop-out, will certainly let the residuals to cross the defined bounds. The moment the residuals cross the defined thresholds, respective sensor fault will be announced on time.

5.5.1 Data Acquisition & Experimentation

In order to validate virtual sensors, an experiment was conducted in steady state conditions while idling. By steady state condition it was meant that: throttle valve and load on engine were kept constant through out the experiment. Under steady state conditions, throttle value remained at 9.8^o. The nominal load on

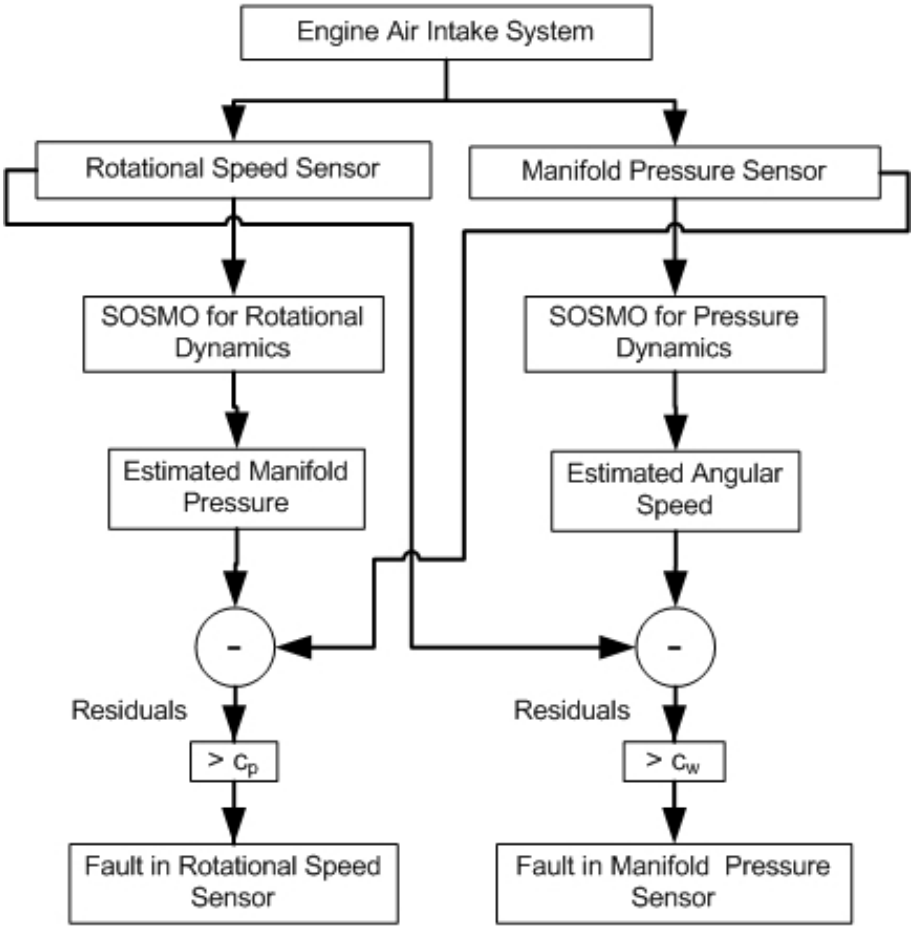

FIGURE 5.20: Air intake system sensors fault diagnosis methodology.

engine was contributed by: engine rotating mass e.g. crank shaft, fly wheel, power train components engaged. As no extra load is induced, load torque remained around 29 Nm. With these inputs to the engine, the pressure and rotational speed remained in steady state conditions.

The prime requirement of the proposed scheme was the convergence of observers in *Eq (4.40)* and *Eq (4.77)*. Figure 5.21 shows the 1.3L engine and SOSM Observers output. The SOSM Observers gains and initial conditions were taken as shown in Table 4.4 and Table 4.5. It can be seen that throughout the experiments, SOSM Observers efficiently track the actual values of manifold pressure and angular speed. The estimators error remain near to zero. The robustness of the scheme can be observed when the observers are tracking the sensors reading even in the presence of variations in engine behavior. Once the observers convergence was achieved, sensors fault diagnosis can be conducted.

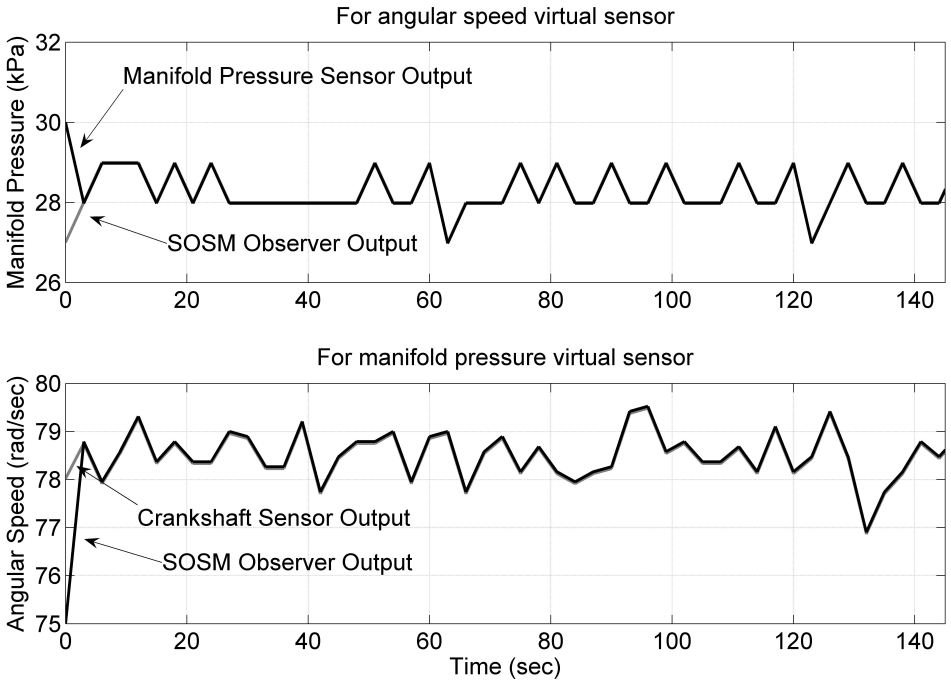

FIGURE 5.21: SOSM Observer convergence for pressure and angular speed dynamics, to be used for sensors fault diagnostics.

Remark 5.6. It was ensured that SOSM Observer parameters (α_1, α_2, λ_1 and λ_2) satisfy Theorem 4.4 by employing Remark 4.5 and these parameters were further tweaked till the virtual sensors outputs started to reproduce/duplicate actual sensor measurements.

5.5.2 Sensor Fault Diagnosis Results

The functioning of the sensors involved in air intake system can be monitored with the help of following virtual sensors developed in previous chapter.

$$\bar{x}_3 = \bar{\omega}_e = \frac{1}{\eta_{vol} A_2 x_1}(A_9 - (\bar{z}_1 + \hat{x}_2)) \qquad Eq\ (5.8)$$

$$\bar{x}_1 = \bar{P}_m = \frac{1}{B_3}(J_e(\hat{x}_4 + \bar{z}_3) + B_4) \qquad Eq\ (5.9)$$

These virtual sensors have been validated against actual sensor as shown in Figure 4.10.

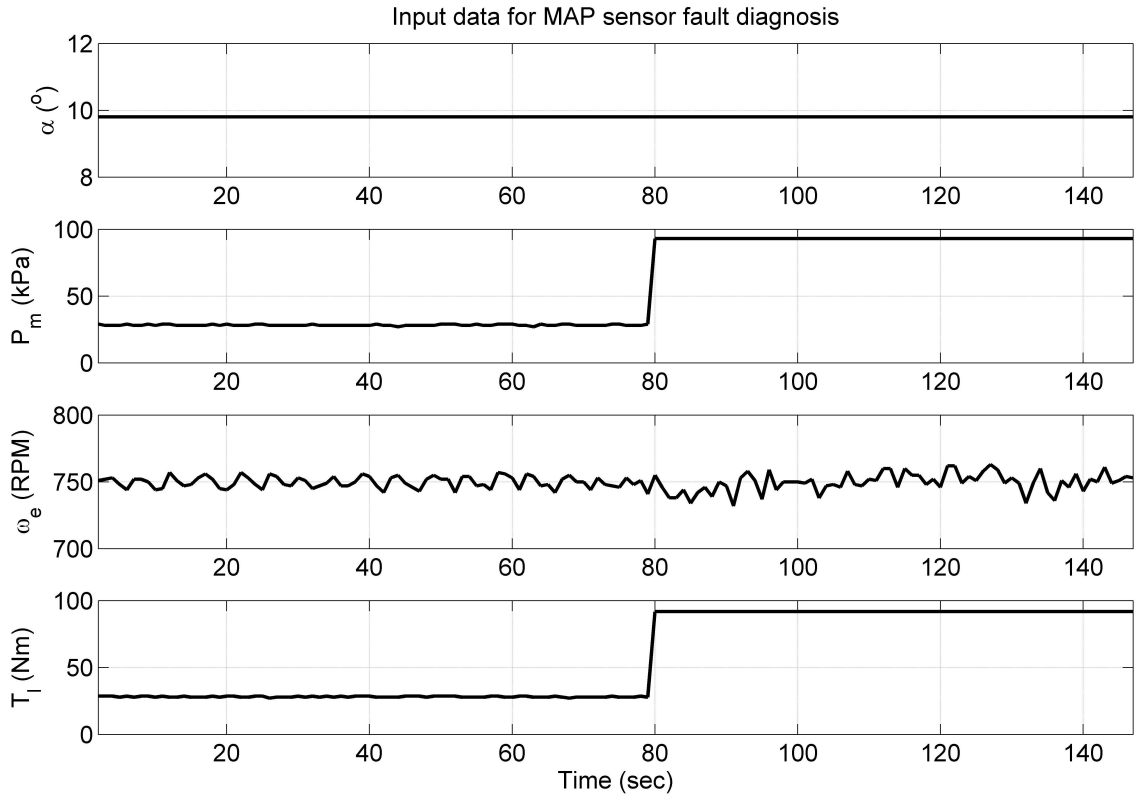

FIGURE 5.22: Input data acquired from OBD-II scanner in the presence of sensor fault diagnosis.

For the pressure sensor fault diagnosis, an experiment was performed that replicated pressure sensor diaphragm damage. When the diaphragm gets ruptured, instead of measuring actual pressure the sensor starts sensing normal air pressure of 93 kPa. This replicates *freeze* sensor fault in nature. This behavior can be visualized in Figure 5.22. On the contrary, engine angular speed demonstrated that engine was working properly as the throttle angle was kept at 9.8^o throughout the experiment. The load torque exhibited the shown response as it was calculated by a relation that is proportional to manifold pressure sensor measurements. Thus, the consequences of the faulty MAP sensor were visible on engine performance. An inevitable outcome of the MAP sensor fault was exhaust emissions. The higher values of MAP sensor measurements indicated false demand of air for air-fuel mixture. As a result more fuel was injected in combustion chamber that resulted in rich mixture and incomplete combustion, thus founding the base for exhaust emissions.

In the second step, the acquired data (Figure 5.22) was supplied to SOSM Observer

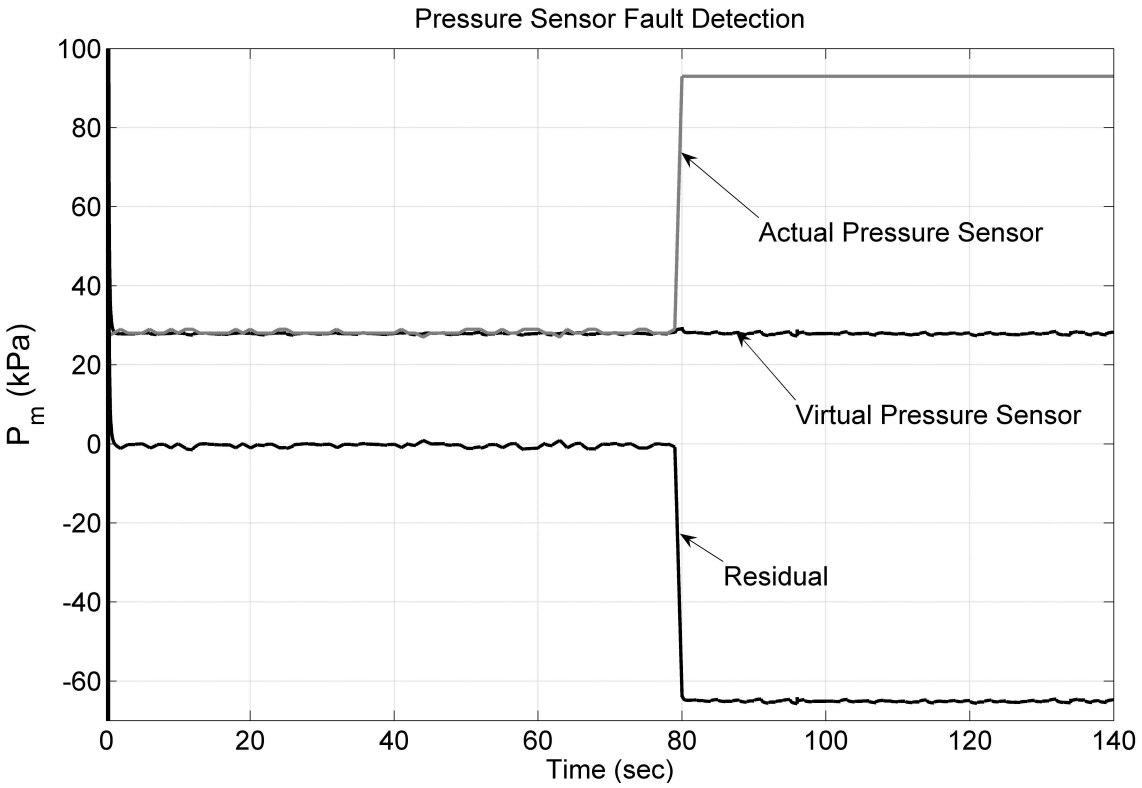

FIGURE 5.23: Manifold pressure sensor fault diagnosis results.

based estimation scheme. The manifold pressure was virtually sensed from angular speed using *Eq (5.9)* and correcting injectors in *Eq (4.41)*. The SOSM Observer convergence was achieved by selecting gains as given in Table 4.5. Figure 5.23 demonstrates the effectiveness and sensitivity of the proposed methodology, as the fault was detected in less than one second. It can be seen that the virtual sensor informed that the pressure is 30 kPa, after the fault has occurred in pressure sensor. Thus, the residual r_1 announced the occurrence of fault in MAP sensor.

Remark 5.7. It may be kept in mind that engine operations during sensor fault diagnosis experiment were working properly (See Figure 5.22), only the pressure sensor started malfunctioning. This is the reason virtual pressure sensor revealed healthy engine operations.

Remark 5.8. When the power of MAP sensor was interrupted, ECU at once announced the fault code for pressure sensor, however for the experiment conducted as shown in Figure 5.23, ECU did not announce any fault code, this depicts the effectiveness of the proposed algorithm.

Remark 5.9. The same methodology can be applied for crankshaft sensor health monitoring. The angular speed virtual sensor devised in Chapter 4 can keep a check on crankshaft sensor working. The experiment for crankshaft sensor fault diagnosis was not conducted as ECU of available production vehicle engine rig does not allow to introduce fault in crankshaft sensor.

5.6 Conclusion

A SOSM Observer based fault diagnosis scheme for automotive engine has been discussed in this chapter. The critical parameters of air intake path were estimated and the estimated values were compared under normal and faulty operating conditions to generate residuals. These residuals were evaluated to diagnose fault in air intake system and its components. The presented scheme was implemented to monitor the health of production vehicle engine and successfully detection of a major set of air intake system faults has been presented. The credibility of the diagnosis scheme can be observed when the engine performance was effected by these faults and on board diagnostic system was unable to detect these faults. However, the proposed scheme diagnosed these faults, thus proving the validity of the proposed scheme.

Chapter 6

CONCLUSION & FUTURE WORK

This manuscript presented a novel health monitoring scheme for automotive gasoline engine. The focus of methodology was air intake subsystem. The prime responsibility of this subsystem is to ensure strict air and fuel proportions in combustion chamber mixture. Any malfunction in this subsystem or its components can disturb the air fuel mixture that will result in poor engine performance, retarded fuel efficiency and harmful exhaust emissions. Among various faults in air intake system, few defects have been discussed along-with their consequences. It has been discussed that

- Clogged air filter may effect the drivability performance of engine, as the engine acceleration time is increased in ECU equipped engines.
- Air leakages in intake manifold may result in degraded drivability performance.
- Any blockade in throttle body may cause low engine angular speeds and if the blockade increases with time, engine may fail to operate during idling.
- Any fault in manifold absolute pressure sensor may result in hazardous emissions.
- Crankshaft sensor malfunction may hinder the engine performance.

It can be seen that the above mentioned failures result in poor engine performance and harmful emissions and yet these faults are not catered in modern gasoline engines equipped with on-board diagnostics. Therefore, for a highly nonlinear air intake system, a nonlinear fault diagnosis scheme was proposed that can timely monitor these malfunctions.

The task of health monitoring was achieved by estimating such critical parameters that are nonlinear & un-measurable in nature and carry credible information

about the air intake system health. Such parameters include air filter discharge coefficient, throttle body discharge coefficient, volumetric efficiency, combustion efficiency and frictional torque were estimated. These parameters were estimated by employing robust second order sliding mode observer. The SOSM Observer was designed with the help of a highly nonlinear two state mean value engine model. The reliability of the engine dynamical model was ensured by validating it against a production vehicle engine. The presented scheme also delivered the solution to devise virtual/soft sensors for manifold pressure and angular speed measurement.

The second order sliding mode observer was selected as it inherits the same robustness as first order sliding mode observer. However, it was preferred due to its quick convergence solution for highly nonlinear systems. It did not require any mandatory initial information of the system for its convergence. It operates sample by sample to deliver estimation results, thus making it computationally cheap. These attributes make SOSM observer based estimation superior than any other estimation technique.

The SOSM Observers were designed for pressure and angular speed dynamics. Once the convergence was achieved by selecting suitable SOSM Observer parameters, the identification of aforementioned parameters was conducted under idle, steady state and healthy operating conditions. The estimation results were verified from the available literature resources. Virtual sensors were validated with actual sensors measurements.

The proposed scheme was validated on a 1300 cc production vehicle engine. The engine was equipped with ECU compliant to OBD-II standards. OBD-II scanner/logger was used to record engine operations. The recorded data was supplied to estimation scheme sample by sample. The proposed estimation scheme was evaluated under healthy and faulty operating conditions to generate residuals. The residuals were later on analyzed for the identification of respective fault. It was shown experimentally that all of the mentioned faults were timely diagnosed successfully.

6.1 Contributions

After going through a brief discussion on the presented work, the main contributions of the thesis can be enumerated as follows,

1. Incorporation of air filter effects on air flow across the intake manifold to refine manifold pressure dynamics. The air filter effects are modeled under air filter discharge coefficient or by measuring pressure drop across air filter.

2. Estimation of

   (a) Air filter discharge coefficient (C_{af})

   (b) Gasoline engine volumetric efficiency (η_{vol})

   (c) Gasoline engine combustion efficiency (η_c)

   (d) Frictional torque (T_f)

   from highly nonlinear gasoline engine pressure and angular speed dynamics. These dynamics were used to develop estimation scheme from super twisting based second order sliding mode observer. The presented scheme required measurements from throttle position sensor, manifold pressure sensor and crankshaft sensor. These sensors are mandatory in every OBD-II compliant vehicle. This practice can serve as replacement for lookup table based solution to acquire values for above parameters.

3. Development of virtual/soft sensor for manifold pressure computation. This task was accomplished by estimating manifold pressure from crankshaft sensor readings.

4. Fabrication of virtual/soft sensor for angular speed quantification. For this purpose, manifold pressure sensor measurements were employed to sense rotational speed virtually.

5. Health monitoring of air filter by generating residuals from estimation of air filter discharge coefficient. These residuals were analyzed to diagnose clogged air filter.

6. Diagnosis of manifold air leakages and throttle body efficiency by analyzing the residuals generated from estimation of throttle discharge coefficient (C_D) and η_{vol}.

7. Development of sensor redundancy for air intake system. This redundancy was exploited for monitoring crankshaft and manifold air pressure sensor functions.

8. The presented scheme can be termed as OBD-II based estimation and fault diagnosis strategy. It only requires measurements that can be accessed from basic OBD-II kit without installing any extra hardware for data acquisition. Thus it can be implemented on any OBD-II kit as discuss in future tasks.

6.2 Future Prospects

The presented work in this manuscript can be extended in several directions. Few of the future tasks are discussed below;

Modeling of Other Engine Subsystems: In this monograph, intake manifold pressure and angular speed dynamics are used to model engine behavior. Rest of the dynamics like intake temperature dynamics, fuel dynamics were assumed to be constant. In future, the engine can be precisely modeled if one can include engine fuel dynamics, intake manifold temperature dynamics and exhaust pressure dynamics [61]. This practice will also contribute in improving estimation results and can help in health monitoring of other auxiliary engine components.

Analysis of Estimation Results: The SOSM Observer based parameter estimation results are sensitive to number of factors. These factors include SOSM Observer gains, SOSM Observer initial conditions, numerical solver, numerical solver sampling time and low pass filter time constant. The presented estimation and fault diagnosis results are applicable for the given values of the mentioned factors. These values were tuned after number of experiments. The sensitivity analysis of estimation results with respect to

these factor may reveal the dependency of the solutions [99], [100]. This can save the time for estimation results tuning and can improve fault diagnostics.

Air Fuel Ratio Estimation: One of the major parameters which cannot be routinely sensed and encompass vital information is, Air Fuel Ratio [56]. This parameter is usually monitored by modeling the engine fuel dynamics. In this manuscript it has been taken as a constant value but one can estimation it using angular speed dynamics. This practice can eliminate the need of modeling fuel dynamics as conventionally these dynamics are used to monitor air fuel ratio.

Fault Diagnosis using Combustion Efficiency: Estimation of combustion efficiency can serve as effective tool for health monitoring of combustion process and its after-effects. The air fuel mixture if not in its proper proportions can reflect itself on combustion efficiency. This is generally sensed by oxygen sensor. So, combustion efficiency can help in health monitoring of combustion process, exhaust emissions and oxygen sensor functions.

Fault Diagnosis using Frictional Torque: Friction estimation can reveal important information about lubrication issues. Generally, frictional torque is modeled as a function of valve lift, oil temperature, oil viscosity, piston speed and other factors. Conversely, estimation of frictional torque from speed dynamics can reveal information about these factors. Any increase or decrease in frictional torque can mention to check any malfunctions due to above factors.

Adaptive Thresholding: When the fault diagnosis is carried out under active diagnosis procedure, it allows to threshold the residuals with constants. However, the generated residuals can be evaluated under more strict conditions. One can avoid a predefined procedures requirement for residual evaluation if adaptive thresholding is employed. The results of presented health monitoring scheme can be improved by extending it to other scenarios with adaptive thresholding for residual evaluation [101], [102]. The adaptive thresholding can be done by fuzzy-based approaches, knowledge based approaches etc.

Implementation on Low Cost Embedded System: The available low cost OBD-II kits does offer a long list of faults that can be diagnosed well in time. However, diagnosis of clogged air filter, manifold leakages, throttle body efficiency and certain MAP sensors faults is still not addressed in current OBD-II kits. The presented scheme analyzes the readily available sensors measurements and is computationally cheap. One can easily implement it on a low cost embedded system for online fault diagnosis of production vehicle engines.

REFERENCES

[1] D. Sandoval and J.B. Heywood. An improved friction model for spark-ignition engines. In *World Congress, SAE, Paper no. 2003-01-0725*, 2003.

[2] Willard W. Pulkrabek. *Engineering Fundamentals of the Internal Combustion Engine.* Prentice Hall, 2003.

[3] Pakistan Automotive Manufacturers Association. Monthly production & sales of vehicles: Production & sales of vehicles - 2010-11, 2011.

[4] CARB. California's obd-ii regulation. Section 1968.1, Title 13, California Code of Regulations, 1993.

[5] Pakistan Environmental Protection Agency. National environmental quality standard for motor vehicle exhaust and noise. Islamabad, Pakistan, 2009.

[6] J. J. Gertler, M. Costin, Xiaowen Fang, R. Hira, Z. Kowalczuk, and Qiang Luo. Model-based on-board fault detection and diagnosis for automotive engines. *Control Engineering Practice*, 1(1):3 – 17, 1993.

[7] V. Krishnaswami, Guan-Chun Luh, and G. Rizzoni. Fault detection in ic engines using nonlinear parity equations. In *American Control Conference, 1994*, volume 2, pages 2001 – 2005 vol.2, June-1 July 1994.

[8] R. Isermann and P. Balle. Trends in the application of model-based fault detection and diagnosis of technical processes. *Control Engineering Practice*, 5(5):709 – 719, 1997.

[9] Heinz Unbehauen. *Control systems, Robotics and Automation, Volume 16.* Encyclopedia of life support systems, UNESCO, 2009.

[10] Giorgio Rizzoni, Simona Onori, and Matteo. Rubagotti. Diagnosis and prognosis of automotive systems: Motivations, history and some results. IFAC *Safeprocess, 2009*, pages 191–202, 2009.

[11] Seungdeog Choi, B. Akin, M.M. Rahimian, and H.A. Toliyat. Implementation of a fault-diagnosis algorithm for induction machines based on advanced digital-signal-processing techniques. *Industrial Electronics, IEEE Transactions on*, 58(3):937 –948, March 2011.

[12] E. Al Ahmar, V. Choqueuse, M.E.H. Benbouzid, Y. Amirat, J. El Assad, R. Karam, and S. Farah. Advanced signal processing techniques for fault detection and diagnosis in a wind turbine induction generator drive train: A comparative study. In *Energy Conversion Congress and Exposition (ECCE), 2010 IEEE*, pages 3576 –3581, 2010.

[13] M. Abbas, A.A. Ferri, M.E. Orchard, and G.J. Vachtsevanos. An intelligent diagnostic/prognostic framework for automotive electrical systems. In *Intelligent Vehicles Symposium, 2007 IEEE*, pages 352 –357, 2007.

[14] H. Versmold and M. Saeger. Plausibility checking of sensor signal for vehicle dynamics control systems. In *8th International Symposium on Advanced Vehicle Control AVEC, Taiwan*, 2006.

[15] F. Perschl and G. Schmidt. Model- and knowledge-based fault detection and diagnosis of gas transmission networks. In *Systems, Man and Cybernetics, 1993. 'Systems Engineering in the Service of Humans', Conference Proceedings., International Conference on*, pages 749 –754 vol.1, October 1993.

[16] M. S. Sangha, J. B. Gomm, D. L. Yu, and G. F. Fault detection and identification of automotive engines using neural networks. In *World congress, Int. Federation of Automation Control*, 2005.

[17] David Antory. Fault diagnosis application in an automotive diesel engine using auto-associative neural networks. In *Proceedings of the International Conference on Computational Intelligence for Modelling, Control and Automation and International Conference on Intelligent Agents, Web Technologies and Internet Commerce Vol-2 (CIMCA-IAWTIC'06) - Volume 02*, pages 109–116, Washington, DC, USA, 2005. IEEE Computer Society.

[18] A.L. Dexter. Fuzzy model based fault diagnosis. *Control Theory and Applications, IEE Proceedings* -, 142(6):545 –550, November 1995.

[19] Yi Lu, Tie Qi Chen, and B. Hamilton. A fuzzy system for automotive fault diagnosis: fast rule generation and self-tuning. *Vehicular Technology, IEEE Transactions on*, 49(2):651 –660, March 2000.

[20] L.R. Rabiner. A tutorial on hidden markov models and selected applications in speech recognition. *Proceedings of the IEEE*, 77(2):257 –286, Feb 1989.

[21] M. Jager and F.A. Hamprecht. Principal component imagery for the quality monitoring of dynamic laser welding processes. *Industrial Electronics, IEEE Transactions on*, 56(4):1307 –1313, April 2009.

[22] Ming Dong and David He. A segmental hidden semi-markov model (hsmm)-based diagnostics and prognostics framework and methodology. *Mechanical Systems and Signal Processing*, 21(5):2248 – 2266, 2007.

[23] Jie Ying, T. Kirubarajan, K.R. Pattipati, and A. Patterson-Hine. A hidden markov model-based algorithm for fault diagnosis with partial and imperfect tests. *Systems, Man, and Cybernetics, Part C: Applications and Reviews, IEEE Transactions on*, 30(4):463 –473, Nov 2000.

[24] P. Baruaha and R. B. Chinnama. Hmms for diagnostics and prognostics in machining processes. *International Journal of Production Research*, 43(6):1275 –1293, Mar 2005.

[25] Xiaodong Zhang, R. Xu, Chiman Kwan, S.Y. Liang, Qiulin Xie, and L. Haynes. An integrated approach to bearing fault diagnostics and prognostics. In *American Control Conference, 2005. Proceedings of the 2005*, pages 2750 – 2755 vol. 4, 8-10 2005.

[26] M. Mostofi, A. H. Shamekhi, and M. Ziabasharhagh. Developing an algorithm for si engine diagnosis using parity relations. *ASME Conference Proceedings*, 2006(47683):199–205, 2006.

[27] Oscar A.Z. Sotomayor and Darci Odloak. Observer-based fault diagnosis in chemical plants. *Chemical Engineering Journal*, 112(1-3):93 – 108, 2005.

[28] F. Heidtmann and D. Soffker. Virtual sensors for diagnosis and prognosis purposes in the context of elastic mechanical structures. *Sensors Journal, IEEE*, 9(11):1577 –1588, Nov. 2009.

[29] T. Orlowska-Kowalska. Application of extended luenberger observer for flux and rotor time-constant estimation in induction motor drives. *Control Theory and Applications, IEE Proceedings D*, 136(6):324 – 330, November 1989.

[30] D. van Schrick. Pi-observer-based reconstruction of effect-variables and construction of characteristic curves. In *Control Conference, 2004. 5th Asian*, volume 2, pages 937 – 942 Vol.2, 2004.

[31] C. Sentouh, S. Mammar, and S. Glaser. Simultaneous vehicle state and road attributes estimation using unknown input proportional-integral observer. In *Intelligent Vehicles Symposium, 2008 IEEE*, pages 690 –696, June 2008.

[32] A. Khedher, K. Benothman, D. Maquin, and M. Benrejeb. State and sensor faults estimation via a proportional integral observer. In *Systems, Signals and Devices, 2009. SSD '09. 6th International Multi-Conference on*, pages 1 –6, March 2009.

[33] M. M. Share Pasand, M. Aliyari Sh., and H. D. Taghirad. Unknown input-proportional integral observer for singular systems: Application to fault detection. In *Electrical Engineering (ICEE), 2010 18th Iranian Conference on*, pages 662 –667, May 2010.

[34] Zhenhai Li and Imad M. Jaimoukha. Observer-based fault detection and isolation filter design for linear time-invariant systems. *International Journal of Control*, 82:171 – 182, 2009.

[35] R. Isermann. Supervision, fault-detection and fault-diagnosis methods – an introduction. *Control Engineering Practice*, 5(5):639 – 652, 1997.

[36] V. Reppa and A. Tzes. Fault detection and diagnosis based on parameter set estimation for measurements corrupted by bounded noise. In *Control Automation (MED), 2010 18th Mediterranean Conference on*, pages 460 – 465, June 2010.

[37] V. Reppa and A. Tzes. Fault detection and diagnosis based on parameter set estimation. *Control Theory Applications, IET*, 5(1):69 –83, 6 2011.

[38] Xiaofang Zha and F. Crusca. A robust least square fault detection approach for linear systems with structured time-varying perturbations. In *Control and Decision Conference, 2008. CCDC 2008. Chinese*, pages 3372 –3377, 2008.

[39] Mattias Nyberg, Andrej Perkovic, and Lars Nielsen. Model-based diagnosis of leaks in the air-intake system of an si engine. In *World Congress, SAE, Paper no. 980514*, 1998.

[40] Depeng Yang, G.D. Peterson, Husheng Li, and Junqing Sun. An fpga implementation for solving least square problem. In *Field Programmable Custom Computing Machines, 2009. FCCM '09. 17th IEEE Symposium on*, pages 303 –306, April 2009.

[41] D. Caveney. Cooperative vehicular safety applications. *Control Systems Magazine, IEEE*, 30(4):38 –53, Aug. 2010.

[42] R. Van der Merwe and E.A. Wan. The square-root unscented kalman filter for state and parameter-estimation. In *Acoustics, Speech, and Signal Processing, 2001. Proceedings. (ICASSP '01). 2001 IEEE International Conference on*, volume 6, pages 3461 –3464 vol.6, 2001.

[43] T. Wenzel. Dual extended kalman filter for vehicle state and parameter estimation. *Vehicle System Dynamics*, 44:153–171(19), February 2006.

[44] M. Reichhartinger and M. Horn. Application of higher order sliding-mode concepts to a throttle actuator for gasoline engines. *Industrial Electronics, IEEE Transactions on*, 56(9):3322 –3329, Sept. 2009.

[45] S. Sayeef, G. Foo, and M.F. Rahman. Rotor position and speed estimation of a variable structure direct-torque-controlled ipm synchronous motor drive at very low speeds including standstill. *Industrial Electronics, IEEE Transactions on*, 57(11):3715 –3723, 2010.

[46] M. Canale, L. Fagiano, A. Ferrara, and C. Vecchio. Vehicle yaw control via second-order sliding-mode technique. *Industrial Electronics, IEEE Transactions on*, 55(11):3908 –3916, Nov. 2008.

[47] Q.R. Butt and A.I. Bhatti. Estimation of gasoline-engine parameters using higher order sliding mode. *Industrial Electronics, IEEE Transactions on*, 55(11):3891 –3898, Nov. 2008.

[48] J. Davila, L. Fridman, and A. Levant. Second-order sliding-mode observer for mechanical systems. *Automatic Control, IEEE Transactions on*, 50(11):1785 – 1789, Nov. 2005.

[49] N.K. M'sirdi, A. Rabhi, L. Fridman, J. Davila, and Y. Delanne. Second order sliding mode observer for estimation of velocities, wheel sleep, radius and stiffness. In *American Control Conference, 2006*, 2006.

[50] Q. Ahmed and A.I. Bhatti. Second order sliding mode observer for estimation of si engine volumetric efficiency amp; throttle discharge coefficient. In *Variable Structure Systems (VSS), 2010 11th International Workshop on*, pages 307 –312, June 2010.

[51] Z. Xu and M.F. Rahman. An adaptive sliding stator flux observer for a direct torque controlled ipm motor drive. In *Electric Machines and Drives, 2005 IEEE International Conference on*, pages 704 –709, 15-15 2005.

[52] M. Iqbal, A.I. Bhatti, S.I. Ayubi, and Q. Khan. Robust parameter estimation of nonlinear systems using sliding-mode differentiator observer. *Industrial Electronics, IEEE Transactions on*, 58(2):680 –689, 2011.

[53] Arie Levant. Higher-order sliding modes, differentiation and output-feedback control. *International Journal of Control*, 76:924–941, 2003.

[54] J.P. Barbot, M. Djemai, and T. Boukhobza. *Sliding Mode Observers, Sliding Mode Control in Engineering*. Marcel Dekker, New York, 2002.

[55] Mattias Nyberg and Lars Nielsen. Model based diagnosis for the air intake system of the si-engine. In *970209, SAE: Transactions of Commercial Vehicles*, 1997.

[56] Yong-Wha Kim, G. Rizzoni, and V. Utkin. Automotive engine diagnosis and control via nonlinear estimation. *Control Systems Magazine, IEEE*, 18(5):84 –99, Oct 1998.

[57] T. Jaroszczyk, J. Wake, and M. J. Connor. Factors affecting the performance of engine air filters. *Journal of Engineering for Gas Turbines and Power*, 115(4):693–699, 1993.

[58] Xinpeng Wang, Kitai Kim, Changhwan Lee, and Jooyong Kim. Prediction of air filter efficiency and pressure drop in air filtration media using a stochastic simulation. *Fibers and Polymers*, 9(1):34 – 38, Feb. 2008.

[59] Norman Kevin, Shean Huff, and Brian West. *Effect of Intake Air Filter Condition on Vehicle Fuel Economy*. ORNL/TM-2009/021, DOE, USA, 2009.

[60] Kihoon Choi, S. Singh, A. Kodali, K.R. Pattipati, J.W. Sheppard, S.M. Namburu, S. Chigusa, D.V. Prokhorov, and Liu Qiao. Novel classifier fusion approaches for fault diagnosis in automotive systems. *Instrumentation and Measurement, IEEE Transactions on*, 58(3):602 –611, March 2009.

[61] Lino Guzzella and Christopher Onder. *Introduction to Modeling and Control of Internal Combustion Engine Systems*. Springer, ETH Zurich, 2004.

[62] R. W. Weeks and J. J. Moskwa. Automotive engine modeling for real-time control using matlab/simulink. In *World Congress, SAE, Paper no.950417*, 1995.

[63] E. Hendricks, A. Chevalier, M. Jensen, and S. C. Sorensen. Modeling of the intake manifold modeling dynamics. In *World Congress, SAE, Paper No. 960037*, 1996.

[64] A. Dutka, H. Javaherian, and M.J. Grimble. Model-based engine fault detection and isolation. In *American Control Conference, 2009. ACC '09.*, pages 4593 –4600, 10-12 2009.

[65] S. Sengupta, S. De, A.K. Bhattacharyya, S. Mukhopadhyay, and A.K. Deb. Fault detection of air intake systems of si gasoline engines using mean value and within cycle models. In *Automation Science and Engineering, 2009. CASE 2009. IEEE International Conference on*, pages 361 –366, 22-25 2009.

[66] Matthew A. Franchek, Patrick J. Buehler, and Imad Makki. Intake air path diagnostics for internal combustion engines. *Journal of Dynamic Systems, Measurement, and Control*, 129(1):32–40, 2007.

[67] N. Weinhold, S.X. Ding, T. Jeinsch, and M. Schultalbers. Embedded model-based fault diagnosis for on-board diagnosis of engine control systems. In *Control Applications, 2005. CCA 2005. Proceedings of 2005 IEEE Conference on*, pages 1206 –1211, Aug. 2005.

[68] E. Balaban, A. Saxena, P. Bansal, K.F. Goebel, and S. Curran. Modeling, detection, and disambiguation of sensor faults for aerospace applications. *Sensors Journal, IEEE*, 9(12):1907 –1917, Dec. 2009.

[69] A.P. Singh, T.S. Kamal, and S. Kumar. Development of ann-based virtual fault detector for wheatstone bridge-oriented transducers. *Sensors Journal, IEEE*, 5(5):1043 – 1049, Oct. 2005.

[70] D. Capriglione, C. Liguori, and A. Pietrosanto. Analytical redundancy for sensor fault isolation and accommodation in public transportation vehicles. *Instrumentation and Measurement, IEEE Transactions on*, 53(4):993 – 999, Aug. 2004.

[71] J.A. Crossman, Hong Guo, Y.L. Murphey, and J. Cardillo. Automotive signal fault diagnostics - part i: signal fault analysis, signal segmentation, feature extraction and quasi-optimal feature selection. *Vehicular Technology, IEEE Transactions on*, 52(4):1063 – 1075, July 2003.

[72] G. Rizzoni and P.S. Min. Detection of sensor failures in automotive engines. *Vehicular Technology, IEEE Transactions on*, 40(2):487 –500, May 1991.

[73] Pau-Lo Hsu, Ken-Li Lin, and Li-Cheng Shen. Diagnosis of multiple sensor and actuator failures in automotive engines. *Vehicular Technology, IEEE Transactions on*, 44(4):779 –789, Nov 1995.

[74] M. Nyberg. Model-based diagnosis of both sensor-faults and leakage in the air-intake system of an si engine. In *World Congress, SAE, Paper no. 1999-01-0860*, 1999.

[75] D. Capriglione, C. Liguori, C. Pianese, and A. Pietrosanto. On-line sensor fault detection, isolation, and accommodation in automotive engines. *Instrumentation and Measurement, IEEE Transactions on*, 52(4):1182 – 1189, Aug. 2003.

[76] Q. Ahmed and A.I. Bhatti. Estimating si engine efficiencies and parameters in second-order sliding modes. *Industrial Electronics, IEEE Transactions on*, 58(10):4837 –4846, Oct. 2011.

[77] I. H. Kazmi and I. A Tirmizi. Modeling and simulation of internal combustion engines for design of model-based control methods. Master's thesis, Ghulam Ishaq Khan Institute of Engineering Sciences and Technology, Topi, Pakistan, 2007.

[78] Rob Karmiggelt and F.E. Veldpaus. Mean value modelling of a s.i. engine. EUT, Department of Mechanical Engineering, 1998.

[79] J.P.R. Jongeneel, H. Nijmeijer, C. Manzie, and D. Nesic. Input redundant internal combustion engine with linear quadratic gaussian control and dynamic control allocation. Internal Report, Eindhoven Uni. of Tech., Eindhoven, Netherlands, 2009.

[80] John J. Moskwa and J. Karl Hedrick. Automotive engine modeling for real time control application. In *American Control Conference, 1987*, pages 341 –346, 10-12 1987.

[81] Kiencke Uwe and Nielsen Lars. *Automotive Control Systems: For Engine, Driveline, and Vehicle*. Springer, 2005.

[82] Elbert Hendricks and Spencer C. Sorenson. Mean value modeling of spark ignition engines. In *World Congress, SAE, Paper no.900616*, 1990.

[83] P. Anderson. *Air charge estimation in turbocharged spark ignition engines*. PhD thesis, Linkoping University Sweden, 2005.

[84] E. Hendricks and J. B. Luther. Model and observer based control of internal combustion engines. In *Modeling, Emission & Control in Automotive Engine*, Sep 2001.

[85] Martin Müller. Volumetric efficiency and pumping torque estimation and compressor recirculation control of turbocharged engines. In *World Congress, SAE, paper No. 2009-01-0587*, 2009.

[86] G. De Nicolao, R. Scattolini, and C. Siviero. Modelling the volumetric efficiency of ic engines: Parametric, non-parametric and neural techniques. *Control Engineering Practice*, 4(10):1405 – 1415, 1996.

[87] P.R. Crossley and J.A. Cook. A nonlinear engine model for drivetrain system development. In *Control 1991. Control '91., International Conference on*, pages 921 –925 vol.2, 25-28 1991.

[88] Donald J. Dobner. A mathematical engine model for development of dynamic engine control. In *World Congress, SAE, paper No. 800054*, 1980.

[89] John Heywood. *Internal Combustion Engine Fundamentals*. McGraw-Hill, 1988.

[90] Alexander A. Stotsky. *Automotive Engines Control, Estimation, Statistical Detection*. Springer, 2009.

[91] J.J. Moskwa and Chung-Hung Pan. Engine load torque estimation using nonlinear observers. In *Decision and Control, 1995., Proceedings of the 34th IEEE Conference on*, volume 4, pages 3397 –3402 vol.4, Dec 1995.

[92] Q. Ahmed, A.I. Bhatti, and M. Iqbal. Virtual sensors for automotive engine sensors fault diagnosis in second-order sliding modes. *Sensors Journal, IEEE*, 11(9):1832 –1840, Sept. 2011.

[93] Ltd. Honda Motor Co. New 1.8l i-vtec engine, 2005.

[94] Chi-Tsong Chen. *Linear System Theory and Design.* Oxford University Press, USA, 3^{rd} edition, 1998.

[95] M. Anguelova. *Observability and Identifiability of nonlinear systems with applications in biology.* Phd thesis, Department of Mathematical Sciences ,Chalmers University of Technology and Gteborg University, Gteborg, Sweden, 2007.

[96] K. Madsen, H.B. Nielsen, and O. Tingleff. *Methods for Non-Linear Least Squares Problems.* Informatics and Mathematical Modeling, Technical University of Denmark, 2004.

[97] Mehrdad Saif, Weitian Chen, and Qing Wu. *High Order Sliding Mode Observers and DifferentiatorsApplication to Fault Diagnosis Problem, Modern Sliding Mode Control Theory.* Springer, Berlin, 2008.

[98] Ltd. Honda Motor Co. New 1.3l i-dsi engine, 2005.

[99] M. Hinkkanen and J. Luomi. Parameter sensitivity of full-order flux observers for induction motors. *Industry Applications, IEEE Transactions on*, 39(4):1127 – 1135, July-Aug. 2003.

[100] Zhenhuan Yuan, Haihui Lu, R.J. Kerkman, T.A. Nondahl, and R.A. Lukaszewski. Parameter sensitivity analysis of flux observers for induction motors. In *Industry Applications Conference, 2007. 42nd IAS Annual Meeting. Conference Record of the 2007 IEEE*, pages 1015 –1022, Sept. 2007.

[101] P.M. Frank. Residual evaluation for fault diagnosis based on adaptive fuzzy thresholds. In *Qualitative and Quantitative Modelling Methods for Fault Diagnosis, IEE Colloquium on*, pages 4/1 –411, apr 1995.

[102] Xiaodong Zhang. Sensor bias fault detection and isolation in a class of nonlinear uncertain systems using adaptive estimation. *Automatic Control, IEEE Transactions on*, 56(5):1220 –1226, May 2011.